An analysis of 5 Gev/c π(^+)P collisions involving many neutral secondary particles

Kamakhy, Khalid Ali

TO MY

PARENTS

An Analysis of 5 Gev/c π^+P Collisions Involving Many Neutral Secondary Particles

A thesis presented

by

Khalid Ali Kamakhy

for the

Degree of Doctor of Philosophy

at the

University of Durham

May, 1973

ABSTRACT

This thesis contains an account of some of the work carried out by the author whilst at Durham University. The work has been carried out by the High Energy Nuclear Physics Group of the University of Durham in collaboration with similar groups from the Universities of Bonn, Nijmegen, Paris, Turin and Strasbourg.

Bubble Chamber analysis is concentrated on those events in which at most there is only one neutral particle involved. The remainder, the NOFIT events, can often amount to a considerable proportion of the total events unless these are analysed they represent a loss in the total knowledge of the physics of the interaction. The events, in a sense, are of lower quality than the normal sets of events that are analysed, since the latter have undergone the fitting process which reduces the effects of errors of measurements and also reduces ambiguities of interpretation.

In this thesis events produced by 5 Gev/c positive pions on protons, in which there are two charged secondary particles and two or more neutral particles have been selected for analysis. The problem of ambiguity of identity of the charged secondaries is discussed at length and a successful method has been devised to divide clearly these two pronged events into those with $P\pi^+$ and those with $\pi^+ \ \pi^+$ as the two charged secondaries.

For each of these groups the effects of measuring errors on the estimated invariant masses is considered in detail and the expected mass resolution in each invariant mass combinations is determined.

With the resolution of ambiguity and the calculated precision of mass determination, resonant particle production is sought. Clear signals corresponding to the production of Δ^{++}, η^{o}, f^{o}, A_1^{+} and A_2^{+} are seen. There is some evidence for the $N^{x+}(1700)$ resonance.

The consideration of mass resolution is preceded by a general consideration of the accuracy of the determination of momentum in the chamber.

CONTENTS

LIST OF FIGURES

Chapter 6

Table

LIST OF TABLES

Page

Chapter 1

Chapter 3

Chapter 4

Chapter 5

Chapter 7

CHAPTER 1

INTRODUCTION

Currently, in preparation for bubble chamber experiments at 300 Gev, there is considerable prediction on the kinds of interactions that will be available for analysis. It is estimated that at 150 Gev about 5% of interactions will comprise charged secondary particles (to form an elastic or an inelastic event, i.e. 4-Constraint FIT channel), about 10% will also include one neutral particle in the final state of known mass (neutral pi-meson or neutron and to form an inelastic event, i.e. 1-Constraint (π^o or n)FIT channel) and where the remaining 85% of events will include two or more neutral particles (i.e. NOFIT channel). Only the 4-C and 1-C (π^o or n) FIT channels (i.e. 15% of the total) will be available for conventional film analysis.

The problem at 300 Gev is obvious. To a lesser extent the problem is still a serious one at 5 Gev/c. In all the inelastic reactions that have been considered by Bonn - Durham - Nijmegen - Paris - Turin (B.D.N.P.T.) collaboration in its analysis of interactions of 5 Gev/c positive pi-mesons in hydrogen about 43% have given 4-C FIT, about 35% have given 1-C (π^o and n) FIT channels whilst the remaining 22% have fallen into the NOFIT category. These numbers are averages over all sizes of interactions (largely two and four pronged events). In table (1-1) there is a detailed break down of the topological cross-sections(4-C FIT, 1-C (π^o or n) FIT and NOFIT channels) for the π^+ P collisions at an incident momentum of 5 Gev/c in

Table (1-1) Cross-Sections for the Various Pronged of π^+ P Reactions at 5.0 Gev/c in the B.N.H.B.C.

REACTION π^+ P 5.0 Gev/c		NO. OF EVENTS	CROSS-SECTION (mb)	% RATIO OF EVENTS
TWO PRONGED INTERACTIONS:-				
P π^+	4-C FIT	13992	5.85 ± 0.18	42.9
P $\pi^+ \pi^o$	1-C(π^o)FIT	3100	1.30 ± 0.03	9.5
n $\pi^+ \pi^+$	1-C(n)FIT	1700	0.71 ± 0.04	5.2
P $\pi^+ \ m_2\pi^o$	NOFIT*	8562	3.57 ± 0.40	26.2
n $\pi^+ \pi^+ \ m_1\pi^o$	NOFIT*	5286	2.21 ± 0.40	16.2
TOTAL		32640	13.64 ± 0.14	
FOUR PRONGED INTERACTIONS:-				
P $2\pi^+ \pi^-$	4-C FIT	6994	2.76 ± 0.04	27.4
P $2\pi^+ \pi^- \pi^o$	1-C(π^o)FIT	7300	2.88 ± 0.04	28.6
n $3\pi^+ \pi^-$	1-C(n)FIT	2164	0.85 ± 0.02	8.5
P $2\pi^+ \pi^- \ m_2\pi^o$	NOFIT	6030	2.39 ± 0.17	23.8
n $3\pi^+ \pi^- \ m_1\pi^o$	NOFIT	2976	1.18 ± 0.17	11.7
TOTAL		25464	10.06 ± 0.06	
SIX PRONGED INTERACTIONS:-				
P $3\pi^+ 2\pi^-$	4-C FIT	1055	0.41 ± 0.02	30.8
P $3\pi^+ 2\pi^- \pi^o$	1-C(π^o)FIT	1597	0.61 ± 0.03	45.9
n $4\pi^+ 2\pi^-$	1-C(n)FIT	279	0.11 ± 0.01	8.3
P $3\pi^+ 2\pi^- \ m_2\pi^o$	NOFIT	378	0.15 ± 0.01	11.3
n $4\pi^+ 2\pi^- \ m_1\pi^o$	NOFIT	140	0.05 ± 0.01	3.7
TOTAL		3449	1.33 ± 0.05	
TOTAL OF 2,4 and 6 PRONGED EVENTS		61553	25.03 ± 0.09	

Where m_1 greater than 0 and m_2 greater than 1

* These are revised in chapter 4.

the British National Hydrogen Bubble Chamber (B.N.H.B.C.) of the two, four and six pronged events (see ref. 1, 2 and 3 respectively) excluding the strange particle events. The total $\pi^+ P$ cross-section (obtained by interpolation from counter results, see ref.4) is 26.60 ± 0.01 mb. In the case of the two pronged events ambiguities between the two NOFIT channels have been divided between both channels on the basis of the laboratory momentum spectra of the charged secondaries (see ref. 2) as observed in the unambiguous and ambiguous events respectively, these are revised in chapter 4. If the two pronged events separately are considered then about 42% of these fall into the NOFIT categories and are lost to conventional analysis. This represents a considerable loss of information and in this thesis an attempt is made to exploit the two pronged NOFIT channels. It begins with an account of resolving the ambiguous events followed by a discussion of the precision of measurements in these channels in Chapter 4.

The aim of the work is to show that the multi-neutral particles final state events can be analysed by using the missing mass technique. The way in which this is done is to predict from the four-pronged events which have been analysed in the normal way what is to be expected in the two pronged NOFIT events. For this purpose, the predictions that may be made are given in chapter 5.

In chapters 6 and 7 results of the observation of resonances in the two pronged NOFIT channels are described and a check has been made on these predictions.

General conclusions are given in a short final chapter 8.

Precision of measurement is an important feature of this

work. Because of this it has been of great interest to examine the basic errors in bubble chamber measurements. The bubble chamber, devised and developed by Glaser (1952), has been of great importance in the study of high energy nuclear physics and elementary particles. The present chambers, when backed by accurate measuring machines, are capable of considerable precision.

When a chamber is placed in a magnetic field, the curvature of a track can be used to calculate the momentum of a particle. In the B.N.H.B.C., 1.5 m long, the magnetic field is 13.5 kilogauss. An accuracy of 1.4% in momentum can be achieved at 5 Gev/c when tracks 100 cm long are measured with nine points over the track. This accuracy can be determined from the spread of the measured points about the fitted track (so called "internal error") or an expected value can be calculated by knowing the basic accuracy of the measuring machines, the length of a track and the geometry of reconstruction from the three views (so called "external error"). The external error is used in subsequent analysis, such as that of hypotheses fitting, whereas the internal error is only used as a guide. It will be worthwhile to consider the validity of error formulae that are used in programmes such as THRESH and GRIND. For this purpose, chapters 2 and 3 have described briefly the exposure at 5 Gev/c in the B.N.H.B.C. for the $\pi^+ P$ collisions followed by the sources of error in a typical bubble chamber whereas the multiple scattering and the measuring error are considered in some detail.

CHAPTER 2

GENERAL EXPERIMENTAL CONSIDERATIONS

2. 1 The Exposure

The exposure took place in the beginning of 1965, using the 02 beam at C.E.R.N., with positive pi-mesons at an incident momentum of 5.0 Gev/c, directed into the British National Hydrogen Bubble Chamber (B.N.H.B.C.). At the end of the exposure, about 150,000 pictures had been obtained. The films have been distributed among the following collaborating laboratories: Bonn - Durham - Nijmegen - Paris (Ecole Polytechnique) and Turin for the analysis of two, four and six prong interactions. Later, the film of Paris was shared by Strasbourg for four prong event analysis.

Brief descriptions of the beam and of the chamber are given in the following two sections.

2. 2 The Beam

The 02 beam (see ref.1) in which 5.0 Gev/c positive pions were selected by electrostatic separation was reduced to about 12 pions per picture for the exposure. The beam momentum as defined by the beam line, and confirmed by measurements on the film was (4.985 $\pm$ 0.006) Gev/c with a momentum bite of 0.15 Gev/c. The contamination of the beam from hadrons is negligible and that from muons and electrons (from pion decay) is estimated (see ref.2) to be 3%.

2. 3 The British National Hydrogen Bubble Chamber (B.N.H.B.C.)

The B.N.H.B.C. (see ref. 3a and 3b) was filled with liquid hydrogen at a temperature of 27°K. Figure (2-1) shows the B.N.H.B.C. with surrounding magnet. Its volume is 150 by 45 by 50 cm^3. The chamber was photographed by three cameras placed, 1.4 m away from the chamber, on the corners of an isosceles triangle, of which the base (= height) is 480 $\pm$ 0.01 mm. The observable volume, therefore, was 300 litres.

2.3.1 The Operation of the Chamber

An automatic system is used to control the operating cycles of the expansion system. The Proton Synchrotron gives a signal before the beam arrives; thereafter the expansion cycle starts from a static pressure P_s (in this experiment P_s = 6.3 Kilograms cm^{-2}) which is higher than the vapour pressure P_v. Then the P_s is rapidly removed and the pressure in the liquid falls below P_v, passing into the sensitive region and decreasing to the minimum pressure Pmin at the time t(Pmin). At this time, the pressure is constant and the chamber is sensitive to ingoing and outgoing particles. The paths of the charged particles appear as a string of bubbles. These are allowed to grow for 1 or 2 ms before they are photographed under strong illumination. The final phase is the recompression cycle, when the pressure is raised back to its initial value of the P_s and the chamber is ready for the next expansion.

However, the expansion and the recompression cycles are the critical parts of the operating system for the following reasons:-

I - if the expansion cycle is not fast enough, the boiling

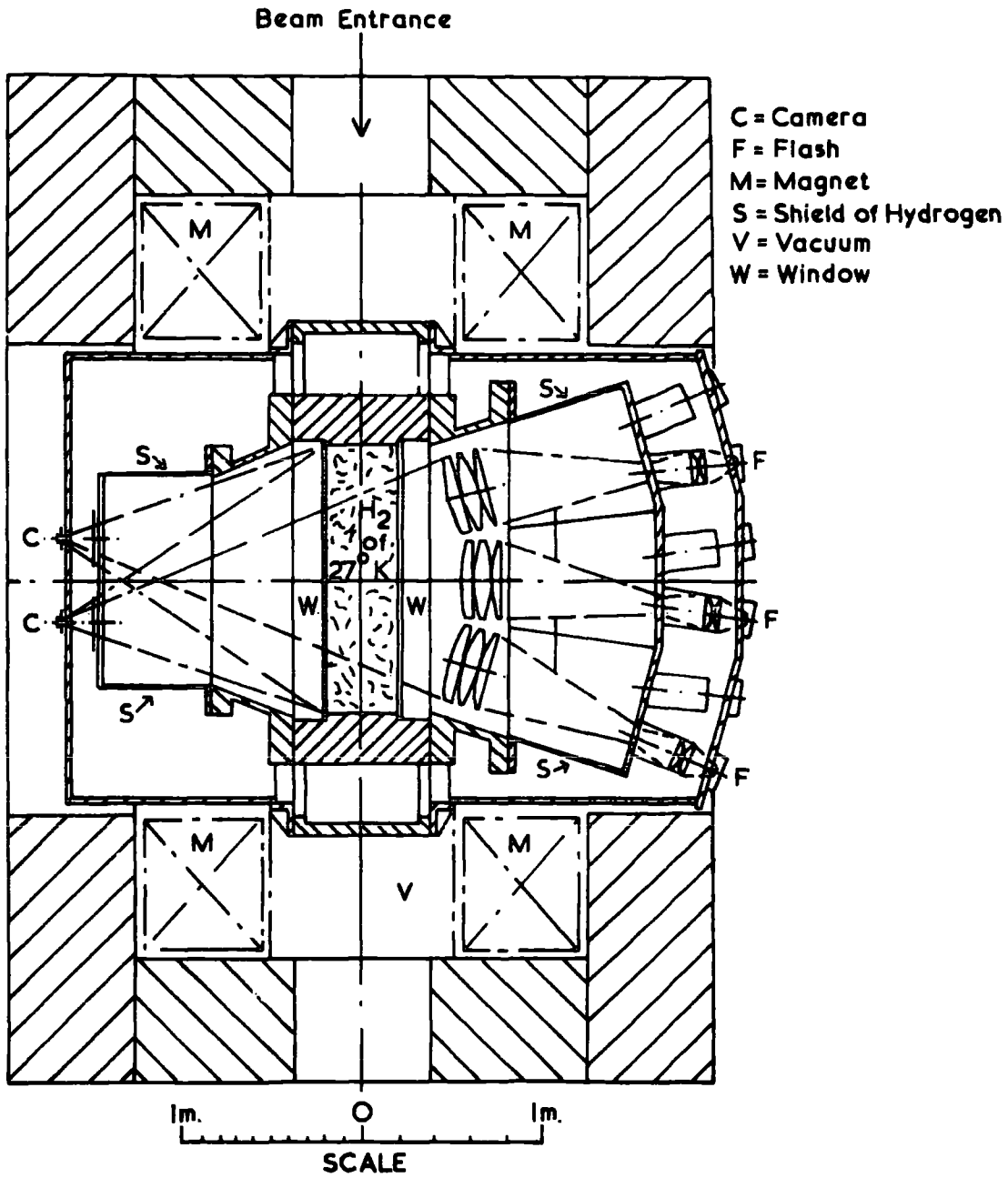

FIG.(2-1) PLAN VIEW OF B.N.H.B.C. SHOWING OPTICAL SYSTEM AND MAGNET

at various surfaces will prevent the P_s from dropping below the P_v and so the liquid will not become sensitive.

II - if the recompression cycle is slow, then so much liquid will be boiling off that it will take a long time before all vapour is returned to the liquid phase.

A typical pressure curve of the operating system is shown in figure (2-2).

Figure (2-3) shows a four prong interaction as observed in the B.N.H.B.C. where the bubbles are photographed some 1 or 2 ms after formation. The bubbles are still small but their apparent size which is determined from their images on the photographic film corresponds to about 250 μm in the chamber. The image on the film is a diffraction image since the problem of depth of focus necessitates that the lens apertures are stopped down and these reduced apertures produce images which are in fact the Airy disc images of the bubbles.

2.3.2 The Relation between Bubble Density and Particle Velocity

Many experiments (see ref.4) have been made to determine a relationship between the bubble density (number of bubbles per cm of track) and the particle velocity (βc). Experimentally, the bubble density n is inversely proportional to the particle velocity squared in the bubble chamber, i.e.

$$n \propto 1/\beta^2 = n_o/\beta^2 \qquad 2.1$$

Rewriting (β) as a function of momentum P and the mass M of the particle, then

$$n = n_o/\beta^2 = n_o(1 + M^2/P^2) \qquad 2.2$$

For large values of momentum n approaches n_o which is the mini-

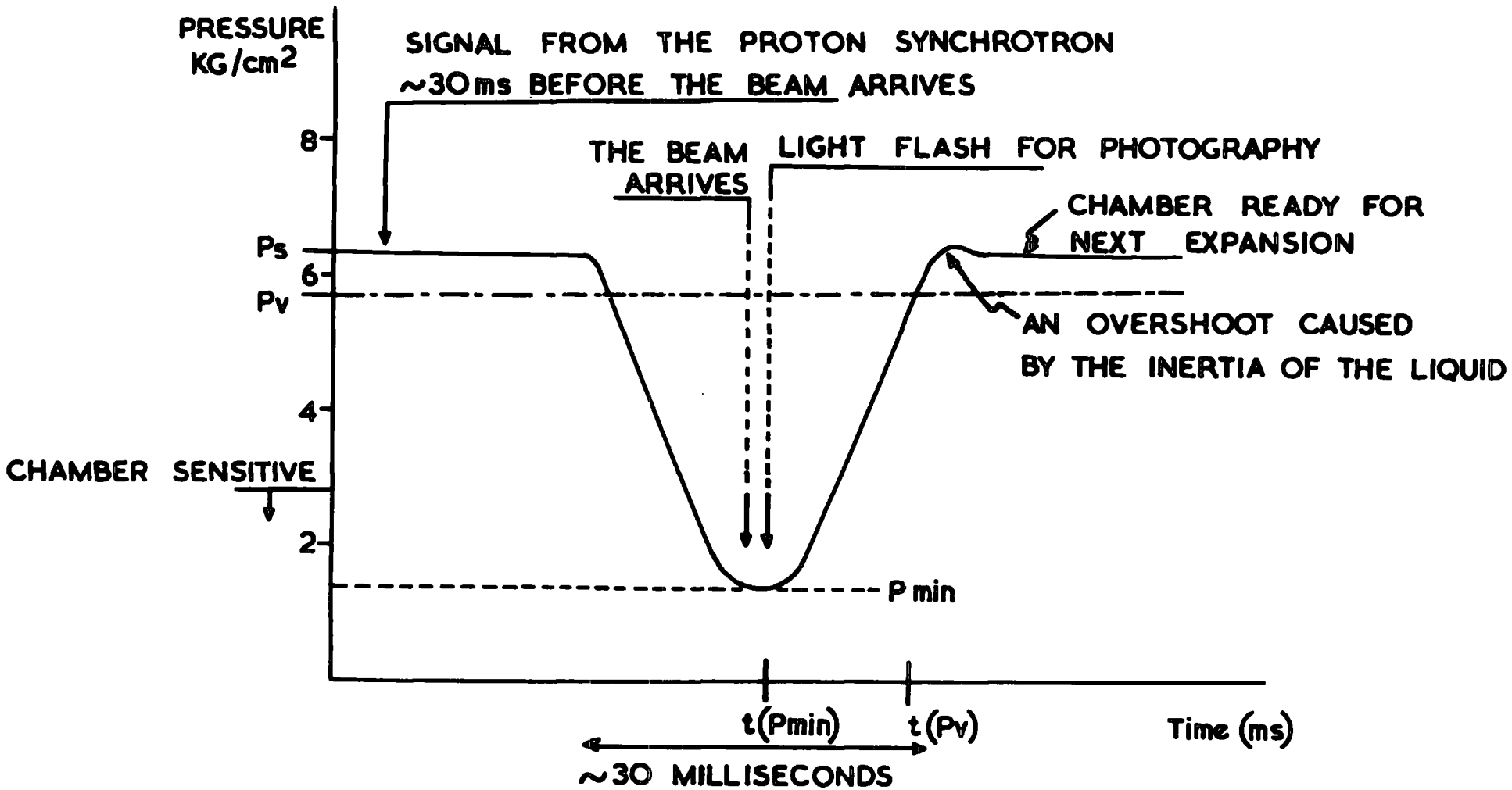

FIG. (2-2) THE SEQUENCE OF OPERATIONS IN THE BUBBLE CHAMBER

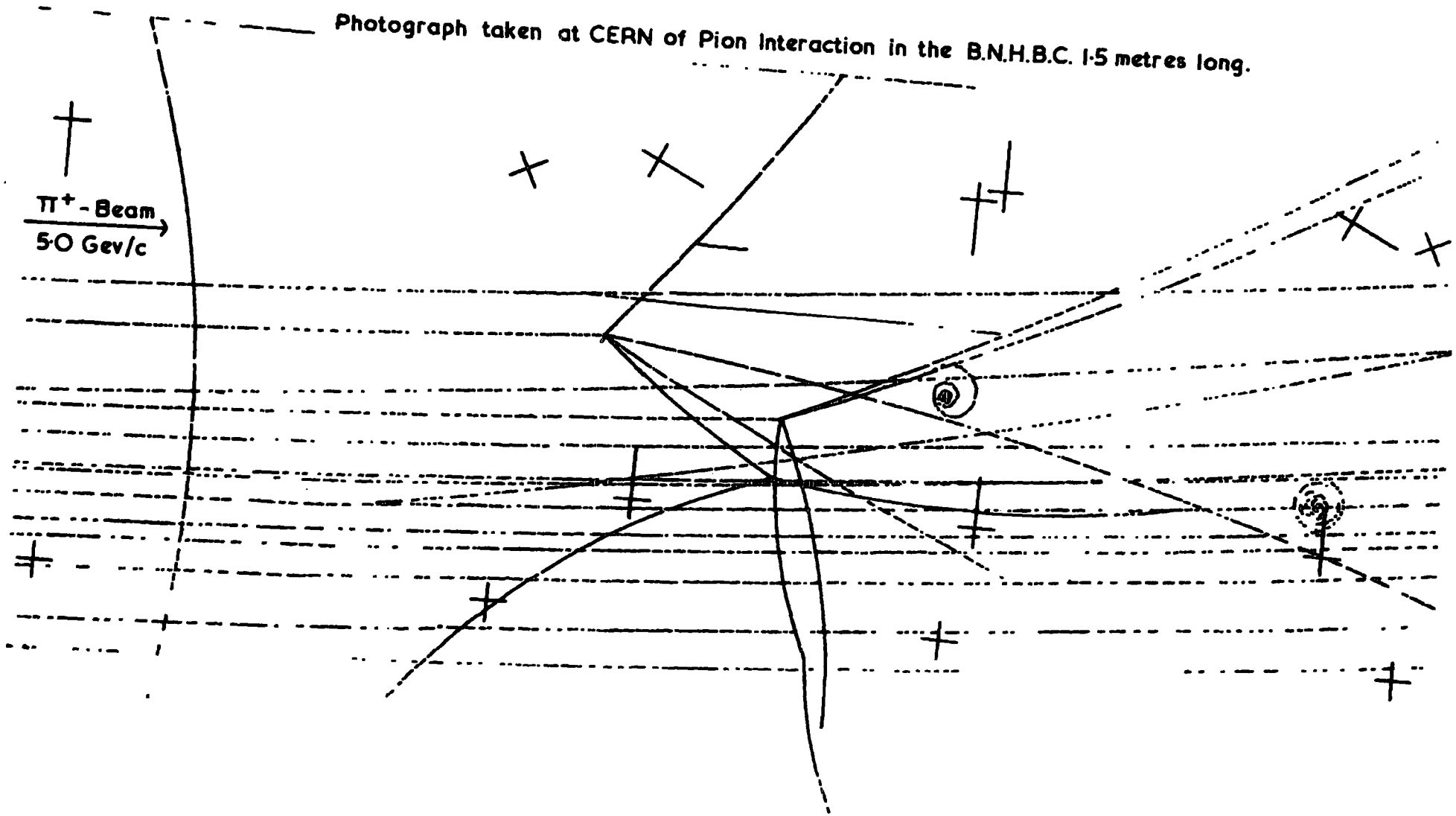

FIG.(2-3) POSITIVE PIONS BEAM MOMENTUM 5·0 Gev/c H = 13·5 KG
Note the 4 pronged reaction in which a K^+ meson is produced and decays.

mum value of the ionisation. Hence the relative bubble density (i.e. bubble density referred to the minimum value) is given by:-

$$n/n_o = 1 + M^2/P^2 \qquad 2.3$$

This is shown in figure (2-4) for pion, kaon and proton. Experimentally, relative bubble density in excess of about 1.4 can be distinguished by eye from the minimum value of 1.0. In terms of momentum it means that pions can be distinguished from protons at momentum below 1.5 Gev/c and pions from kaons below 0.8 Gev/c.

2. 4 The Limitation of Accuracy in a Typical Chamber

The accuracy of the chamber is an important feature of an experiment, obviously, since it controls the overall precision. Indirectly it is important in that selection criteria are based on assumptions about the precision. In this section the precision is considered theoretically and later, in chapter 3, an experimental check on the accuracy is described.

There are many different sources of error which contribute to the overall inaccuracy of the determination, from its track, of momentum (or curvature) and the spatial angles of a particle in the chamber in a known magnetic field. These may be divided into two groups. Firstly there are the intrinsic errors in the chamber due to thermal convection, thermal turbulence and multiple (Coulomb) scattering, and secondly there are errors due to distortion in the optical system, inaccuracy in the strength of the magnetic field and errors in measurement. The multiple scattering and the measuring error are very important and are considered in some detail. The other sources are considered first and described briefly.

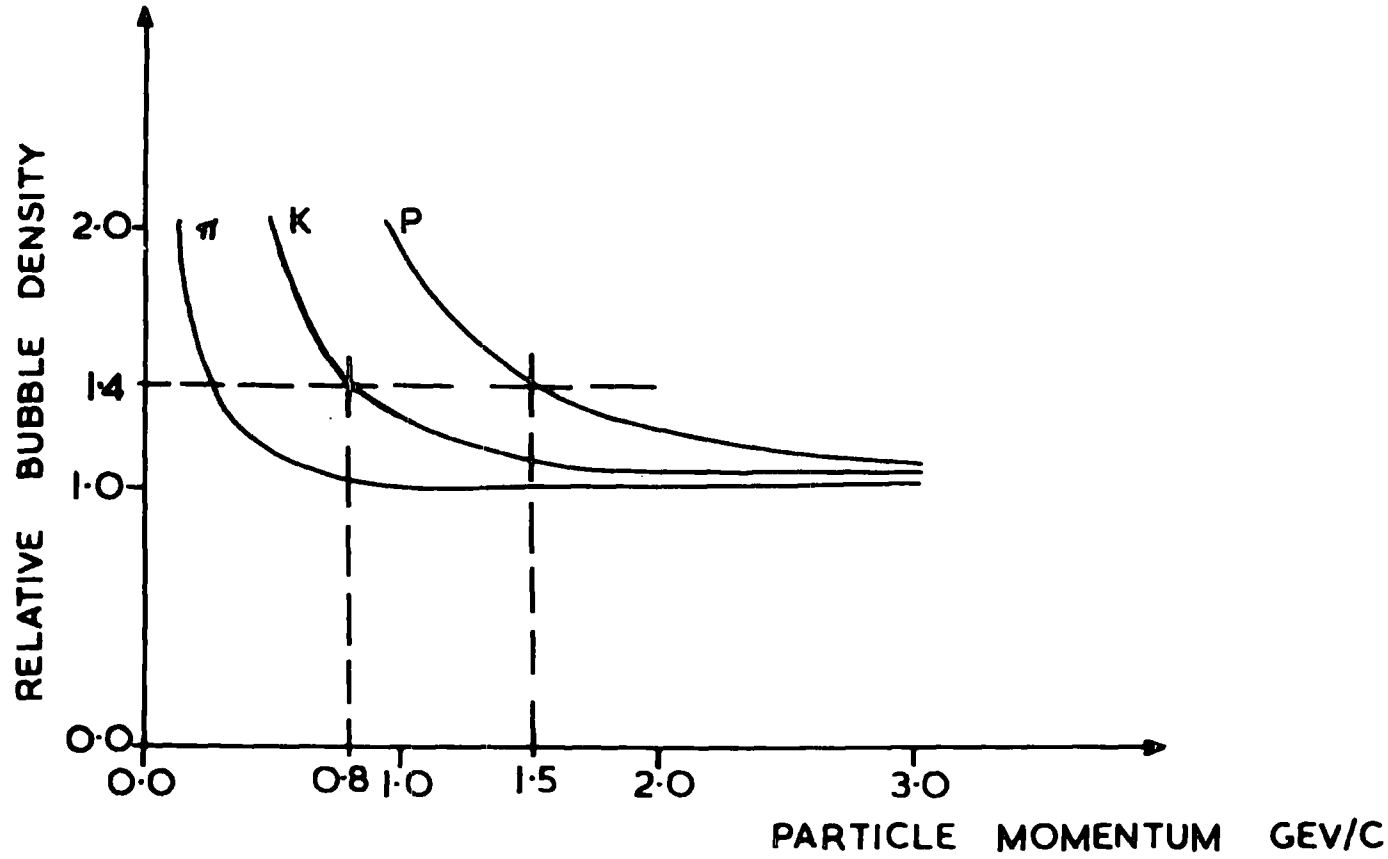

FIG.(2-4) THE RELATIVE BUBBLE DENSITY AS A FUNCTION OF THE PARTICLE MOMENTUM (PION, KAON AND PROTON)

2.4.1 Variation of Magnetic Field

The magnetic field in the chamber is usually denoted by its central value (see ref.5) and in the B.N.H.B.C. this is (13.46 ± 0.03) kilogauss. However, the field varies throughout the chamber but the variation, which is worst at the edges, amounts to about 5%. Since the field is the saturation value of the electromagnet, current variations produce virtually no field variation. The magnetic field is accurately mapped and the deviations from the central value known to about 1%. Hence variations in the paths of a particle due to field variations may be corrected.

2.4.2 Optical Distortions of the Chamber and Camera System

By accurate surveying of the system, it is found (see ref.6) that the distortions can be represented as a simple power series. By means of that the apparent coordinates (x', y') on the ideal film plane can be written as follows:-

$$x' = x(1 + a_1x + a_2y + a_3xy + a_4x^2 + a_5y^2 + a_6(x^2 + y^2)^2 + \ldots)$$
$$y' = y(1 + b_1x + b_2y + b_3xy + b_4x^2 + b_5y^2 + b_6(x^2 + y^2)^2 + \ldots) \quad 2.4$$

when the effect of film stretch has been removed. The terms including a_i and b_i correspond to distortions in the optical system and these are determined from measurements on the film of the known positions of the fiducial marks (they are shown in figure (2-5)). Usually terms with i less than 7 are sufficient.

2.4.3 Thermal Convection and Turbulence

These are motions of the liquid arising from the temperature differences in the system. The convection gives rise to liquid

FIG.(2-5) DIAGRAM OF FIDUCIAL MARKS IN THE B.N.H.B.C. 1·5 METRES LONG

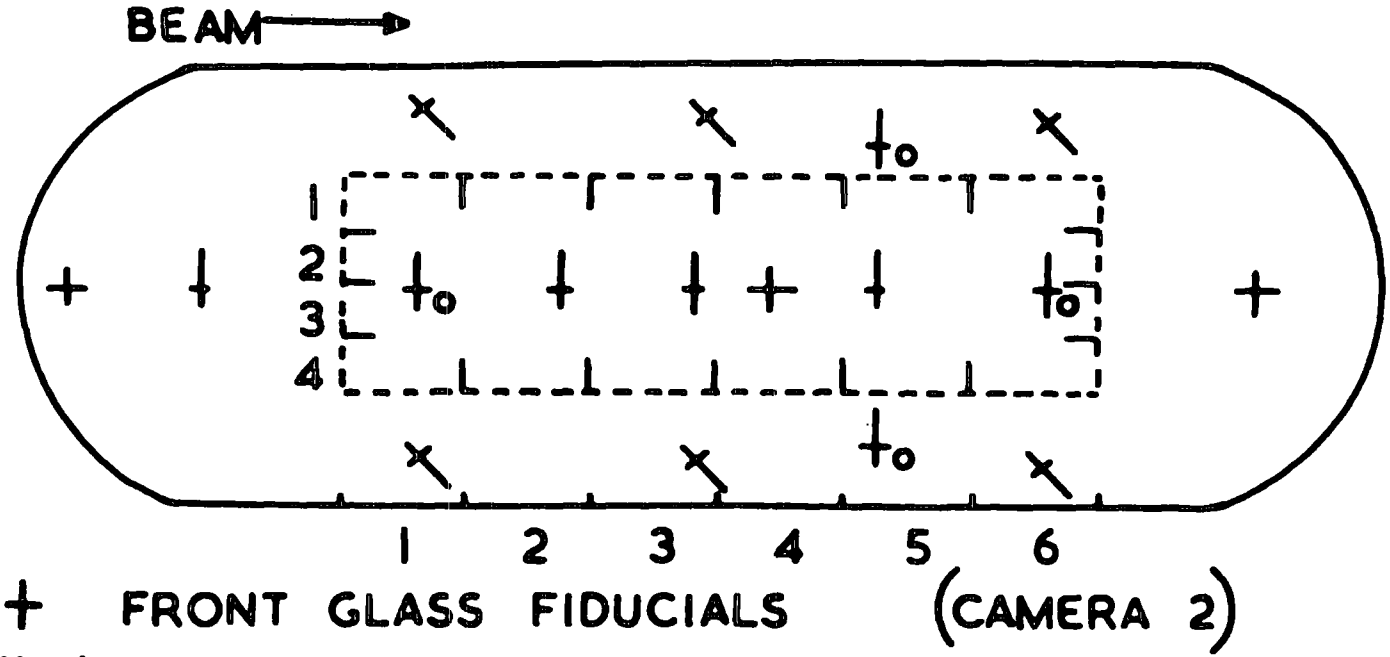

(and hence bubble velocities) of about 3 cm.sec^{-1}. For a growth time of 1 ms for the bubble before photography, the bubble will have moved 30 μm from its original position.

The optical effects of turbulence result from associated variations in refractive index of the liquid. Thomas (see ref.7) has estimated the r.m.s. deviation of the apparent movement of the bubble due to this "twinkling" effect. In liquid hydrogen he has shown that at distance S cm (from bubble to chamber window) where the heat flux is H_f watts cm^{-2} the deviation is given by:-

$$E_t = 45.6 \quad H_f^{7/8} S^{3/2} \ \mu m \qquad 2.5$$

For example, assuming that S = 40 cm and $H_f = 10^{-3}$ watts cm^{-2}, then the above expression gives, E_t = 27 μm. Both of these are small compared to the apparent size of a bubble.

2.4.4 Multiple Scattering

Multiple scattering gives a spurious curvature to a track even when the magnetic field is zero. In the presence of a magnetic field this error in the measured curvature is interpreted as an error in the momentum. Similarly there are errors in the measurement of angles (see ref.8,9 and 10). The experimental analysis which follows later (in chapter 3) is concerned almost entirely with primary tracks. These are selected because their momentum is constant and known. Their angles are not so well defined. Hence, in what follows, the errors on momentum only are considered.

The relative error in the measured momentum P from the multiple scattering is given by:-

$$dP/P = 45.0/(\beta H\, L^{1/2} x_o^{1/2}) \qquad 2.6$$

The scattering constant (45.0 in hydrogen) represents the basic quality of the liquid to cause multiple scattering. It depends upon the atomic number. (βc) is the velocity of the particle and H is the magnetic field in kilogauss. L and x_o are the length of a track and the radiation length of the liquid, both in cm.

From the above expression, it can be seen that the multiple scattering becomes important for short tracks and for low values of β (H and x_o are constants).

Now, writing momentum P in terms of the magnetic field and the radius of curvature (R in cm) as follows:-

$$P = 0.3\ HR \quad Mev/c \qquad 2.7$$

$$= 0.3\ H/C \quad Mev/c \qquad 2.8$$

where C is the curvature (C = 1/R), then

$$|dP/P| = |dC/C| \qquad 2.9$$

Therefore,

$$|dP/P|_{M.S.} = |dC/C|_{M.S.} = 45.0/(\beta H\, L^{1/2} x_o^{1/2}) \qquad 2.10$$

2.4.5 Measuring Error

The source of the measuring error on the film can be seen from the determination of curvature of the track by three point location.

Assuming that the track of length L, which is accurately known, has a sagitta S (both in cm) and that it is measured symmetrically at three points (see figure (2-6)) then the curvature C is given by:-

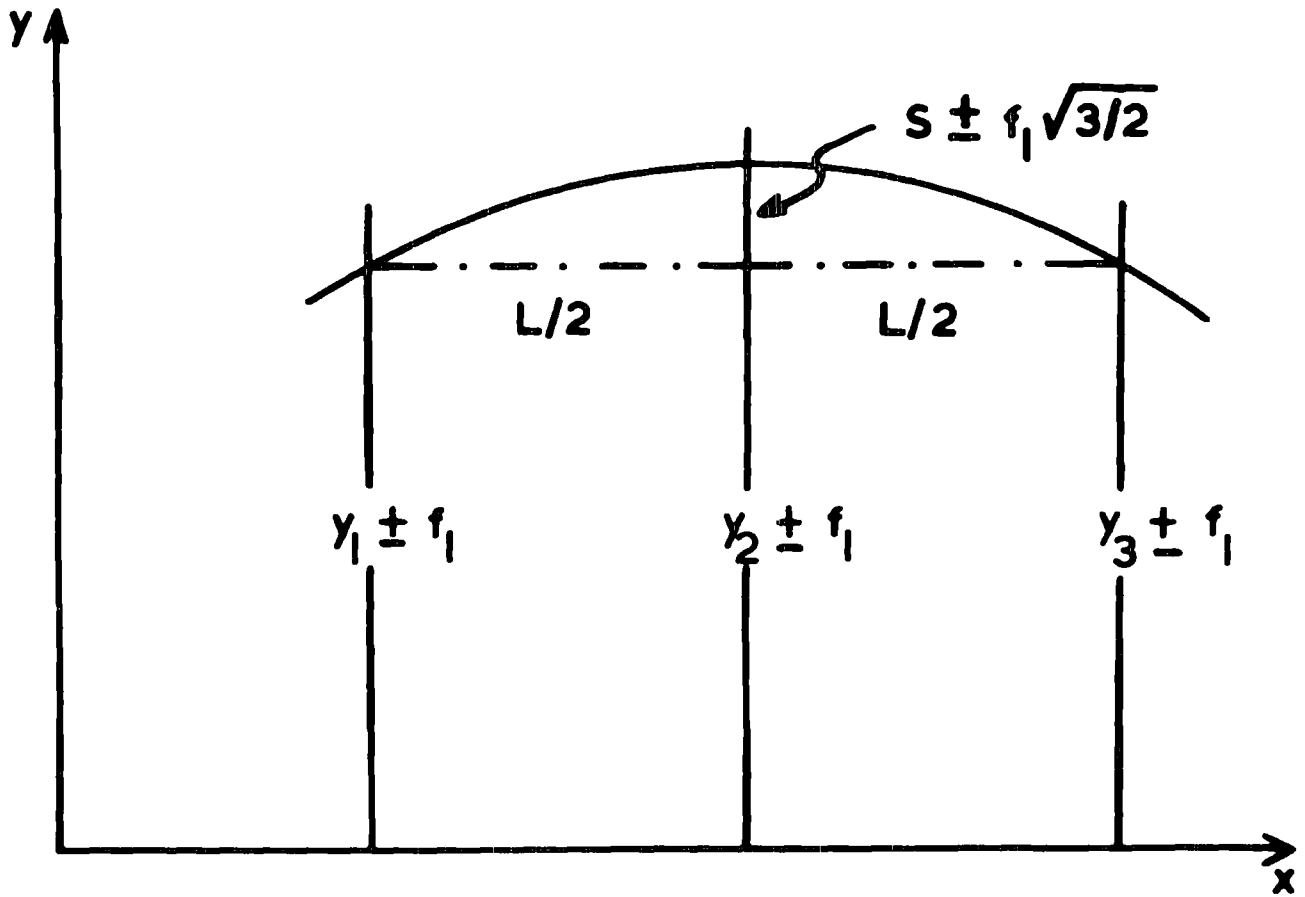

FIG. (2-6) THE (xi, yi) OF THE THREE POINTS LOCATION OF THE TRACK, i=1,2,3. SAGITTA S PARALLEL TO THE y AXIS AND $\Delta x = \Delta y = f_1$

$$C = 8S/L^2 \qquad cm^{-1} \qquad 2.11$$

Hence, the relative error in the measured curvature is related to that in the sagitta by:-

$$dC/C = dS/S \qquad 2.12$$

But $dS = f_1(3/2)^{1/2}$, where f_1 is the r.m.s. error made in measuring a point on a track, the relative error on curvature is

$$dC/C = 8f_1(3/2)^{1/2}/CL^2 \qquad 2.13$$

where substitution has been made for S. This calculation refers to measurements made on a single film. In practice three stereographic films are measured and from these three-dimensional reconstruction is made in chamber space. Equation 2.13 will hold approximately inside the chamber where C is now the curvature of the track (rather than on the film), provided L is interpreted as the length in chamber space and f_1 is the "measuring error in chamber space". Usually about N = 9 points are used in measurement which leadsto an improvement in accuracy given approximately by $(N/3)^{1/2}$. Then the relative error in the measured curvature due to the measuring error is given by:-

$$(dC/C)_{M.E.} = 8(3/2)^{1/2}f_1/((N/3)^{1/2}CL^2) \qquad 2.14$$

Hence, the relative error in the curvature is given by:-

$$(dP/P)_{M.E.} = (dC/C)_{M.E.} = 8f_1P/(0.3(2)^{1/2}HL^2) \qquad 2.15$$

where substitution has been made for C.

In practice the uncertainties in the three-dimensional reconstruction of the track tend to increase the error in the curvature. It is found that for tracks measured with nine points that the working value of the measuring error in curvature (or momentum) in chamber space is given by, (CERN kine-

matics programme, GRIND),

$$(dP/P)_{M.E.} = (dC/C)_{M.E.} = (60)^{1/2} f_1 P / (0.3\ HL^2) \qquad 2.16$$

where f_1 and L in cm, P in Mev/c and H in kilogauss.
Rewriting the above expression when f_1 in μm and P in Gev/c

$$(dP/P)_{M.E.} = (dC/C)_{M.E.} = (60)^{1/2} f_1 P / (3.0\ HL^2) \qquad 2.17$$

The total relative error in the curvature (or momentum) from the multiple scattering and the measuring error can be written in the form

$$(dP/P)_T = (dC/C)_T = \left((dP/P)^2_{M.S.} + (dP/P)^2_{M.E.} \right)^{1/2} \qquad 2.18$$

using equations 2.10 and 2.17.

One can define a momentum P_E when the relative errors from the multiple scattering and the measuring error are equal as follows (using equations 2.10 and 2.17):-

$$P_E = 135\ L^{3/2} / \left((60)^{1/2} \beta f_1\ x_o^{1/2} \right) \text{ Gev/c} \qquad 2.19$$

The total relative error in momentum is not a minimum at P_E, but below P_E the coulomb term dominates and above P_E the error is dominated by the measuring error.

Similarly, it can be seen that the track length L_E when both are equal is given by:-

$$L_E = \left((60)^{1/2} \beta f_1 P\ x_o^{1/2} / 135 \right)^{2/3} \text{ cm} \qquad 2.20$$

Again, the total relative error is not a minimum at L_E, but below this length the error is dominated by measuring error and above L_E by multiple scattering. For any given value of momentum P it is possible to calculate a track length L_E for a given f_1 (β and x_o are constants). For example in the B.N.H.B.C. this length L_E is of about 96 cm at P = 5.0 Gev/c, f_1 = 100 μm, β = 1.0 and x_o = 1050 cm (liquid hydrogen at 27°K).

In figure (2-7) the expected inaccuracies due to Coulomb scattering and measuring error are compared for primary particles of 5.0 Gev/c in the B.N.H.B.C. For most of the lengths (L = 100 cm) available in this exposure, measuring error is the dominating source of inaccuracy (using primary tracks only).

Similarly, in the CERN 2M H(D) BC the critical length L_E is in excess of about 168(152) cm at P = 11.7 Gev/c, f_1 = 100 μm, β = 1.0 and x_o = 1050 (= 764) cm. In the exposures which are considered later the lengths available are less than 100.0 cm and so the precision is dominated by measuring error.

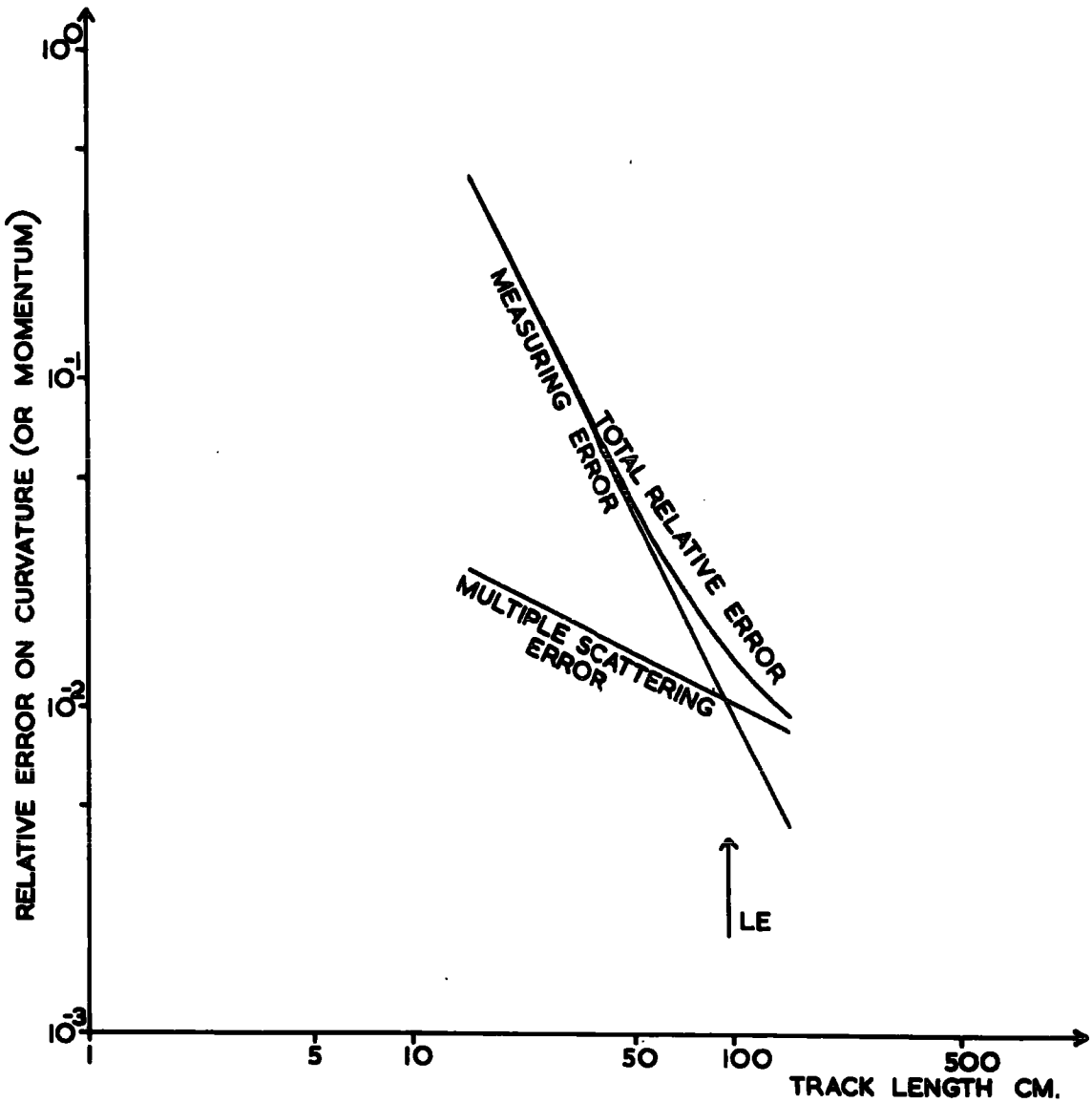

FIG.(2-7) THE EXPECTED ERROR AS A FUNCTION OF THE PRIMARY TRACK LENGTH IN THE B.N.H.B.C.

CHAPTER 3

THE EXPERIMENTAL DETERMINATION OF CURVATURE ERRORS

In section 2. 4 an outline of sources of error in a bubble chamber experiment has been given, in particular theoretical estimates of the magnitudes for the important multiple scattering and measuring error have been presented. With the accumulation of data from three experiments in Durham (these are, the 5.0 Gev/c π^+P in B.N.H.B.C. and 11.7 Gev/c π^+P(d) in CERN 2MH(D)BC) an experimental check on accuracy has been possible. The methods and the results are given in the ensuing sections.

3. 1 The Experimental Data

No special attempt has been made to measure tracks specifically for the purpose of determining error. Instead the accumulated data on GRIND output tapes has been used. This accummulated data is the better sample to test since:-

a) it has been measured under ordinary working conditions

b) the track lengths are the normal ones available, in that they have been selected by scanning for interactions.

In the B.N.H.B.C. and the CERN 2MH(D)BC films the maximum length of these primary tracks is about 100 cm. From figures (2-7) and (3-1) it is not expected that the measurements on the primaries will be limited in any way by Coulomb scattering. The only way of making measurements under multiple scattering limitation is by selecting secondary tracks whose measured momenta are relatively small.

The advantage of using primary tracks is that they are of

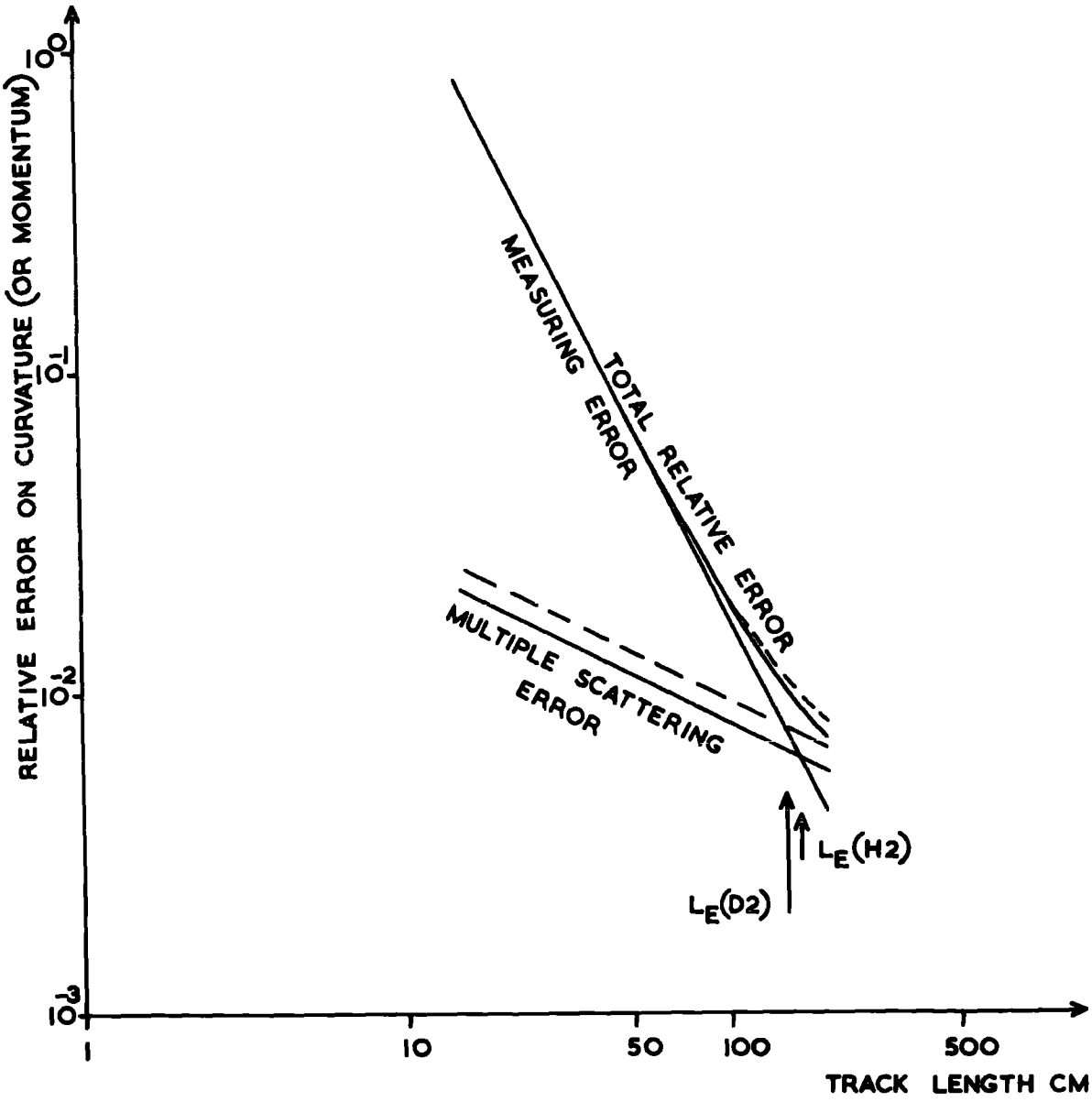

FIG.(3-1) THE EXPECTED ERROR AS A FUNCTION OF THE PRIMARY TRACK LENGTH IN THE CERN 2M B.C.

a) —— LIQUID HYDROGEN

b) — — LIQUID DEUTERIUM

well determined momentum from the characteristics of the beam line. The danger of selecting secondary tracks is that they are selected on their measured momentum rather than their true (but unknown) momentum.

A summary of the data is given in table (3-1).

3. 2 A comparison of Expected and Measured Errors as Determined in THRESH and GRIND

The CERN programmes THRESH and GRIND have been used to reconstruct events in chamber space and to determine their kinematics. In THRESH the curvature is estimated from the nine points measured on a track in each view. From the reconstructed track an "internal error" on the curvature is estimated from the spread of these points about the fitted curve by least squares fitting. In GRIND the "external error" on the curvature is calculated from equation 2.17 assuming that measuring error alone is important. The measurement is defined to be good when the internal error is less than three times the external error.

Obviously, the average value of the internal error should be equal to the average value of the external error and it should vary with length according to equation 2.18. A comparison of the errors calculated in THRESH and GRIND will form an experimental check on equations 2.17 and 2.18.

An overall comparison of errors is given in table (3-1) where the average internal and external errors (columns 9 and 10) for all data are compared. A more detailed check has been made by dividing primary track lengths into groups in 10 cm steps. For each group the average internal and external error

TABLE (3-1) SUMMARY OF DATA ON PRIMARY TRACKS

1	2	3	4	5	6	7	8	9	10	11
CHAMBER	Magnetic field (KG)	Incident momentum (Gev/c)	Range of lengths used and average (cm)	Number of primaries used (No)	Primary curvatures (μm^{-1})			Errors on curvature (μm^{-1})		
					Unweighted mean (C_o)	Weighted mean (C_{oi})	(C_{oe})	Internal (THRESH)	External (GRIND)	Experimental
B.N.H.B.C.	13·5	5·0	(15 – 85) 40·0	1683	8·022 ± 0·029	8·026 ±0·029	8·018 ±0·029	0·726 ±0·013	0·735 ±0·013	1·007 ±0·017
CERN 2M H.B.C.	17·5	11·7	(15 – 95) 48·7	3196	4·488 ± 0·012	4·446 ±0·012	4·452 ±0·012	0·455 ±0·005	0·508 ±0·006	0·586 ±0·007
CERN 2M D.B.C.	17·5	11·7	(15 – 95) 55·0	1717	4·471 ± 0·017	4·438 ±0·017	4·429 ±0·017	0·395 ±0·006	0·425 ±0·007	0·638 ±0·012

C_o is the "unweighted" mean of the curvature ($= \sum_{j=1}^{No} C_j/No$)

C_{oi} is the "weighted" mean of the curvature ($= \sum_{j=1}^{No}(C_j/E_{ij}) / \sum_{j=1}^{No} 1/E_{ij}$)

C_{oe} is the "weighted" mean of the curvature ($= \sum_{j=1}^{No}(C_j/E_{ej}) / \sum_{j=1}^{No} 1/E_{ej}$)

where E_{ij} and E_{ej} are the internal error and the external of the j th track

has been determined from GRIND output records. In figure (3-2) the average internal errors are shown for the three sets of the primary data. Through them is drawn the line corresponding to the average external errors (i.e. a line of slope = -2, see equation 2.17). In each case it can be seen that there is a good agreement between the internal and the external error.

In table (3-2) the fitted slopes to the internal errors (by least squares fitting) are given. There is some indication that the internal errors do not fall off quite so rapidly as a slope of -2 would imply.

TABLE (3-2)

CHAMBER	B.N.H.B.C.	CERN 2M H.B.C.	CERN 2 M D.B.C.
The fitted slopes by Least Squares Fitting	-1.76 ± 0.04	-1.64 ± 0.03	-1.60 ± 0.04

Some further evidence for this is given in figure (3-3). There the internal errors and the external errors are directly compared for the 11.7 Gev/c $\pi^+ P$ exposure. Through them is drawn the line corresponding to the ratio between the average values of the internal error and the external over all the data (E_{oi}/E_{oe}); the dashed line is the expected line and corresponds to the average internal error (E_{oi}) being equal to the average external (E_{oe}). It can be seen that the internal error is about 90% of the external. This means that the internal error is related to the external as follows:-

$$E_i = t\, E_e \qquad 3.1$$

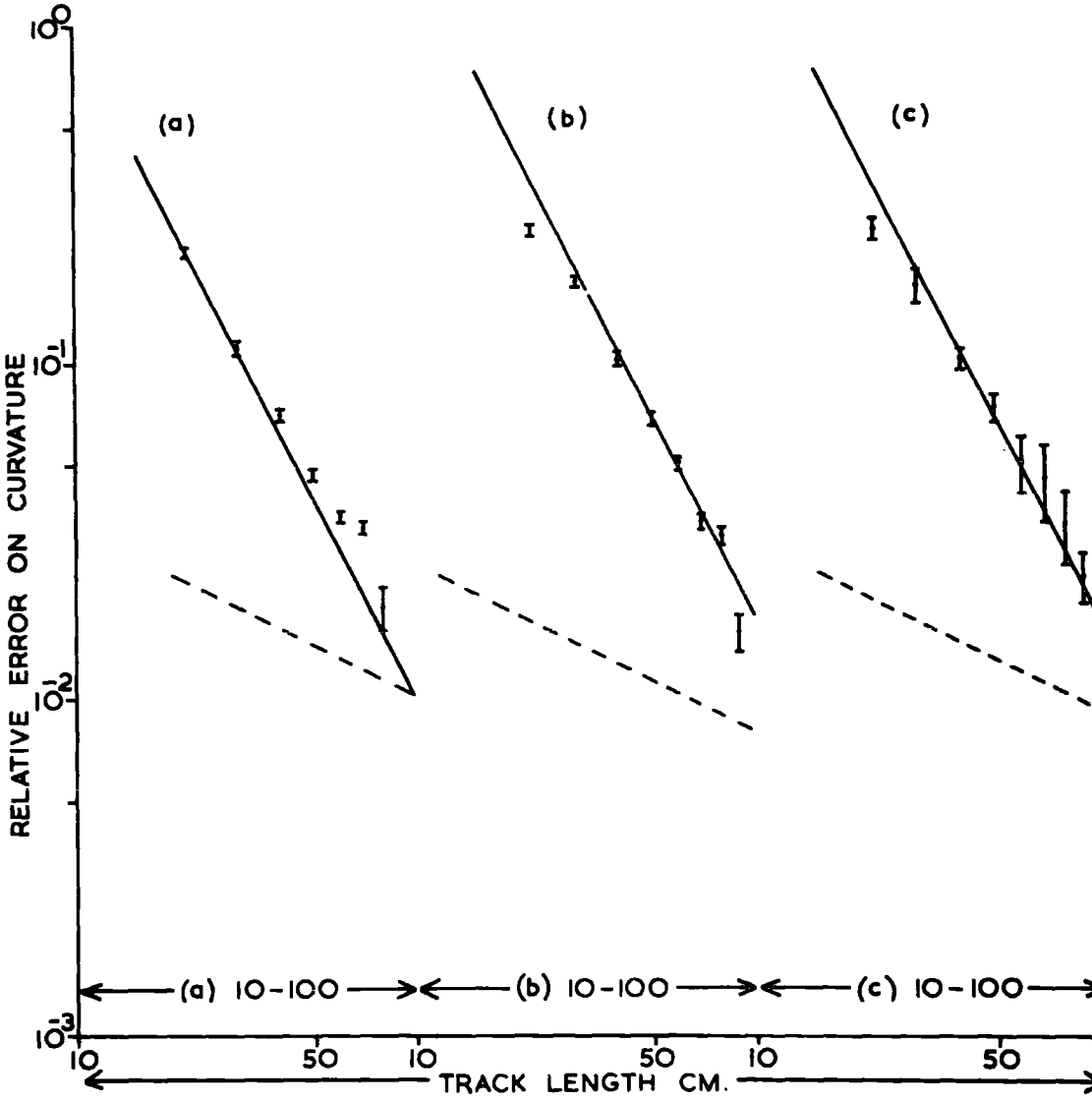

FIG.(3-2) THE RELATIVE ERROR AS A FUNCTION OF THE TRACK LENGTH

(a) IN THE B.N.H.B.C.
(b) IN THE CERN 2M H.B.C.
(c) IN THE CERN 2M D.B.C.

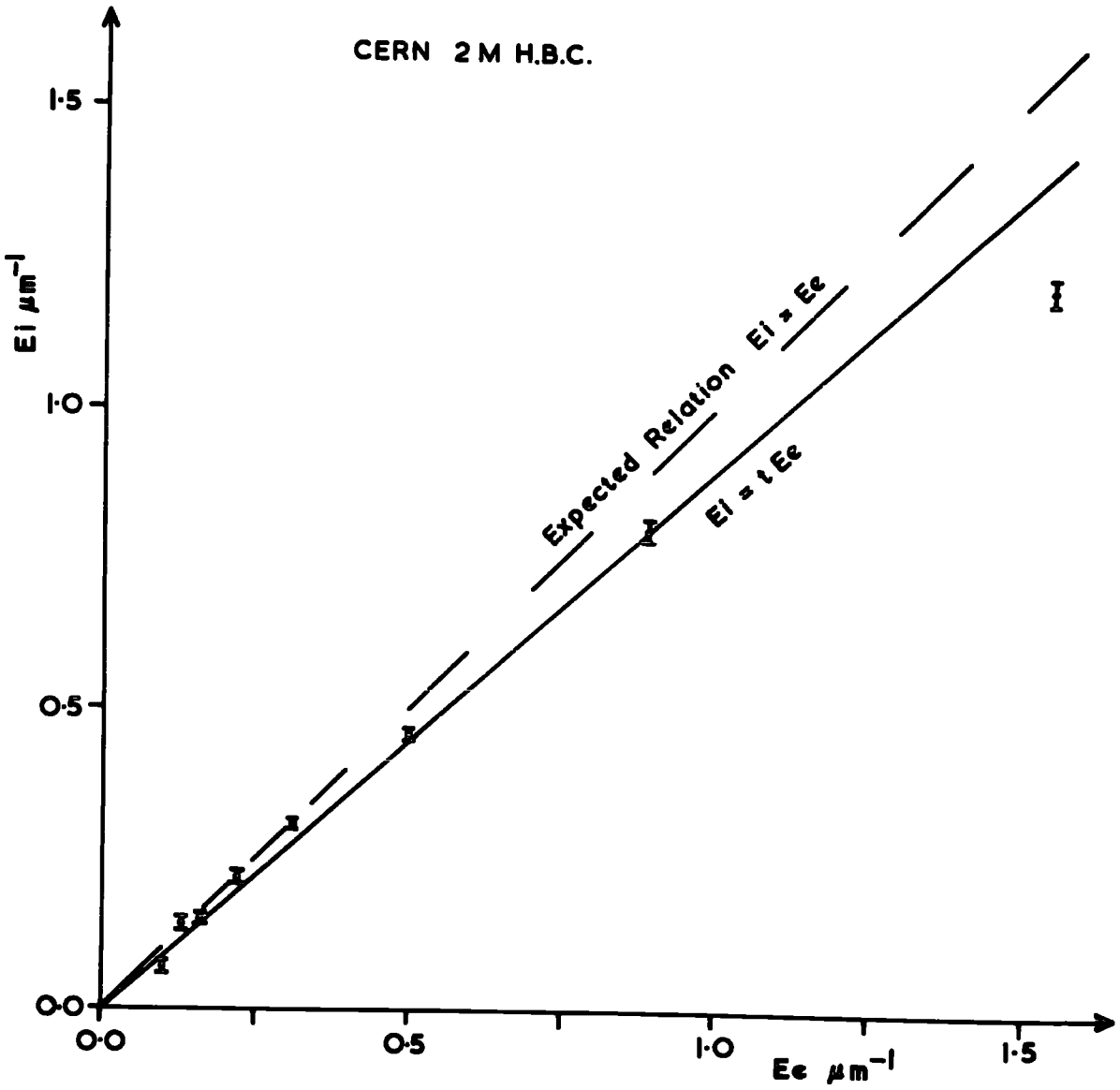

FIG.(3-3) THE INTERNAL ERROR (Ei) AS A FUNCTION OF THE EXTERNAL ERROR (Ee)

where t is the slope (equal to about E_{oi}/E_{oe}). A summary of the results for the three exposures is given in table (3-3) where the value of t (the fitted slope by least squares fitting) of equation 3.1 and the ratio between the errors calculated in THRESH and GRIND are shown.

TABLE (3-3)

CHAMBER	B.N.H.B.C.	CERN 2M H.B.C.	CERN 2M D.B.C.
t	0.92 ± 0.03	0.83 ± 0.02	0.83 ± 0.03
E_{oi}/E_{oe}	0.98 ± 0.04	0.89 ± 0.02	0.93 ± 0.03
The Expected value is $t = E_{oi}/E_{oe} = 1$			

As indicated in section 3. 1 Coulomb scattering is not expected to contribute to the overall accuracy. This can be seen also in figure (3-2) where the dashed lines corresponding to the expected multiple scattering contribution are shown.

3. 3 Demonstration of Multiple Scattering Limitation

In figure (3-4) the expected multiple scattering (dashed line), measuring error (solid line) and the total error (solid curve) are shown for tracks with momentum of 2.0 Gev/c (in the CERN 2M HBC). From equation 2.20 and figure (3-4) it can be seen that for lengths in excess of about 50 cm the accuracy should be limited by Coulomb scattering. On the other hand, below this length the accuracy should be limited by measuring error.

About 370 secondary tracks with a variety of lengths whose measured values of momentum were in the range (1.6 - 2.4) Gev/c

were selected from interactions in the CERN 2M HBC at an incident momentum of 11.7 Gev/c. It is assumed that these measured values correspond to an average true momentum of 2 Gev/c. For various intervals of track lengths the average internal errors were determined. The relative errors on the curvature are displayed in figure (3-4).

The transition from limitation by measuring errors to limitation by Coulomb errors can be clearly seen. There may be a discrepancy in the apparent size of the multiple scattering as displayed by the internal error. This could arise from the fitting procedure in THRESH which adjusts the curvature of the fitted circle to a track, until the r.m.s. deviations are a minimum. This process will tend to reduce the effect of multiple scattering.

3.4 An Experimental Check on the Measuring Errors

The results in figures (3-2), (3-3) and (3-4) seem to show that errors calculated in THRESH and GRIND are consistent with one another. This may not be so surprising since the expression in GRIND which is used to determine the external error contains a parameter f_1 (see equation 2.17) which can be adjusted to give consistency. A much better check on accuracy would be afforded by a direct comparison of the error calculated in THRESH with the experimental error determined by some experimental means. Working with primaries provides this possibility since they form a monoenergetic sample of known momentum. Measured momenta or curvatures can be compared directly with the known values. From their r.m.s. deviations an error can be determined experimentally and compared with that estimated error

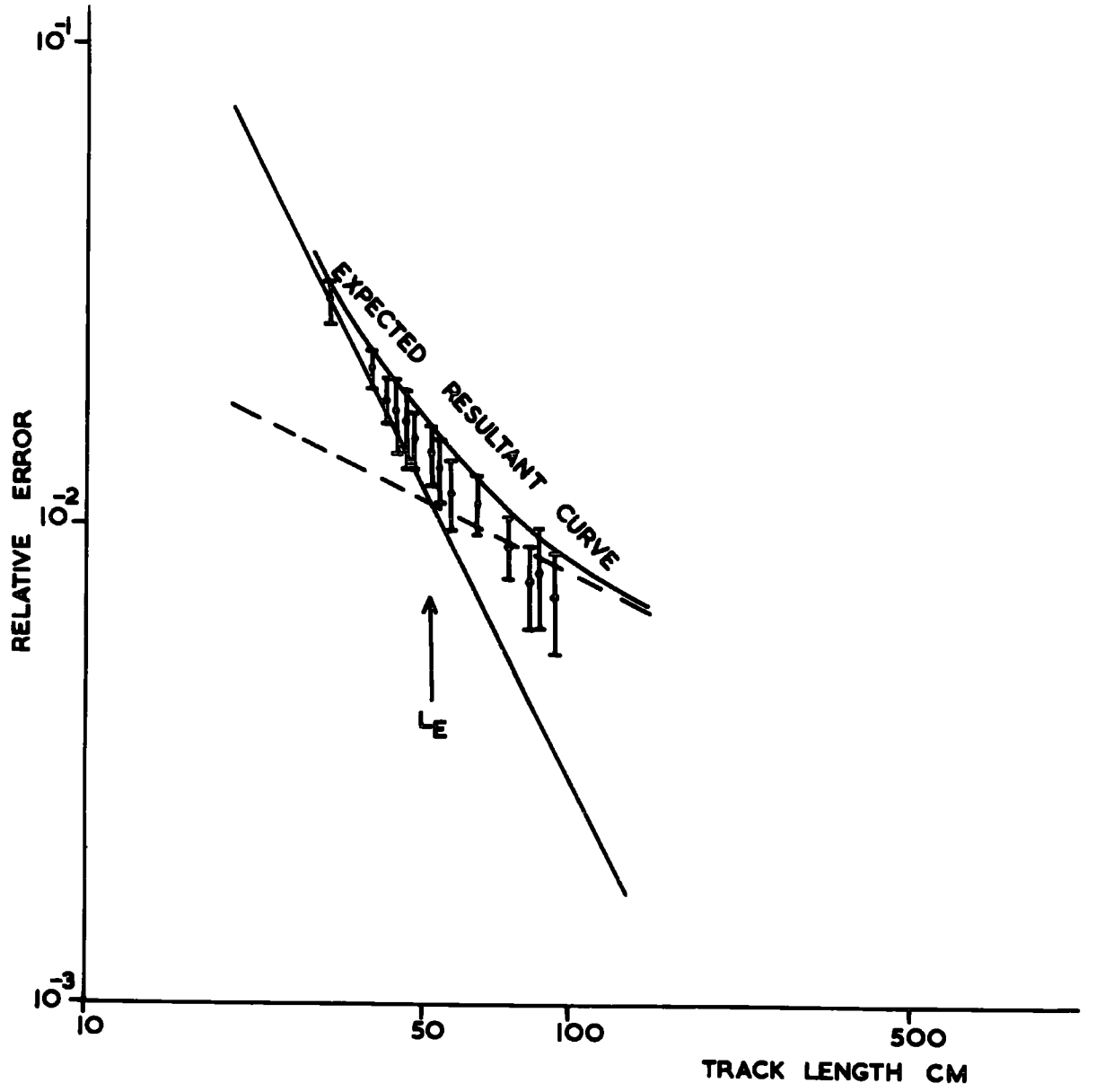

FIG. (3–4) EXPECTED AND OBSERVED RELATIVE ERRORS AS A FUNCTION OF THE SECONDARY TRACK LENGTH IN THE CERN 2M H.B.C.

by THRESH or that calculated error by GRIND.

The data in table (3-1) was used for this purpose. The primaries, as before, were divided into groups according to length. For each group the average internal error was determined from THRESH. Also for each group the deviations of the measured curvatures from the average primary curvature were determined and from these the r.m.s. deviations were found. A comparison of both estimates of error is shown in figure (3-5) for the data from 11.7 Gev/c $\pi^+ H_2$. It can be seen that zero internal error does not correspond to a zero of the experimentally determined error. The relation between the errors can be seen when their squares are plotted. It is found that the experimentally determined error D_c is related to the internal error E_i as follows:-

$$D_c^2 = A^2 + S^2 E_i^2 \quad \mu m^{-2} \qquad 3.2$$

where $A = 0.149 \pm 0.003 \ \mu m^{-1}$ and $S = 1.195 \pm 0.022$. This is shown also on figure (3-5) as the solid curve. On the whole the measured errors are about 28% larger than the expected errors from the programmes THRESH or GRIND. An adjustment to the programmes would correct this. However, from the expression 3.2 the minimum value of D_c is $A(= 0.149 \pm 0.003) \ \mu m^{-1}$. Now this minimum is reached with extremely long tracks only and this result means that the benefit of measuring long tracks is not being fully realised. For example, for tracks of 90 cm length the standard deviation determined above would be, from figure (3-5), equal to $(0.12 \pm 0.01) \ \mu m^{-1}$ which is twice as large as the value expected from THRESH or GRIND, for this length, which is about $(0.07 \pm 0.01) \ \mu m^{-1}$.

The corresponding results for the other two exposures of

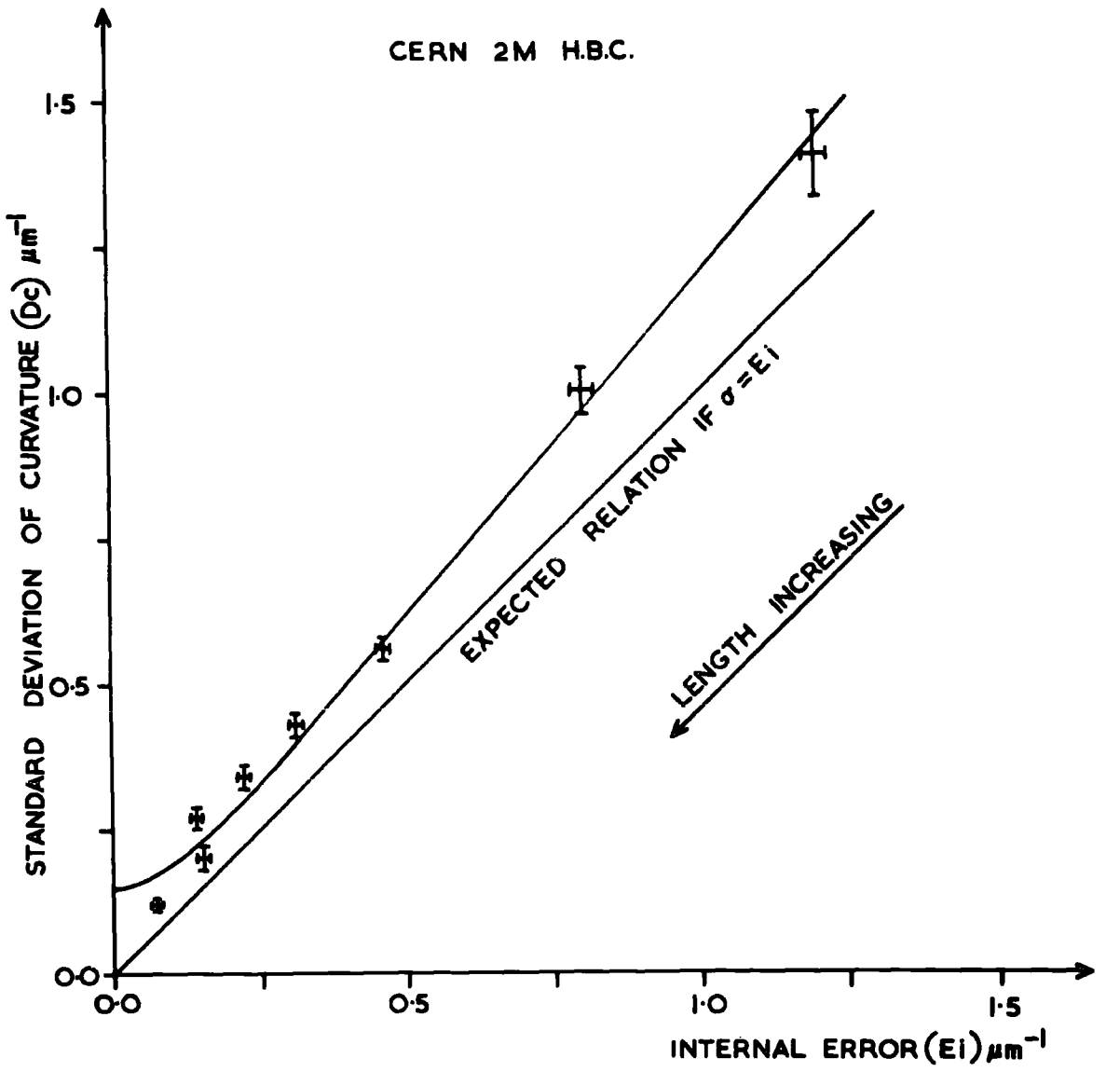

FIG. (3–5) THE STANDARD DEVIATION OF THE CURVATURE AS A FUNCTION OF THE INTERNAL ERROR.

the fitted values of A and S of equation 3.2 are contained in table (3-4). The standard deviation for the three experiments is about 20% to 50% larger than the expected value.

TABLE (3-4)

CHAMBER	THE VALUES OF A AND S BY LEAST SQUARES FITTING			
	D_c v E_i		D_c v E_e	
	A (μm^{-1})	S	A (μm^{-1})	S
B.N.H.B.C	0.377 ± 0.010	1.360 ± 0.033	0.470 ± 0.012	1.220 ± 0.030
CERN 2M H.B.C.	0.149 ± 0.003	1.195 ± 0.021	0.206 ± 0.004	0.957 ± 0.017
CERN 2M D.B.C.	0.358 ± 0.010	1.232 ± 0.030	0.428 ± 0.011	0.917 ± 0.024
The Expected values are A = 0.0 and S = 1.0				

3.4.1 The Origin of A

The intercept A indicates a source of error other than that appearing in the internal error. It is not due to any randomness in the position of bubbles in the track which would arise from the measuring error, the Coulomb scattering, turbulence or field variations since these would appear also in the internal error.

One possibility is that A arises from the basic property of THRESH. This programme reconstructs tracks in three dimensional chamber space. To do this it is forced to take the demagnified image on film, estimate the magnification from the measurements there and reconstruct in chamber space. For this the measurer measures four-fiducial crosses on each of the three-views and THRESH matches these with their known position on the

window. Suppose the fiducials are measured somewhat roughly, so that in the matching of the crosses the track is, for example, straightened. In this way no further randomness will be introduced to the measured points but the curvature will be smaller (in this case) than its expected value.

Hence, the internal error will be unchanged but the standard deviation of curvatures will be increased. To test this, an event with a well measured long primary track was selected from the records and the measurements of its fiducial marks were replaced in turn by those of the next 100 measured events. For these 100 artificial events the curvature of the same primary was determined using the original fiducial marks and then using the replacement fiducial crosses. The standard deviation of the variation between the two determinations was found. It accounts for about one half of the value of A. No source has been found for the remainder of the error.

3. 5 A Detailed Consideration of the Distribution of the Measured Error

So far we have examined average errors on a variety of track lengths and find that in general the external error as calculated in GRIND and the internal error as estimated in THRESH are in reasonable agreement. When these are compared with errors calculated from r.m.s. deviations of the curvature of primaries, discrepancies were observed in that GRIND and THRESH errors underestimate the real errors by about 28%. In this section the distribution of the error on individual tracks rather than averages is considered.

The measurements on individual primary tracks have lead to

the measured estimates of their curvature c_j and their internal error E_{ij}. In figure (3-6), for example, the distribution is shown of the curvature measurements in the 11.7 Gev/c $\pi^+ P$ exposure in the CERN 2M HBC. Since the tracks are of different lengths the values of E_i will vary. To obtain one common distribution the normalised quantities

$$(C_j - C_{oi}) \; / \; E_{ij}$$

are plotted where C_{oi} is the weighted average curvature

$$C_{oi} = \sum_{j=1}^{N_o} (C_j/E_{ij}) \Big/ \sum_{j=1}^{N_o} (1/E_{ij}) \qquad 3.3$$

where N_o is the number of primaries. This distribution should be Gaussian with a standard deviation of unity provided that the internal error is a good estimate of precision. If internal error really underestimates the true value of error, for example in the 11.7 Gev/c $\pi^+ P$ exposure by about 28%, then the standard deviation of the experimental distribution should be larger than unity by this amount.

This Gaussian (with standard deviation equal to 1) is drawn on figure (3-6) as the full line on the histogram. By inspection it can be seen that there are discrepancies between the observed and the normal distributions. There is an excess of large deviations from the mean value at the expense of small deviation. This can be summarised in the standard deviation of the experimental distribution. This is found to be 1.26 ± 0.02 which is significantly different from the expected value of unity. This and the corresponding results for the other two exposures (and for normalising against the external error) are contained in table (3-5).

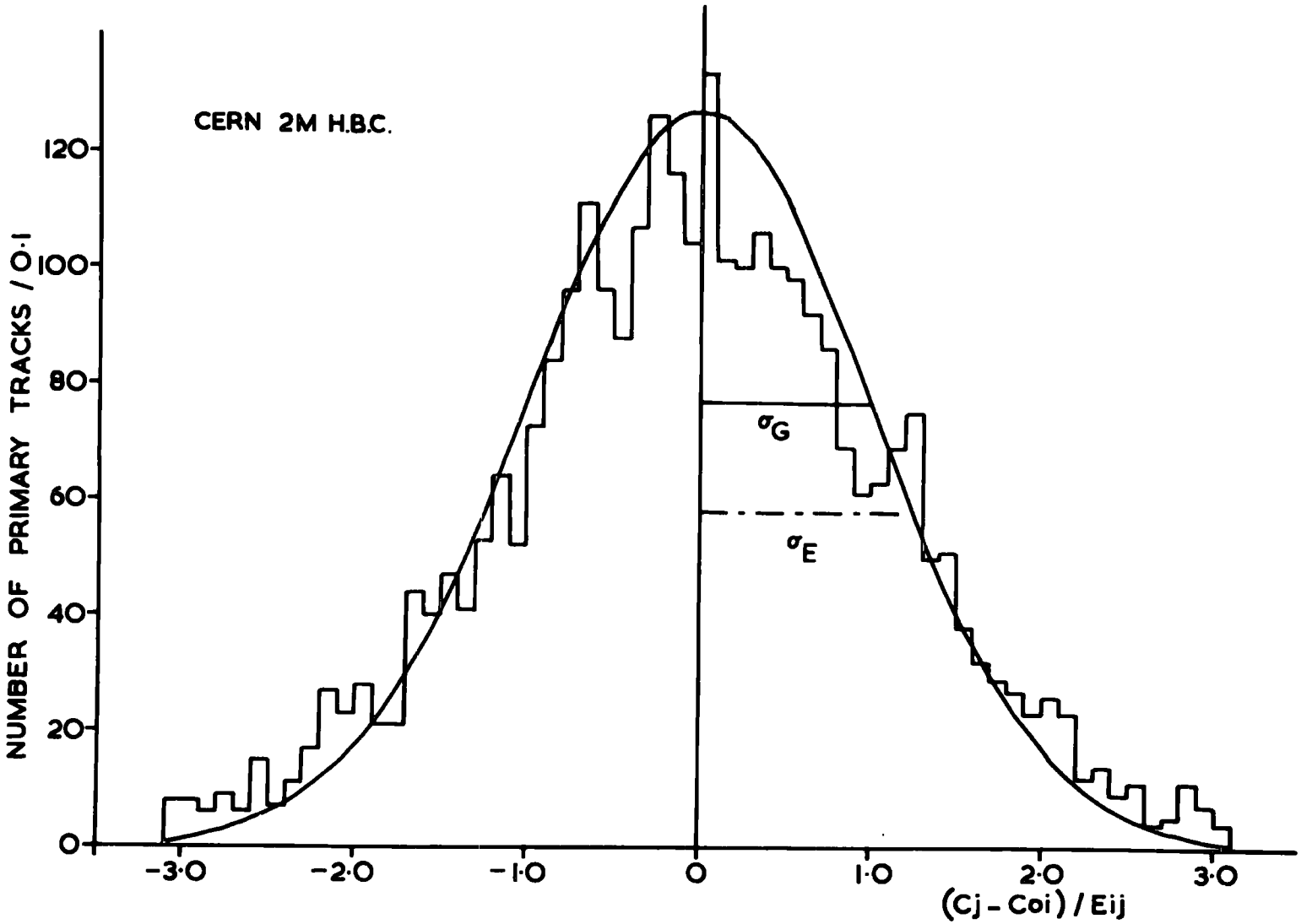

FIG. (3-6) THE DISTRIBUTION OF THE CURVATURE. THE SOLID CURVE SHOWS THE GAUSSIAN DISTRIBUTION WITH $\sigma_G = 1$.

TABLE (3-5)

EXPOSURE	Standard Deviation using Internal Error	Standard Deviation using External Error
5.0 Gev/c π^+P	1.27 ± 0.02	1.27 ± 0.02
11.7 Gev/c π^+P	1.26 ± 0.02	1.13 ± 0.02
11.7 Gev/c π^+d	1.43 ± 0.04	1.28 ± 0.02

These values of standard deviation confirm the result found earlier that the internal error and the external do underestimate the true error by about 20% to 50%.

It is convenient to display the data in an alternative way. If the distribution of the data is Gaussian, i.e. $N = K \text{ Exp } \left(-(C_j - C_{oi})^2 / 2 E_{ij}^2\right)$, then a plot of $\text{Log}_e N$ against $(C_j - C_{oi})^2/E_{ij}^2$ should give a straight line graph of slope equal to - 0.5. In figure (3-7) data is plotted in this way from the 11.7 Gev/c π^+P exposure. The slopes instead of being equal to-0.5 are typically about -0.3. The results are summarised in table (3-6) for the three experiments.

The values of these slopes can be accounted for if the errors involved in the experiment are given by equation 3.2, that is by $D_c^2 = A^2 + S^2 E^2$. A detailed calculation of the shape of the expected distribution of $(C - C_o)/E$, if the true errors are as given above, is presented in the appendix (I). In summary, after suitable approximation, the slope t in figure (3-7) should be given by:-

$$t = - E^2 / 2(A^2 + S^2 E^2) \qquad 3.4$$

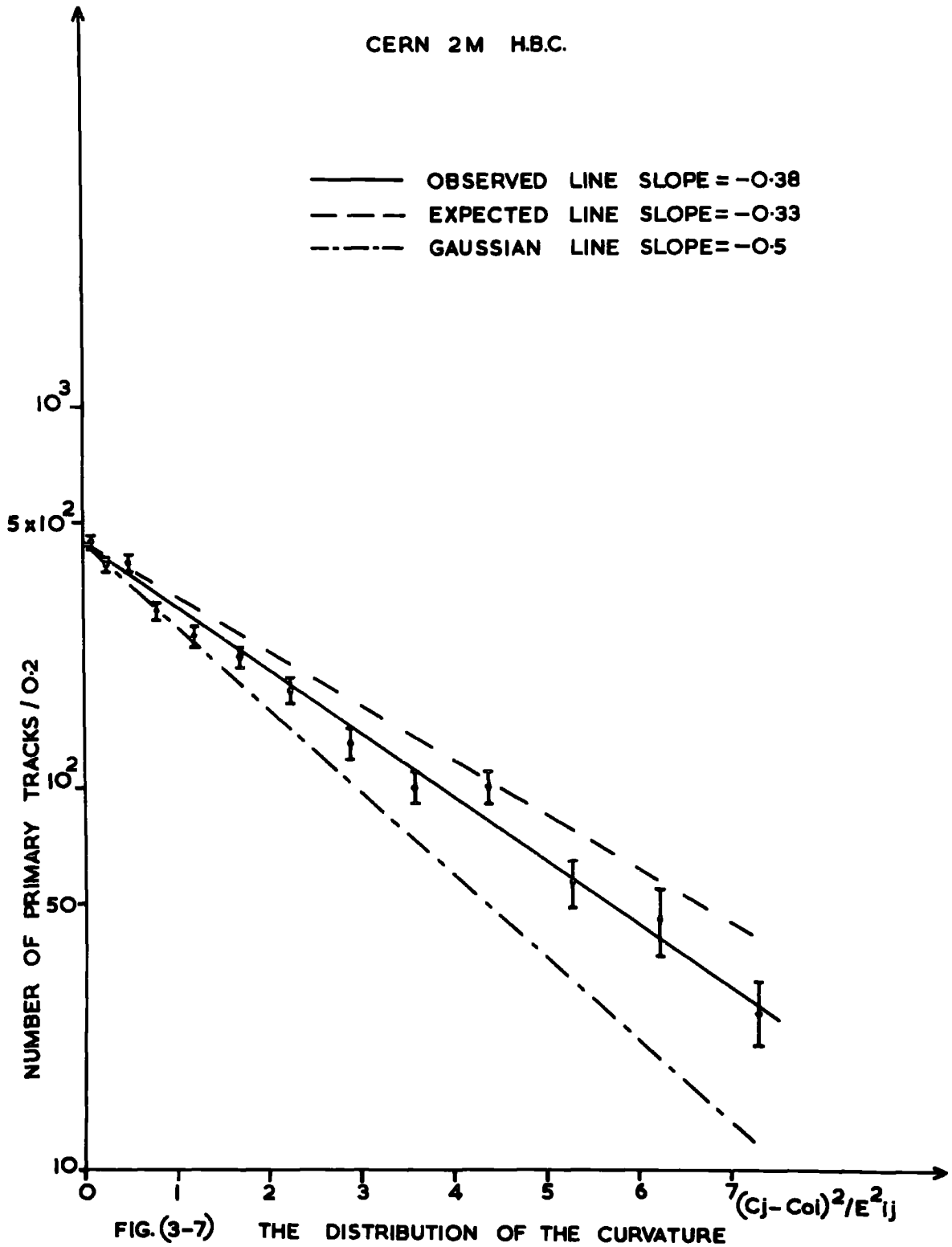

FIG. (3-7) THE DISTRIBUTION OF THE CURVATURE

where E is the average internal or external errors over all data. Using the value of E in table (3-1), columns 9 and 10, and the values of A and S in table (3-4); the expected slopes (using equation 3.4) and the observed slopes (by least squares fitting) are shown in table (3-6) for the three exposures. The expected slope of the 11.7 Gev/c π^+P experiment is drawn on figure (3-7), solid line, and also compared with the experimental one by least squares fitting, dashed line, on the graph.

TABLE (3-6)

Exposure	The Expected and Observed Slopes			
	Using the Internal Error		Using the External Error	
	Expected	Observed	Expected	Observed
5.0 Gev/c π^+P	-0.24	-0.31 ± 0.01	-0.27	-0.28 ± 0.01
11.7 Gev/c π^+P	-0.33	-0.38 ± 0.01	-0.46	-0.48 ± 0.01
11.7 Gev/c π^+d	-0.22	-0.24 ± 0.01	-0.27	-0.30 ± 0.01

These results further confirm the validity of the error expression given above(by equation 3.2), that is, internal and external errors of THRESH and GRIND are underestimates of the true error.

3. 6 Conclusions

In the three exposures the maximum length of available primary tracks is about 100 cm. The measurements on these primaries are not limited by Coulomb scattering since this should only appear in excess of about 100 cm. The transition from limitation by measuring error to limitation by Coulomb scattering has been clearly seen by selecting secondary tracks whose measured momenta are relatively small.

I - Internal, External and Experimental Errors

It was found that, there was good agreement between the estimated error in THRESH and the calculated error in GRIND that is the internal error E_i is related to the external error E_e as follows:-

$$E_i = t\ E_e$$

where t which should be unity is found experimentally to be about 0.95. On the other hand, it was found that the error experimentally determined from the distribution of measured curvatures of primaries D_c is related to the error returned by THRESH or GRIND by:-

$$D_c^2 = A^2 + S^2\ E^2$$

where E is the internal or the external error, A and S are constants. This means that both internal and external error underestimate the experimental error.

II - Use of Errors

a - As Rejection Criteria

In THRESH the internal error E_i is just used as a guide to the quality of measurement; in GRIND the external error E_e is calculated and if this is such that E_i is greater than three times E_e the track is flagged as badly measured. This current flagging of E_i greater than 3 E_e is of course not effected by the underestimation of internal and external errors since both are underestimated in the same way.

b. In the Fitting of Data to Kinematic Hypotheses

External errors are used in GRIND in fitting hypotheses.

For particularly long tracks the error used is badly underestimated (since we should use $D^2_c = A^2 + S^2 E^2$) and this will lead to an overestimation of the chi-squared of the fit and hence to a lower probability of the fit. Usually there is a lower probability limit to the acceptance of a fit and hence it is possible that some fits will wrongly be rejected.

CHAPTER 4

RESOLUTION AND PRECISION IN THE TWO-PRONG NOFIT CHANNELS

In chapter 1 it was pointed out that NOFIT interactions represent a considerable proportion of the events (and hence of the information) in an experiment. At 5 Gev/c it was seen that in the case of two pronged reactions about 42% of the events, because they are NOFIT, are normally not available for standard analysis. In this and the subsequent chapters this problem is reconsidered and an attempt is made to extract the physics underlying the NOFIT interactions. It begins with an account of resolving the events into the two NOFIT channels and then a consideration of the precision of measurements in these channels. In chapter 6 and 7 resonance production in these channels is examined.

Two pronged events were produced in the exposure of 185K pictures to 5 Gev/c, positive pions in the B.N.H.B.C., according to the following main elastic and inelastic reactions:-

π^+P	$\rightarrow$	P	π^+	; 4-C FIT	(A)
π^+P	$\rightarrow$	P	π^+ π^0	; 1-C(π^0)FIT	(B)
π^+P	$\rightarrow$	n	π^+ π^+	; 1-C(n)FIT	(C)
π^+P	$\rightarrow$	P	π^+ (m_2 π^0)	; NOFIT	(D)
π^+P	$\rightarrow$	n	π^+ π^+(m_1 π^0)	; NOFIT	(E)

with m_1 greater than zero and m_2 greater than 1. Strange particles are produced in only about 2% of the interactions and these are ignored in the following sections.

Experimentally, measured events do not fall unambiguously into these five categories (A,...,E). What is observed in

the chamber is a primary pion approaching the interaction point and secondary charged tracks leaving it. For example, in the case of reactions (A), (B) and (D) it is observed that a secondary pion and proton leave the interaction, but for interactions (C) and (E) two secondary pions leave. By accurate measurement of the momenta of the particles (beam and secondaries) from their tracks in the chamber it is possible to determine into which of the categories above an event should be classified. For example, if the event is described by reaction (A) then the following sums over the secondary particles should be satisfied

$$P_o(x) = \sum_{i=1}^{2} P_i(x) = \sum_{i=1}^{2} P_i * \cos\lambda_i * \cos\theta_i \qquad 4.1$$

$$P_o(y) = \sum_{i=1}^{2} P_i(y) = \sum_{i=1}^{2} P_i * \cos\lambda_i * \sin\theta_i \qquad 4.2$$

$$P_o(z) = \sum_{i=1}^{2} P_i(z) = \sum_{i=1}^{2} P_i * \sin\lambda_i \qquad 4.3$$

$$(P_o^2 + m_o^2)^{1/2} = \sum_{i=1}^{2} (P_i^2 + m_i^2)^{1/2} - M_p \qquad 4.4$$

where P_o and P_i refer to the primary and secondary momenta in the laboratory system, m_o is the mass of beam and m_i refers to the mass of secondary particles, λ_i and θ_i are the dip and azimuthal angle of the secondary tracks. If the secondary particles are all charged and provided the event is well measured then p_i, λ_i and θ_i are known for every particle involved. Then there are four simultaneous equations and no unknowns. This is known as a 4-C FIT, as in reaction (A). If there is one neutral secondary (unobserved) as in reactions (B) and (C) then the three values p, λ and θ are unknown for the neutral particle. Then there are 4 simultaneous equations with three unknowns. The equations can be reduced to one equation with

no unknowns. This is a 1-C FIT. For reactions such as (D) and (E) with at least two unseen neutrals then there are four equations and six unknowns. Hence the equations can not be solved and the event is classified as a NOFIT interaction .

Fitting techniques combined with ionisation estimates are used conventionally to resolve reactions (A), (B) and (C). In the case of the NOFIT channels, such as reaction (D) or (E), the fitting techniques have obviously not been successful. Reaction (D) can only be distinguished from reaction (E) if the proton can be recognized by ionisation. The quality of the chamber and the film is such, in this experiment, that pion and proton can be distinguished by eye from each other up to a momentum of 1.5 Gev/c in the laboratory system (see sub-section 2.3.2 in chapter 2). On the other hand, no track which has a momentum in excess of 1.5 Gev/c can be identified unambiguously as a pion or a proton.

By making use of the ionisation estimate events can be classified as follows:-

I - Unambiguous Events

a - If both secondary tracks have momenta below 1.5 Gev/c they can both be identified and then the event is completely unambiguous and it can be classified into either reaction (D) or reaction (E).

b - If a track with a momentum less than 1.5 Gev/c is identified as a proton then, even if the other track is unident-

ifiable by ionisation, baryon conservation demands that it is due to a pion and the event is classified into reaction (D).

II - Ambiguous Events

a - In the case of a track with a momentum less than 1.5 Gev/c which is identified as a pion, when the other track is due to a particle with a momentum greater than 1.5 Gev/c, there is no corresponding conservation law which will help to distinguish between pion and proton ambiguities. The event must remain ambiguous between reaction (D) and reaction (E).

b - If both secondary tracks have momenta above 1.5 Gev/c, a pion and a proton ambiguity always results and again the event is ambiguous between both reactions (D) and (E).

A similar discussion could be given for the reaction (B) and (C) in the 1-C FIT channels. The relevant numbers of the 1-C FIT and the NOFIT channels are given in table (4-1) with the percentage of the ambiguous events in the total number. In this table only the 1-C (π^0) FIT and the 1-C (n) FIT are included. The rather rare use of the 1-C (η^0) FIT, where η^0 decays entirely into neutral secondary particles, is ignored at this stage.

TABLE (4-1)

1	2	3	4	5	6
CHANNEL	TOTAL NO. OF EVENTS	No. of Unambiguous Events		No. of Ambiguous Events	
		P π^+	π^+ π^+	P $\pi^+/\pi^+\pi^+$	Fraction %
1-C FIT & NOFIT	19660	9491	2136	8033	40.8
1-C FIT: (B)+(C)	6365	3188	85	3092	48.6
NOFIT: (D)+(E)	13295	6303	2051	4941	37.2

4. 1 Resolution of the Ambiguous Events

In table (4-1) it can be seen that about 41% of the total number of events are ambiguous. The experimental problem is to resolve the ambiguities between the inelastic reactions, for example, the ambiguous events between reactions (B) and (C), 1-C FIT channel, or (D) and (E), NOFIT channel, arising from the inability to identify tracks with high momentum. For this purpose several attempts have been made to find a characteristic of unambiguous events and to use this as a criterion to resolve the ambiguous ones. The only method that has been found to be successful with these data is to predict from the distribution of measured momenta of identified protons (that is momentum less than 1.5 Gev/c in the laboratory system) how many protons would have momenta in excess of 1.5 Gev/c. These protons would be unidentifiable and the events in which they are produced would be ambiguous, but they should be properly classified as reactions (B) or (D).

4.1.1 Momentum Distribution of the Identified Protons in Channel (D)

The experimental distribution of the momenta of identified protons is shown in figure (4-1) for reaction (D), NOFIT channel. The maximum momentum shown is 1.5 Gev/c which is seen to correspond to the momentum below which pions and protons can be resolved by ionisation. The data are presented again in figure (4-2) in a logarithmic plot. The data have further been subdivided into events which probably include a Δ^{++} formed between proton and pion and those which do not (i.e. where the mass of the Δ^{++} is in the region 1.12 - 1.35 Gev). The spectra of the

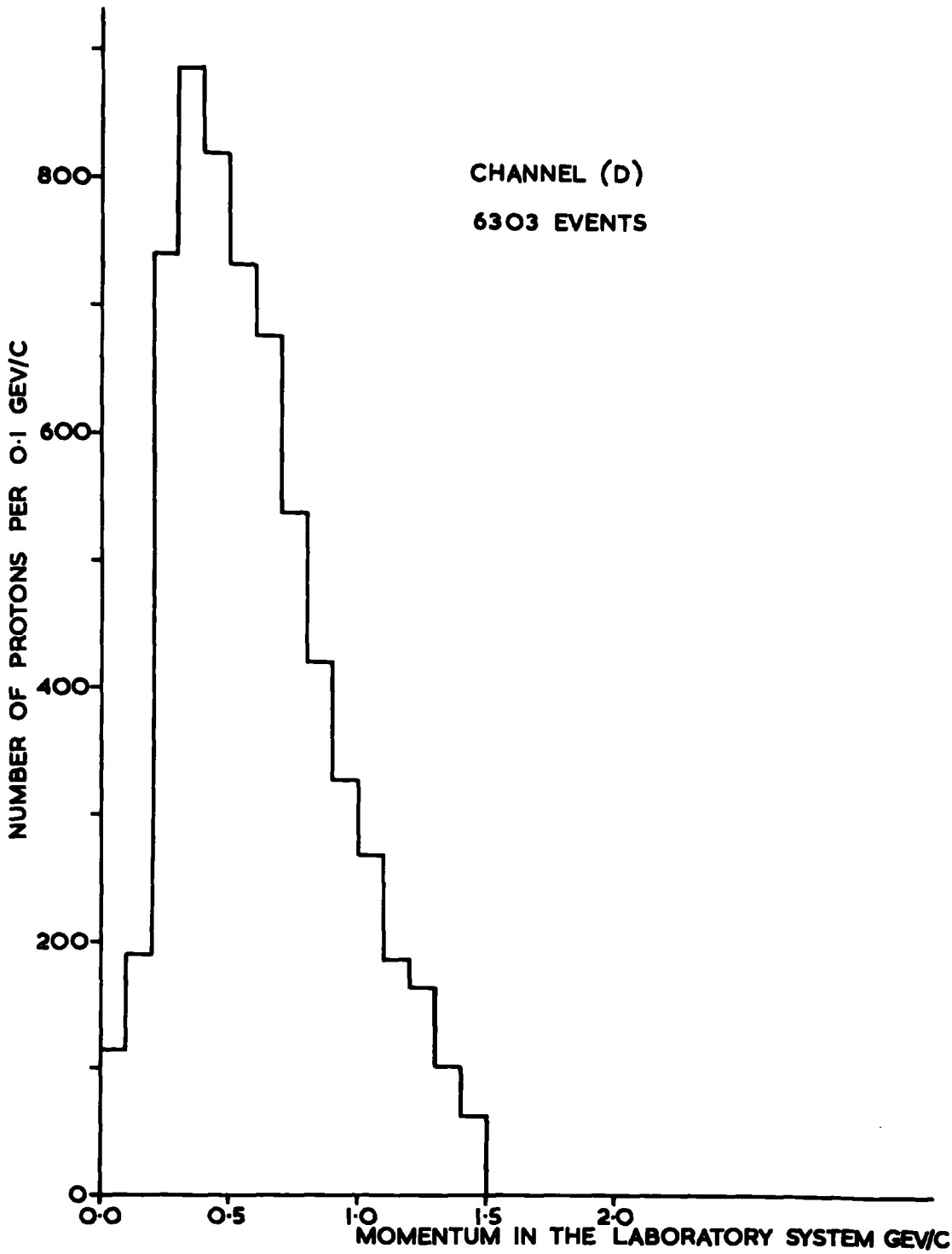

FIG. (4–1) THE EXPERIMENTAL DISTRIBUTION OF IDENTIFIED PROTON MOMENTA

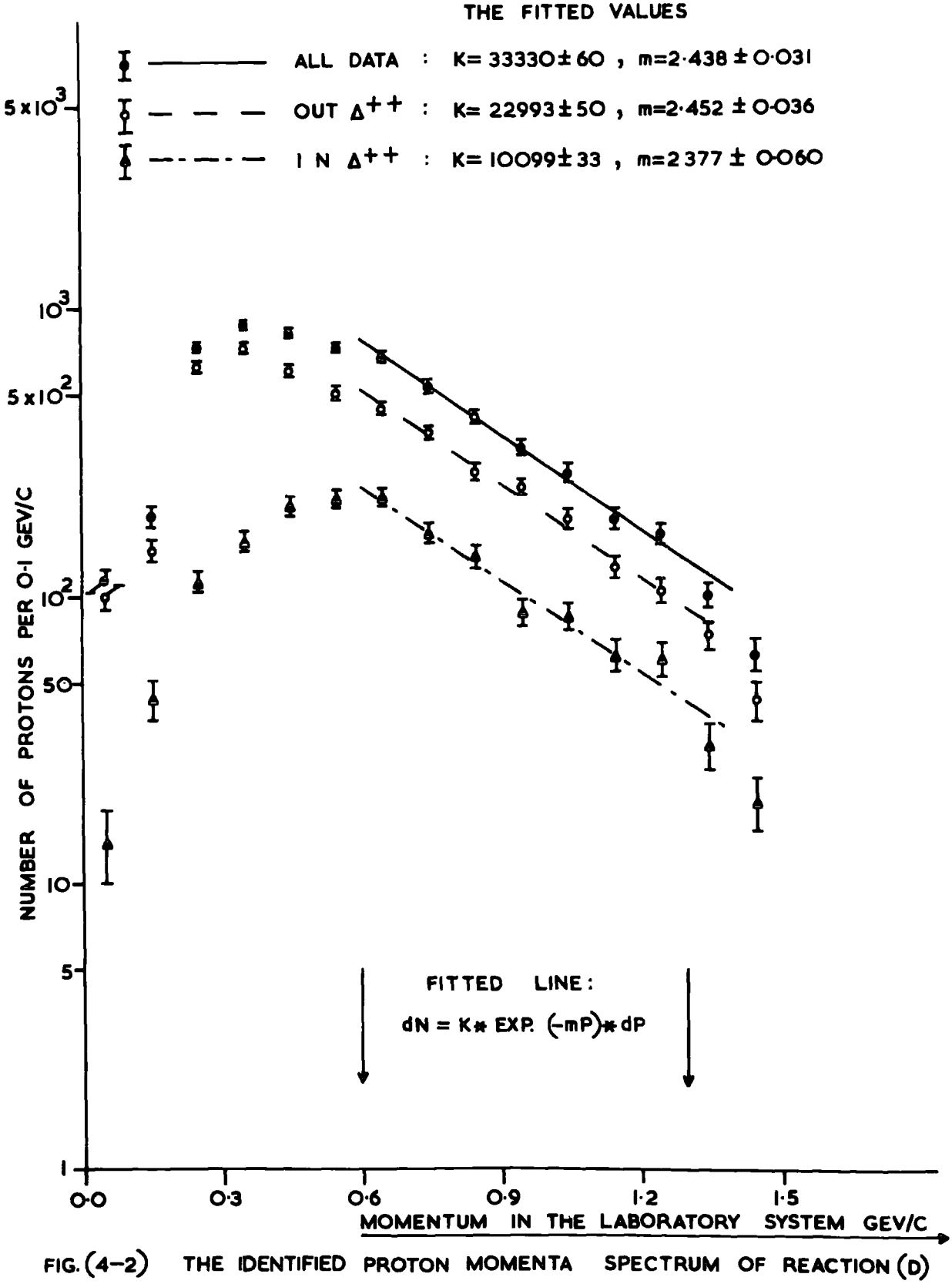

FIG. (4–2) THE IDENTIFIED PROTON MOMENTA SPECTRUM OF REACTION (D)

momenta of identified protons are not very different if they do or do not arise from Δ^{++} production, see figure (4-2). Above a momentum of about 0.4 Gev/c it can be seen that the distributions fall off approximately as an exponential. In the region 0.6 - 1.3 Gev/c the data have been fitted with a distribution of the form

$$dN = K \, Exp(- mP) \, dP \qquad 4.5$$

where K and m are constants and P is the momentum of identified protonsin the laboratory system. The fitted value of m is about 2.44 ± 0.03. If the tail is truly exponential then some fall off in the efficiency of identification of protons appears to set in at about 1.3 Gev/c. However, if the fall off of the tail represents the true spectrum then the projection from the assumed exponential (equation 4.5) behaviour will lead to an overestimate of protons with momenta above 1.5 Gev/c.

The discussion above has concerned the NOFIT reaction (D) and a similar discussion could be given for the FIT reaction (B). Moreover, the NOFIT and FIT channels can be considered jointly before fitting. In this case the combined data form the UNFIT reaction

$$\pi^+ P \rightarrow P \quad \pi^+ \; (m_1 \; \pi^o); \text{UNFIT} \qquad (F)$$

with m_1 greater than zero. The fitted value of m of equation 4.5 and the percentage of protons with momenta in excess of 1.5 Gev/c are given in table (4-2) where all events have been used in which a proton has been identified for the UNFIT channel firstly and then for its sub-channels the 1-C (π^o) FIT and the NOFIT, reaction (D), channels.

TABLE (4-2) The Percentage of Protons with Momenta above 1.5 Gev/c.

1	2	3	4	5	6
CHANNEL	SLOPE (m)	NUMBER OF EVENTS			RATIO
		N	N_1	$N_2=N+N_1$	N_1/N %
I-UNFIT:					
ALL EVENTS	2.29 ± 0.02	9491	576	10067	5.7
OUT Δ^{++}REGION	2.18 ± 0.03	7383	478	7861	6.1
IN Δ^{++}REGION	2.54 ± 0.06	2108	116	2224	5.2
II-1-C(π^o)FIT:					
ALL EVENTS	1.92 ± 0.03	3188	248	3436	7.2
OUT Δ^{++}REGION	1.68 ± 0.03	2728	290	3018	9.6
IN Δ^{++} REGION	3.85 ± 0.18	460	4	464	0.9
III-NOFIT(D):					
ALL EVENTS	2.44 ± 0.03	6303	353	6656	5.3
OUT Δ^{++}REGION	2.45 ± 0.04	4655	237	4892	4.8
IN Δ^{++}REGION	2.38 ± 0.06	1648	120	1768	6.8

In table (4-2) column 3 gives the number of identified protons, column 4 gives the number of protons in excess of 1.5 Gev/c (estimated from equation 4.5) , column 5 gives the total number of protons and in column 6 the percentage of unidentified protons belonging to these channels is given. These are the events in the ambiguous category which really belong to channels (B) or (D).

From table (4-2), column 2, it can be seen that:-

I - the fitted values of the slope in the 1-C(π^o) FIT

channel are different from that in the NOFIT channel (D) for the following reasons.

1 - The number of secondary particles (seen and unseen tracks) in the final states is not constant (e.g. three particles in the 1-C(π^0) FIT and four, or more, particles in the NOFIT channel (D). Because of this difference the momentum distribution to the protons will necessarily be different.

2 - The energy of Δ^{++} in the c.m.s. in the 1-C(π^0) FIT is higher than the energy when Δ^{++} is produced in the NOFIT channel (D). Therefore, the momentum in the laboratory system of a proton associated with Δ^{++} is lower in the 1-C(π^0) FIT channel than the momentum in the NOFIT channel (D) and this would lead to a smaller value of slope in the NOFIT (Δ^{++}) channel (D).

II - for the 1-C(π^0) FIT channel, again, the fitted values of the slope are not identical although the number of the outgoing particles in the final state is constant. The Δ^{++}, in general, is produced in the backward direction in the c.m.s. so that maximum proton momentum in the laboratory system will occur for the proton emitted backwards from the Δ^{++} relative to its c.m.s. direction. The higher the c.m.s. momentum of Δ^{++}, the lower is the proton laboratory momentum. In the FIT reaction a Δ^{++} has energy of 1.84 Gev in the c.m.s. for 5 Gev/c π^+P collisions. This means that the maximum momentum in the laboratory system of the forward proton associated with Δ^{++} is 1.32 Gev/c.

III - in the case of the NOFIT channel (D), it can be seen that the fitted values of the slope are identical.

In columns 4 and 6 of table (4-2) for the all events of the NOFIT channel (D) it can be seen that there are less than 353 events (i.e. about 5.3%) of type (D) which are contained in the ambiguous group of reactions (D)/(E). Consequently, all but approximately 353 events of the ambiguous group must belong to reaction (E) and so without much loss of accuracy all ambiguous events can be grouped as channel (E). Then the situation is that identified events in reaction (D) comprise 94.7% of this reaction. Events taken as reaction (E) will comprise all such unambiguous and ambiguous events and will contain no more than a small admixture (about 4.8%) of channel (D). Despite the ambiguities it would appear that quite pure samples of reactions (D) and (E) can be obtained.

Accepting this method of separation then the numbers in table (4-1), NOFIT channel only, (columns 3, 4 and 5) have been revised and are shown in table (4-3) together with the cross-section for the processes. It should be noted that these cross-sections are somewhat different from those published previously by the collaboration (see ref.1).

TABLE (4-3) The Revised Numbers and the Cross-Section of the Two Pronged NOFIT channels.

1	2	3	4	5	6
CHANNEL	Total No. of Events	No. of Events and the Cross-Sections			
		"p π^+"		" π^+ π^+"	
		N	σ (mb)	N	σ (mb)
NOFIT: (D)	6303	6303	2.63 ±0.03	-	-
NOFIT: (E)	6992	353	0.15 ±0.01	6619	2.77 ± 0.03
NOFIT: TOTAL	13295	6656	2.78 ±0.03	6619	2.77 ± 0.03

In table (4-3) columns 3 and 5 give the numbers of each type " P π^+ " and " π^+ π^+ " and columns 4 and 6 show the cross-sections. These correspond to a microbarn equivalent of 0.418 ± 0.003 μb/event.

In figure (4-2) it was seen that the spectra of identified proton momenta in the NOFIT reaction (D) are identical whether or not a Δ^{++} is produced. This means that events containing Δ^{++} production are subject to the same problem of proton ambiguity. Hence, if all ambiguous events are classified as reaction (E) then a calculable number of these have resulted from Δ^{++} events in reaction (D). Anticipating results presented later Δ^{++} is produced in about 26% of the NOFIT channel (D) events. Hence, the number of Δ^{++} events from reaction (D) which have been wrongly classified in reaction (E) is expected to be 26% of the misclassified events with proton momenta in excess of 1.5 Gev. For the 353 events discussed above then about 92 Δ^{++} events are expected to be wrongly classified in the ambiguous group. This can be used as a check on the misclassification. For this purpose, all events ambiguous between reactions (D) and (E) have been reinterpreted in figure (4-3) as reaction (D). There the invariant " P π^+ " mass is plotted. The number of events above the hand-drawn background in the region of Δ^{++} (1.12 - 1.35) Gev is about 100 ± 12 events. This number of Δ^{++} events is consistant with the number expected from the misclassification of about 353 events of reaction (D) and confirms the general correctness of this method of the resolution of ambiguities.

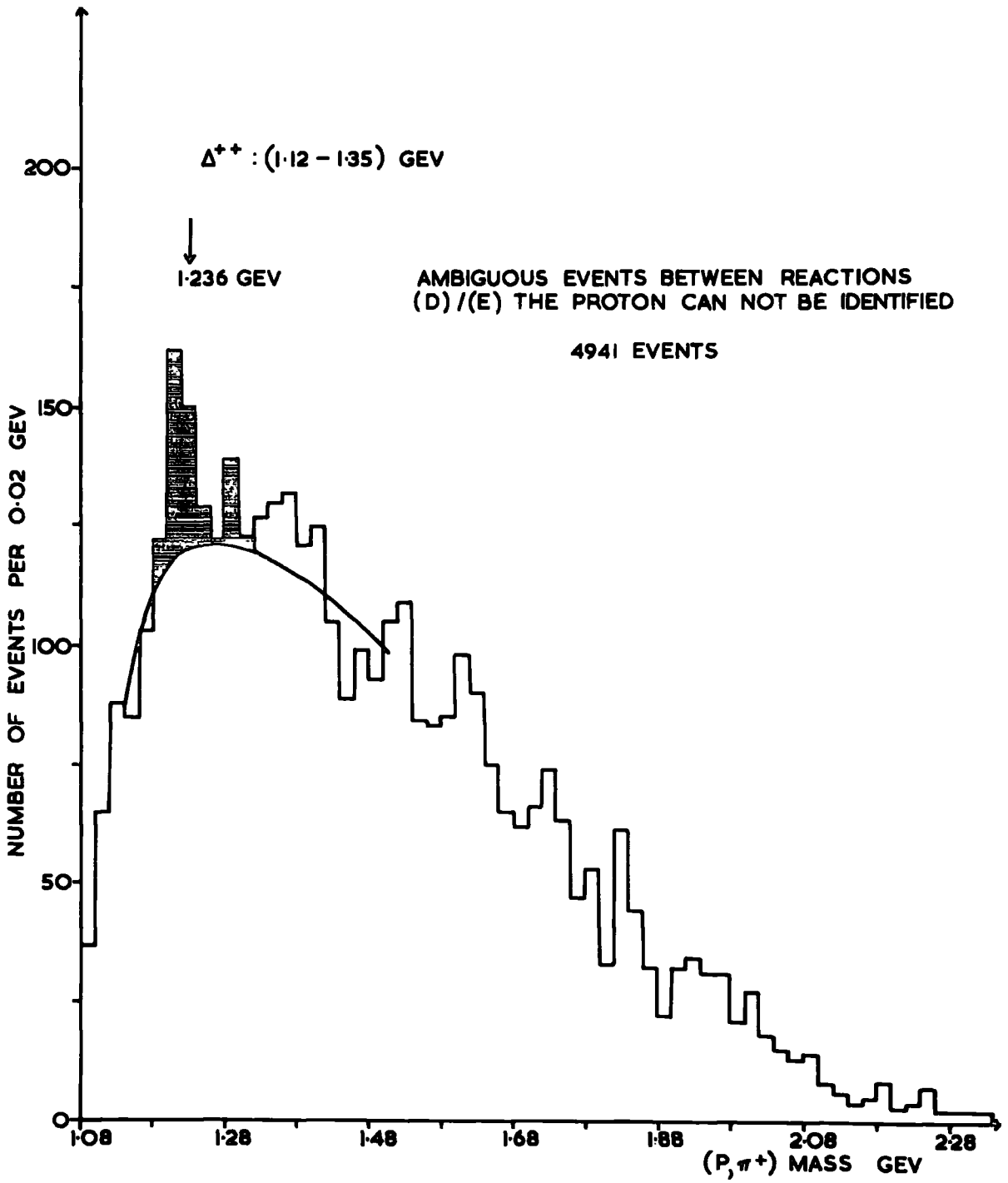

FIG. (4 – 3) THE INVARIANT (P π^+) MASS IN THE π^+P COLLISION AT 5 GEV/C

4. 2 Mass Resolution in the NOFIT Channels

In two pronged interactions the number of visible tracks is so small (two tracks) that missing and invariant masses and their errors involve almost identical variables. For example, in the laboratory system a two pronged NOFIT event is shown in figure (4-4) with the appropriate measured variables. The neutral particles, of which there must be at least two, form the missing mass (MM) as follows:-

a - in the NOFIT channel (D) the missing mass is at least two neutral pions, see figure (4-4)a.

b - in the case of the NOFIT channel (D) the missing mass will be a neutron and at least one neutral pion, see figure (4-4)b.

However, the missing mass is given in terms of the missing energy ME and missing momentum MP by:-

$$MM^2 = ME^2 - MP^2 \qquad 4.6$$

which in turn is a function of the measured variables

$$MM^2 = F(M_i, P_i, \lambda_i, \theta_i),\ i = 1,2,3 \qquad 4.7$$

the variables are the particle masses M_i, their momenta P_i, the dip and azimuthal angles λ_i and θ_i and i runs over the primary and the two secondary particles. The error on the missing mass is given by:-

$$(\Delta MM)^2 = (\partial F/\partial P_1)^2\, d^2P_1 + \ldots + (\partial F/\partial \lambda_1)^2\, d^2\lambda_1 + \ldots\ldots + (\partial F/\partial \theta_3)^2\, d^2\theta_3 \qquad 4.8$$

The invariant mass (IM) combination for the two visible secondaries is

$$IM^2 = F(M_i, P_i, \lambda_i, \theta_i) \quad i = 2,3 \qquad 4.9$$

FIG. (4-4) DIAGRAMMATIC REPRESENTATION OF A TYPICAL TWO PRONGED NOFIT EVENT IN THE LABORATORY SYSTEM.

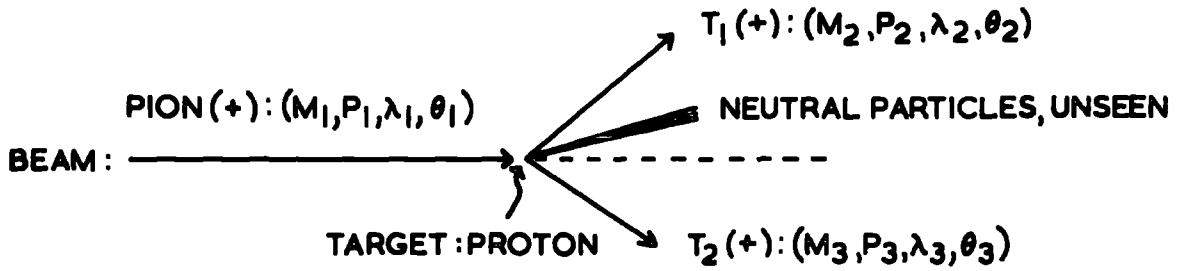

---

a. IN THE NOFIT CHANNEL (D)

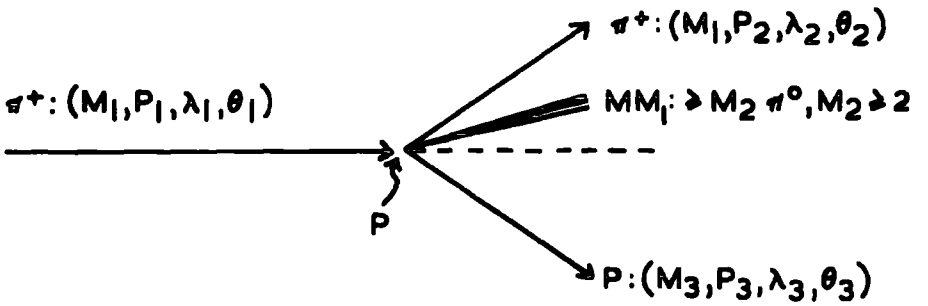

b. IN THE NOFIT CHANNEL (E)

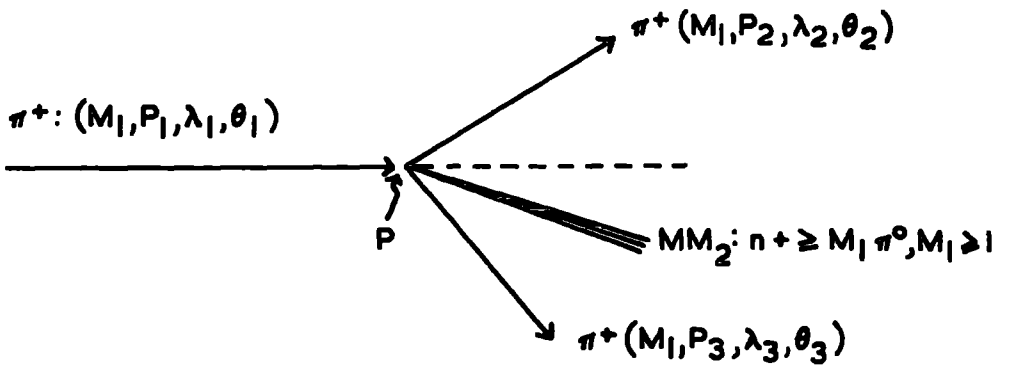

and the error by

$$(\Delta IM)^2 = (\partial F/\partial P_2)^2 d^2 P_2 + .. + (\partial F/\partial \theta_3)^2 d^2 \theta_3 \quad 4.10$$

Expression 4.10 has six terms comprising the error. The same six terms together with a further three form the error expression 4.8. This means that the error on invariant mass is smaller than the error on the missing mass.

It is difficult to appreciate the simultaneous effect of all these variables on the error. Instead, a consideration of errors calculated in GRIND and subsequent programmes give a good guide to mass resolution in the NOFIT channels. These are summarised in the next two sections.

4. 3 The P π^+ Channel (D)

The invariant mass combinations of interest are the missing mass (MM_1) and the invariant combinations (P, π^+), (P,MM_1) and (π^+, MM_1).

4.3.1 The Missing Mass (MM_1)

In figure (4-5) the error on the missing mass (as calculated by GRIND etc) is displayed. It is shown for all events which include "P π^+", channel (F), firstly and then for its sub-channels the 1-C (π^0)FIT and the NOFIT channel, reactions (B) and (D). From the figure it can be seen that the error is relatively dependent on the mass.

1 - For the UNFIT channel (F) the error on the determination of missing mass decreases with the mass. For example, for missing mass in excess of 1 Gev the error is less than 40 Mev. Below 1 Gev the error rises, and for missing mass in the region of

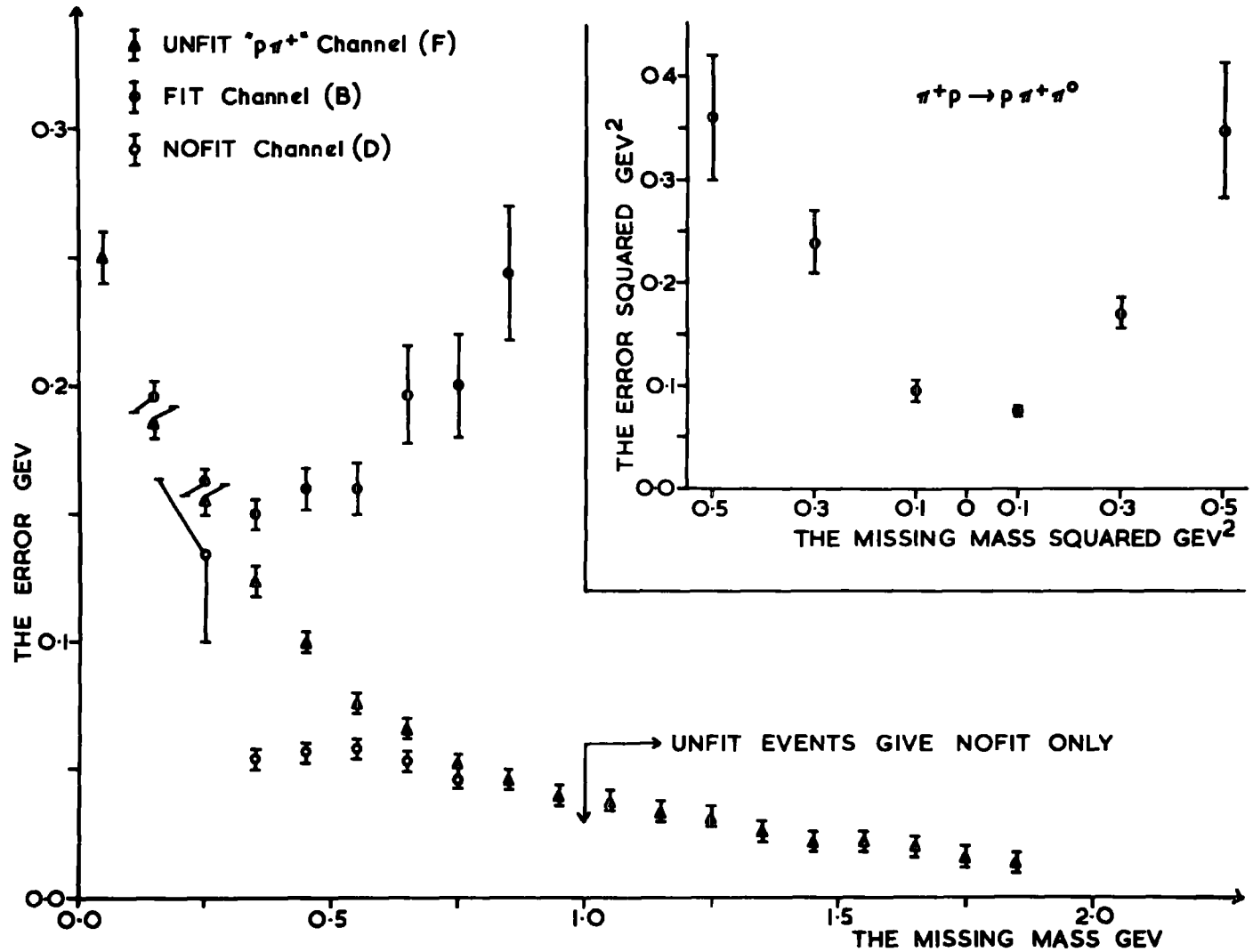

FIG. (4–5) THE ERROR ON THE MISSING MASS (SQUARED) AS A FUNCTION OF THE MISSING MASS (SQUARED) FOR THE INELASTIC TWO PRONGED ($p\pi^+$) EVENTS.

one neutral pion the error on the mass is as large as 200 Mev.

2 - Events in the UNFIT channel (F) subsequently form 1-C (π^0) events and NOFIT events. These are shown, also in figure (4-5). As might have been expected it is the events with the larger error on the missing mass that are pulled into the FIT channel. The events remaining in the NOFIT channel are, on average, more precisely determined.

3 - Since events with missing mass up to 1 Gev are pulled into the FIT channel then the possibility exists that the signal of a resonant missing mass examined in the NOFIT channel below 1 Gev might be seriously distorted by the fitting process. For example, it is expected that the missing mass spectrum corresponding to the all neutral decay of the η^0 - meson may be distorted. To avoid this possibility of distortion if it exists, in the subsequent analysis, the missing mass spectrum to the UNFIT channel (F) (rather than NOFIT) could be used. A more detailed consideration will be given in chapter 7.

The expected full width at half height (Γ_f), by assuming a normal distribution, is given by (for a resonance):-

$$\Gamma_f = (\Gamma_n^2 + \Gamma_e^2)^{1/2} \qquad 4.11$$

where Γ_n is the natural full width of resonant signal and Γ_e refers to the experimental full width which is given by

$$\Gamma_e = 2\ E\ (2\ \mathrm{Log}_e\ 2)^{1/2} = 2.355\ E \qquad 4.12$$

where E is the measured error. Now, in the η^0 - meson region the error on the missing mass is about E = 60 Mev. Consequently, the η^0 signal (mass = 549 Mev) should appear as a broad Gaussian distribution with a full width at half height (Γ_f) of about 140 Mev because the natural full width (Γ_n) of the η^0 - meson is

about 2.63 Kev. On the other hand, the f^o - meson (mass = 1260 Mev) decaying to two neutral pions will be subject in the missing mass to an error of about E = 30 Mev. This will only slightly alter the natural width of the f^o signal (Γ_n = 150 $\pm$ 25 Mev) and it should appear as a Breit-Wigner signal with Γ_f of about 180 Mev, where the expected full width at half height (by using a Breit-Wigner signal) is given by:-

$$\Gamma_f = \Gamma_n + E \qquad 4.13$$

4.3.2 - The Invariant (P, π^+) Mass Combination

Similar discussion to that for missing mass can be presented here for the invariant (P, π^+), (P, MM_1) and (π^+, MM_1) (where MM_1 contains two neutral pions at least) mass combinations by reference to figures (4-6), (4-7) and (4-8) respectively. The resonant signals expected are in general not affected by the fitting process (as was the case with missing mass). However, the NOFIT channel (D) rather than UNFIT channel (F) is preferred for use in the subsequent analysis of the invariant mass spectra because the combinations from the 1-C (π^o) FIT will give Δ^{++}, Δ^+ and ρ^+ signals in the UNFIT channel in the invariant (P, π^+), (P, π^o) and (π^+, π^o) mass spectra respectively.

As can be seen from figure (4-6) the error in the region of the Δ^{++} (mass = 1236 Mev) is so small (E = 10 Mev) that the Δ^{++} should appear as a Breit Wigner signal with virtually no broadening in the (P, π^+) events.

4.3.3 The Invariant (P, MM_1) Mass Combination

Again, the NOFIT channel (D) will be used and in the region of N^{*++}(1700), see ref.2, decaying to P π^o π^o, the error on the (P, MM_1) combination is about E = 40 Mev, see figure (4-7).

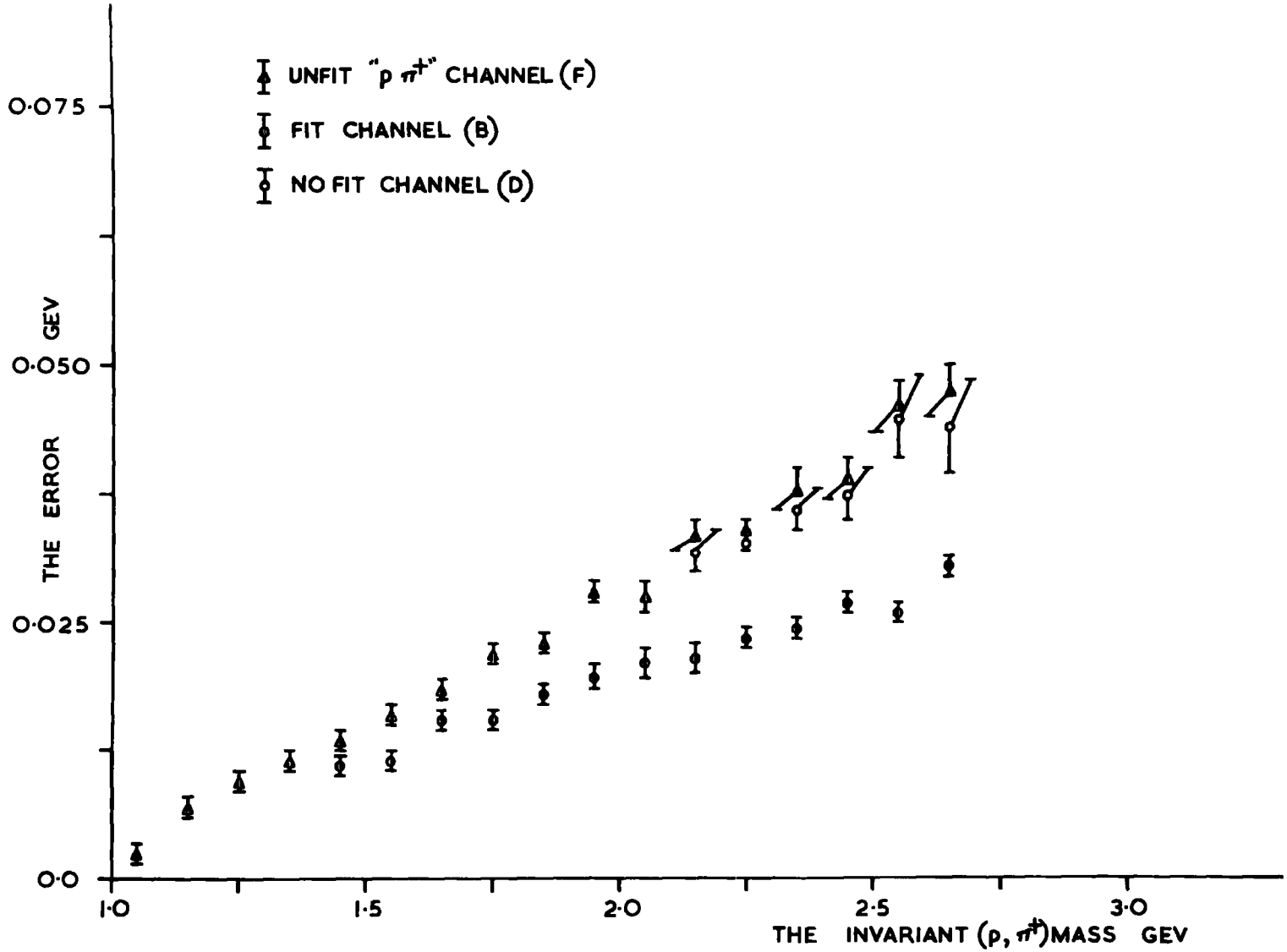

FIG. (4–6) THE ERROR ON THE (p,π^+) MASS SYSTEM AS A FUNCTION OF THE (p,π) MASS FOR THE INELASTIC TWO PRONGED $(p\ \pi^+)$ EVENTS.

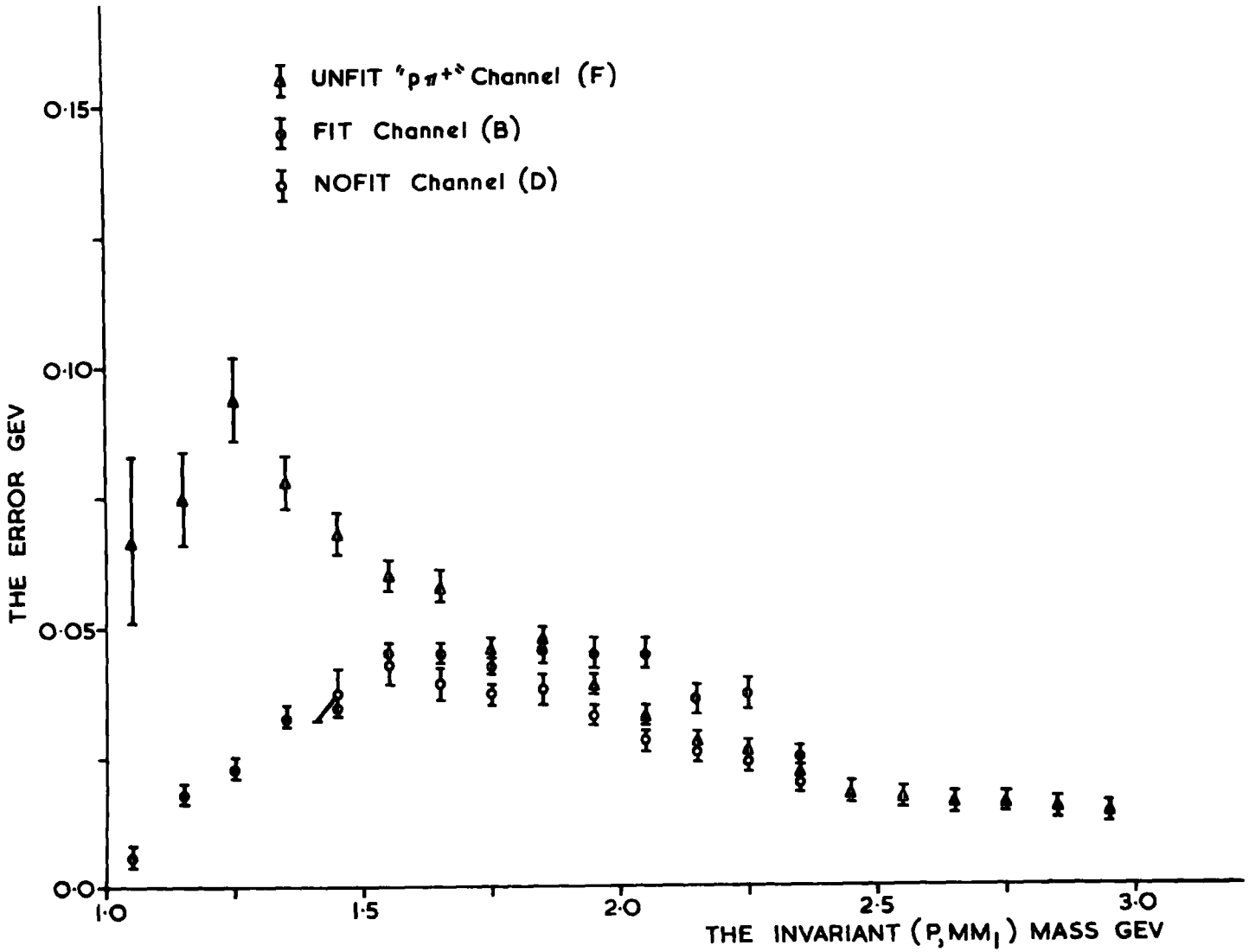

FIG. (4–7) THE ERROR ON THE (p,MM) MASS SYSTEM AS A FUNCTION OF THE (p,MM) MASS FOR THE INELASTIC TWO PRONGED (pπ+) EVENTS.

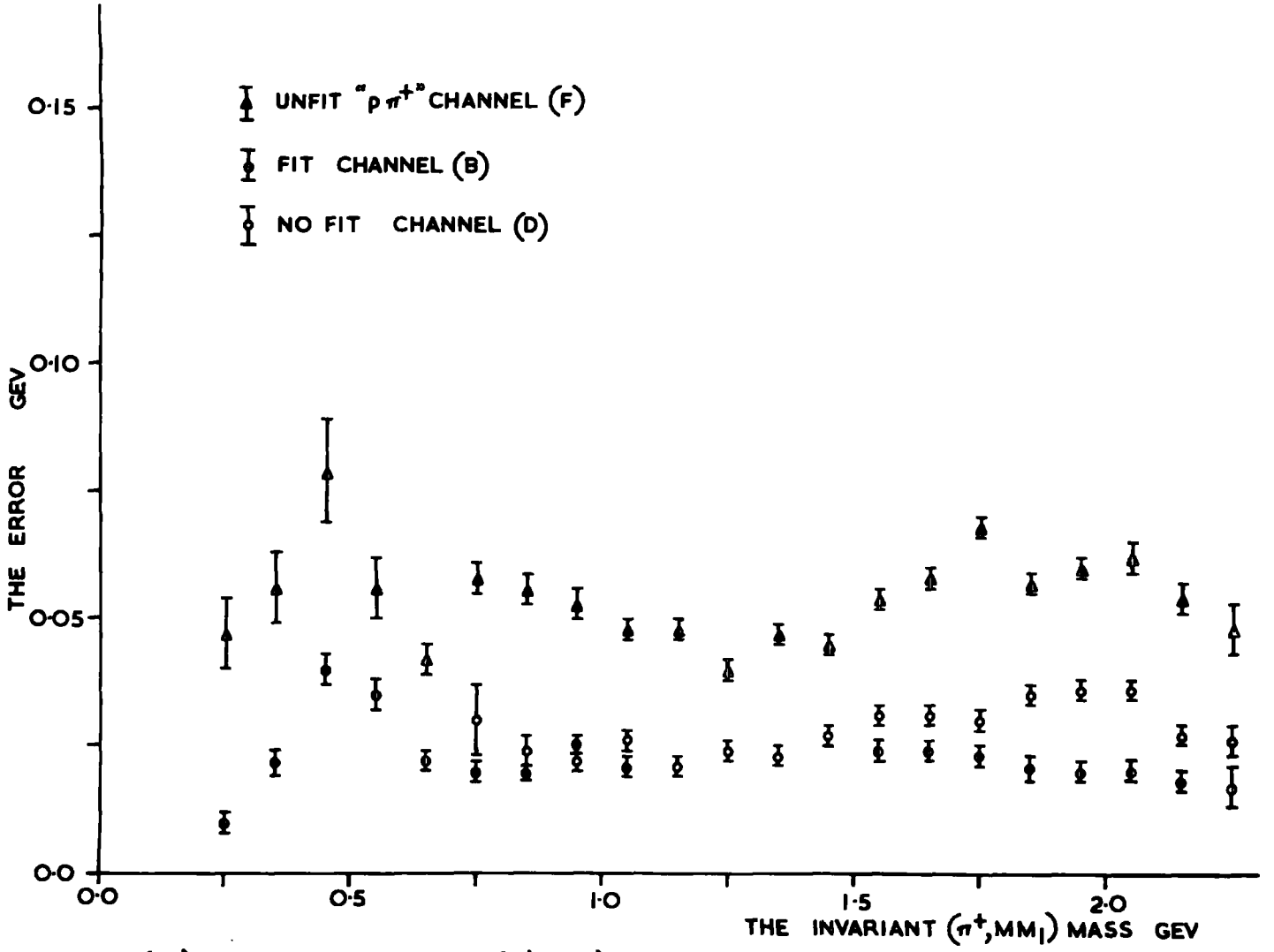

FIG. (4-8) THE ERROR ON THE (π^+, MM_1) MASS SYSTEM AS A FUNCTION OF THE (π^+, MM_1) MASS FOR THE INELASTIC TWO PRONGED $(p\,\pi^+)$ EVENTS.

This will alter the natural width of the $N^{*+}(1700)$, $\Gamma_n = 66 \pm 26$ Mev (see ref.2) and it should appear as a Breit-Wigner signal with $\Gamma_f = 115$ Mev. A more detailed account on the $N^{*+}(1700)$ will be given in chapters 6 and 7.

4.3.4 The Invariant (π^+, MM_1) Mass Combination

Finally, the NOFIT events, channel (D), will be used in the subsequent analysis of the (π^+, MM_1) mass spectrum. For example, in the region of the A_2^+- meson, decaying to $\pi^+ \pi^o \pi^o$ via $\rho^+ \rightarrow \pi^+ \pi^o$, the error in its region (mass = 1300 Mev) is about E = 25 Mev, see figure (4-8), on the (π^+, MM_1) combination. The natural width of the A_2^+ ($\Gamma_n = 92 \pm 28$ Mev) (see ref.3) will be slightly altered and the A_2^+ should appear as a Breit-Wigner signal with $\Gamma_f = 120$ Mev.

4.4 The $\pi^+ \pi^+$ Channel (E)

To distinguish the two charged pions in the final state of channel (E) rewrite the reaction as follows

$$\pi^+ \; P \rightarrow n \; \pi^+_s \; \pi^+_f \; (m_1 \; \pi^o) \quad ; \text{ NOFIT} \qquad (E)$$

with m_1 greater than zero, where s and f refer to the slow and the fast pions as seen in the laboratory system. Moreover, the FIT and the NOFIT channels (C) and (E) can be considered jointly before fitting and the combined data from the UNFIT reactions

$$\pi^+ \; P \rightarrow n \; \pi^+_s \; \pi^+_f \; (m_o \; \pi^o) \quad ; \text{ UNFIT} \qquad (G)$$

with m_o equal or greater than 0 . Again, the invariant mass combinations of interest are the missing mass (MM_2) and the invariant combinations (π^+_s, π^+_f), (π^+_f, MM_2) and (π^+_s, MM_2).

4.4.1 The Missing Mass (MM_2)

Figure (4-9) shows the error on the missing mass (as calculated by GRIND etc) firstly for all events which include "π^+_s π^+_f" channel (G), and then for its sub-channels the 1-C(n) FIT and the NOFIT channel (E). Their characteristics are similar to those of reaction (D). A detailed discussion of this figure is not given since, as will be seen later, there is no significant resonant signal in the NOFIT channel (E).

4.4.2 The Invariant (π^+_s, π^+_f) and (π^+_f, MM_2) Mass Combinations

In the NOFIT channel (E) and for the invariant (π^+_s, π^+_f) and (π^+_f, MM_2) mass combinations the resonant signals expected are in general not affected by the fitting process by reference to figures (4-10) and (4-11) respectively. However, the NOFIT channel (E) rather than the UNFIT channel (G) will be used in the subsequent analysis of the above invariant mass distributions because the combination from the 1-C(n)FIT will give signals in the UNFIT channel (G) in the invariant (π^+_s, π^+_f) and (π^+_f, n) mass spectra.

Now, in the subsequent analysis of these two mass spectra, as will be seen in chapter 6, there are no significant resonant signals in the (π^+_s, π^+_f) and (π^+_f, MM_2) mass systems.

4.4.3 The Invariant (π^+_s, MM_2) Mass Combination

Again, the NOFIT channel is preferred for use in the subsequent analysis of the (π^+_s, MM_2) mass distribution since otherwise the UNFIT channel will give signal in the (π^+_s, n)

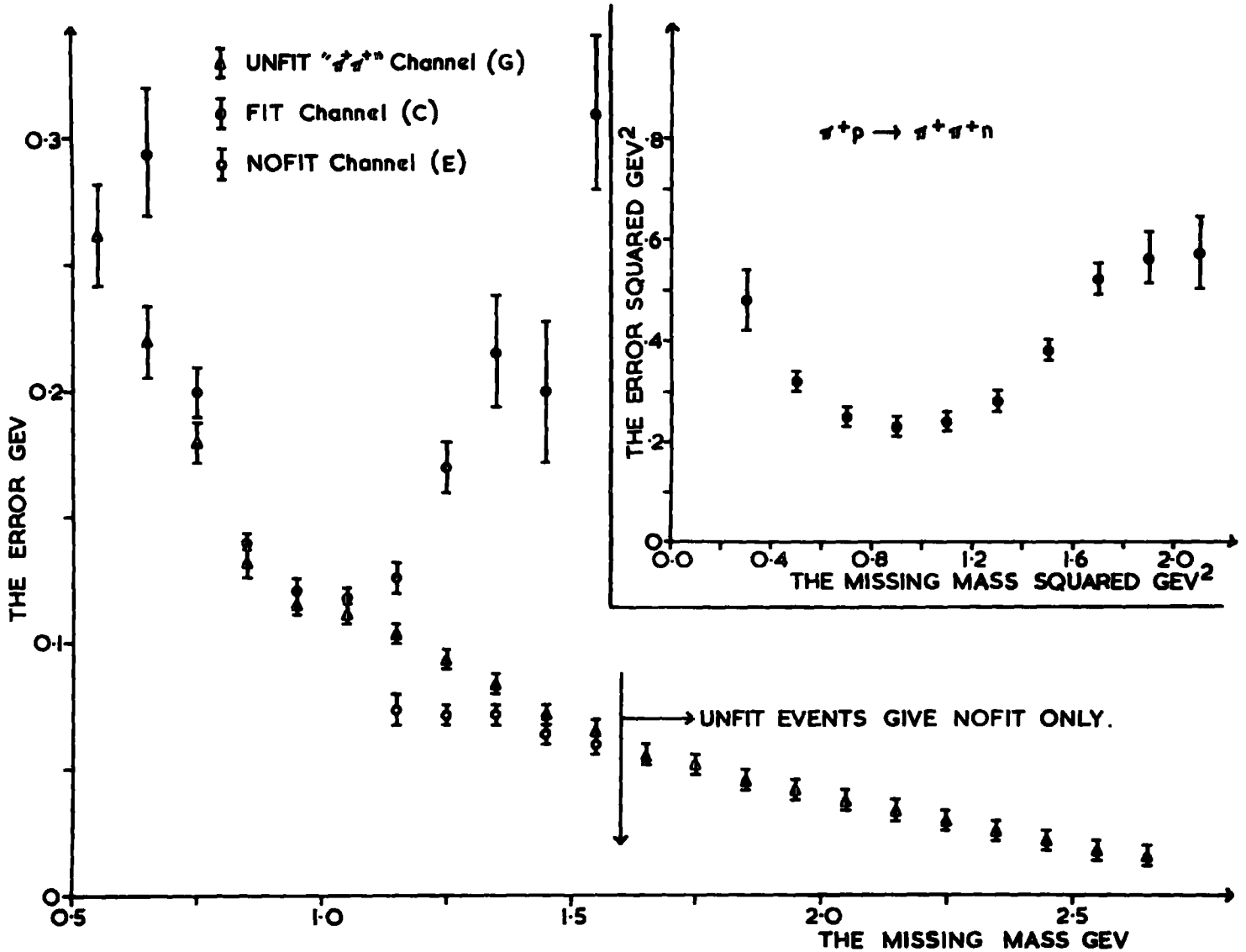

FIG. (4–9) THE ERROR ON THE MISSING MASS (SQUARED) AS A FUNCTION OF THE MISSING MASS (SQUARED) FOR THE INELASTIC TWO PRONGED ($\pi_s^+\pi_f^+$) EVENTS.

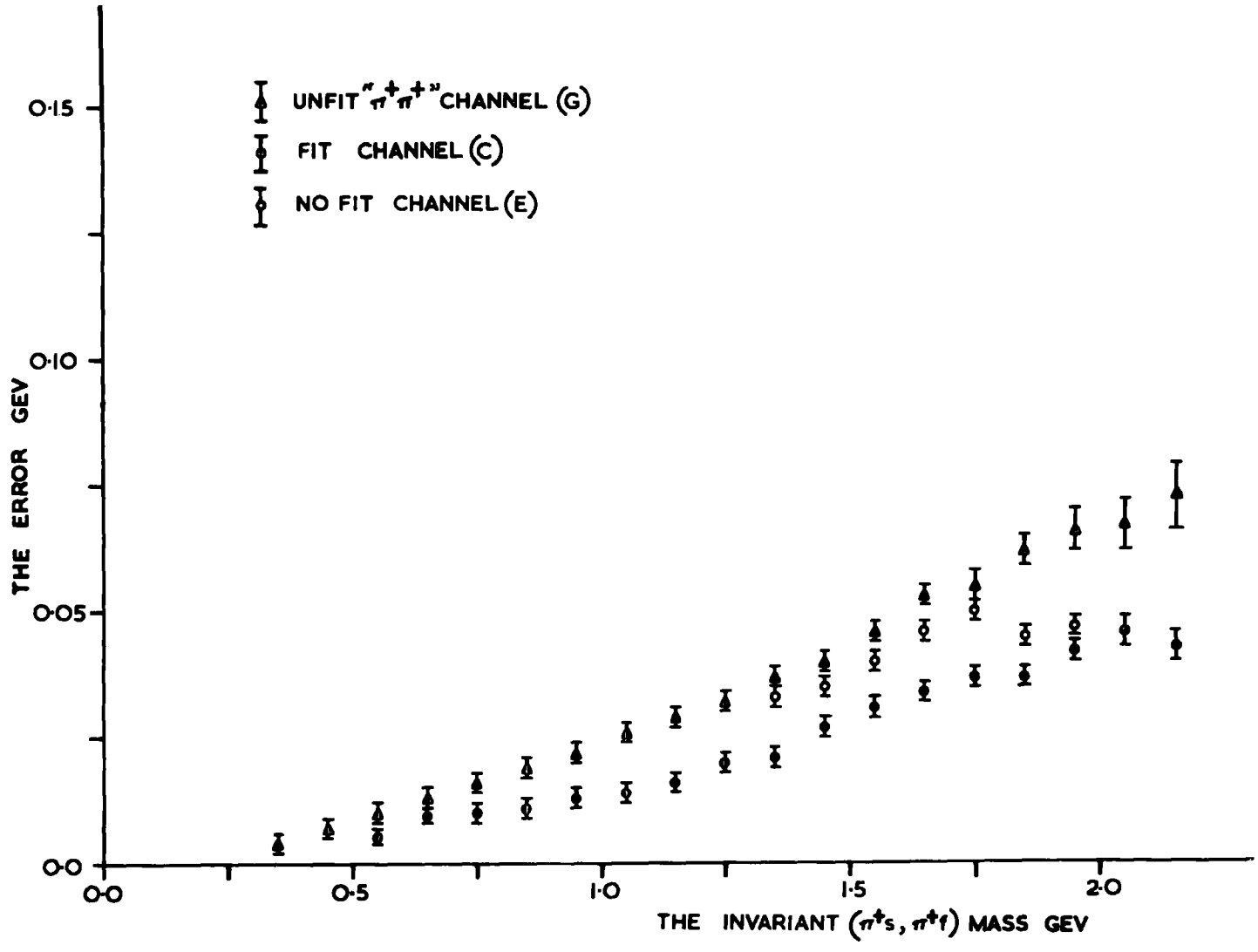

FIG. (4–10) THE ERROR ON THE (π^+_s, π^+_f) MASS SYSTEM AS A FUNCTION OF THE (π^+_s, π^+_f) MASS FOR THE INELASTIC TWO PRONGED $(\pi^+_s\ \pi^+_f)$ EVENTS.

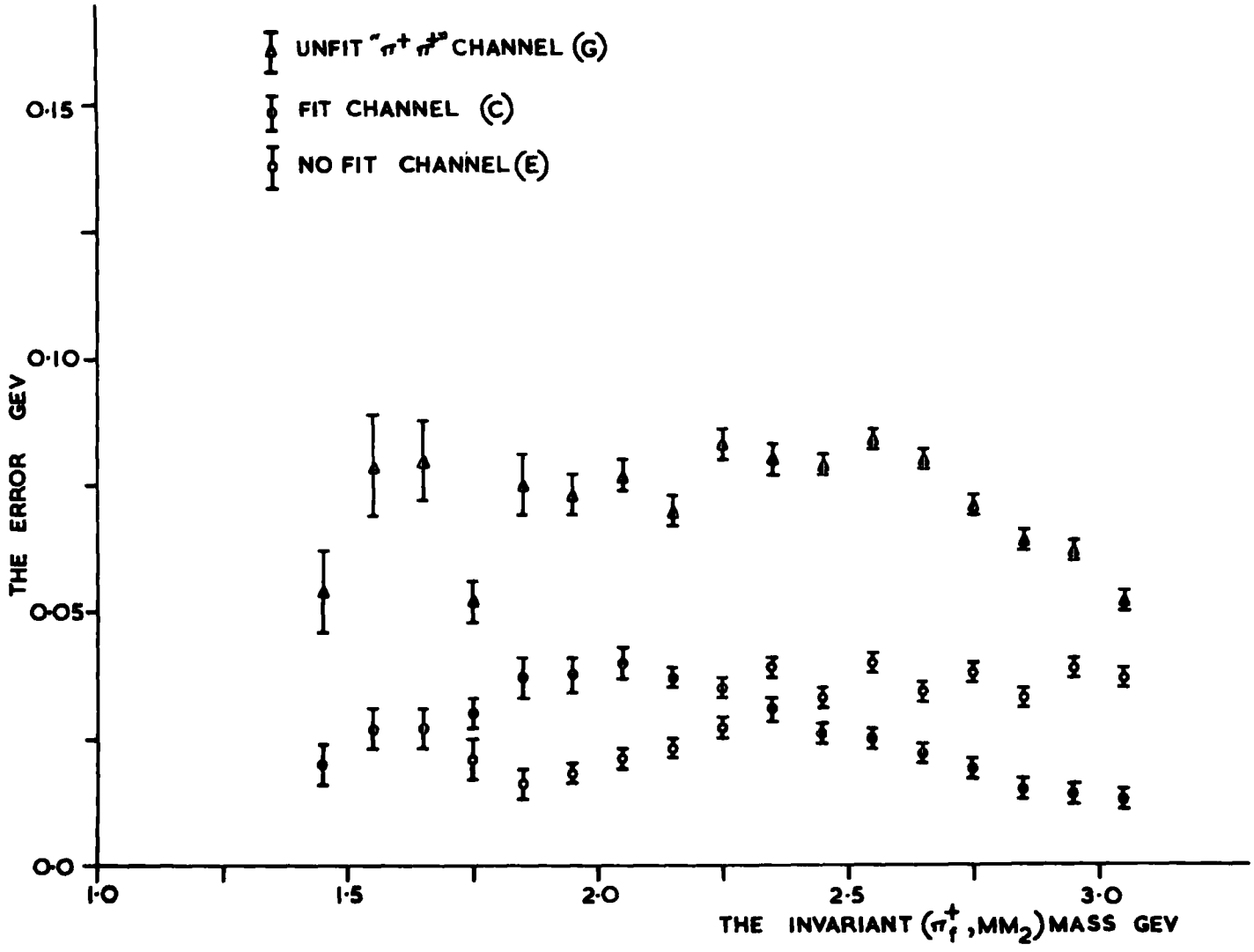

FIG. (4-11) THE ERROR ON THE (π_f^+, MM_2) MASS SYSTEM AS A FUNCTION OF THE (π_f^+, MM_2) MASS FOR THE INELASTIC TWO PRONGED (π_s^+, π_f^+) EVENTS.

combination from 1-C (n)FIT. Figure (4-12) shows the error on the (π^+s, MM_2) mass combination . Now, if $N^{*+}(1700)$ (see ref. 2) exists it should be manifest in the (π^+s, MM_2) mass distribution. For the (π^+s, MM_2) mass combination in the region of $N^{*+}(1700)$, decaying to n π^+s π^o, the error is about E = 20 Mev, see figure (4-12). This will only slightly alter the natural width. The $N^{*+}(1700)$ should appear as a Breit-Wigner signal with a full width at half height of about 80 Mev.

4. 5 Check on the Estimates of Errors

As stated earlier (in sections 4. 3 and 4. 4) the errors on the missing masses and the errors on the invariant mass combinations , displayed in figures (4-6) to (4-12), are those calculated by GRIND and similar programmes and not by any direct method. That these errors are adequate estimates can be seen by a comparison of the errors on the missing masses with the width of the neutral pion (π^o) peak and the neutron (n) peak in the FIT data of reactions (B) and (C) shown in the missing mass or the missing mass squared spectra.

From figure (4-5) it can be seen that the error in the region of the neutral pion is about E = 200 Mev and this corresponds to a full width at half height of Γ_f = 470 Mev. In figure (4-13) the missing mass spectrum is shown for those events which subsequently give a 1-C (π^o)fit. It can be seen that the width at half height Γ_f is in agreement with that expected above. The maximum of the distribution, figure (4-13), can be seen to be displaced from the π^o mass (mass = 135 Mev) to about 200 Mev. In fact in the missing mass squared distribution, figure (4-14), the peak is approximately Gaussian and correctly placed at

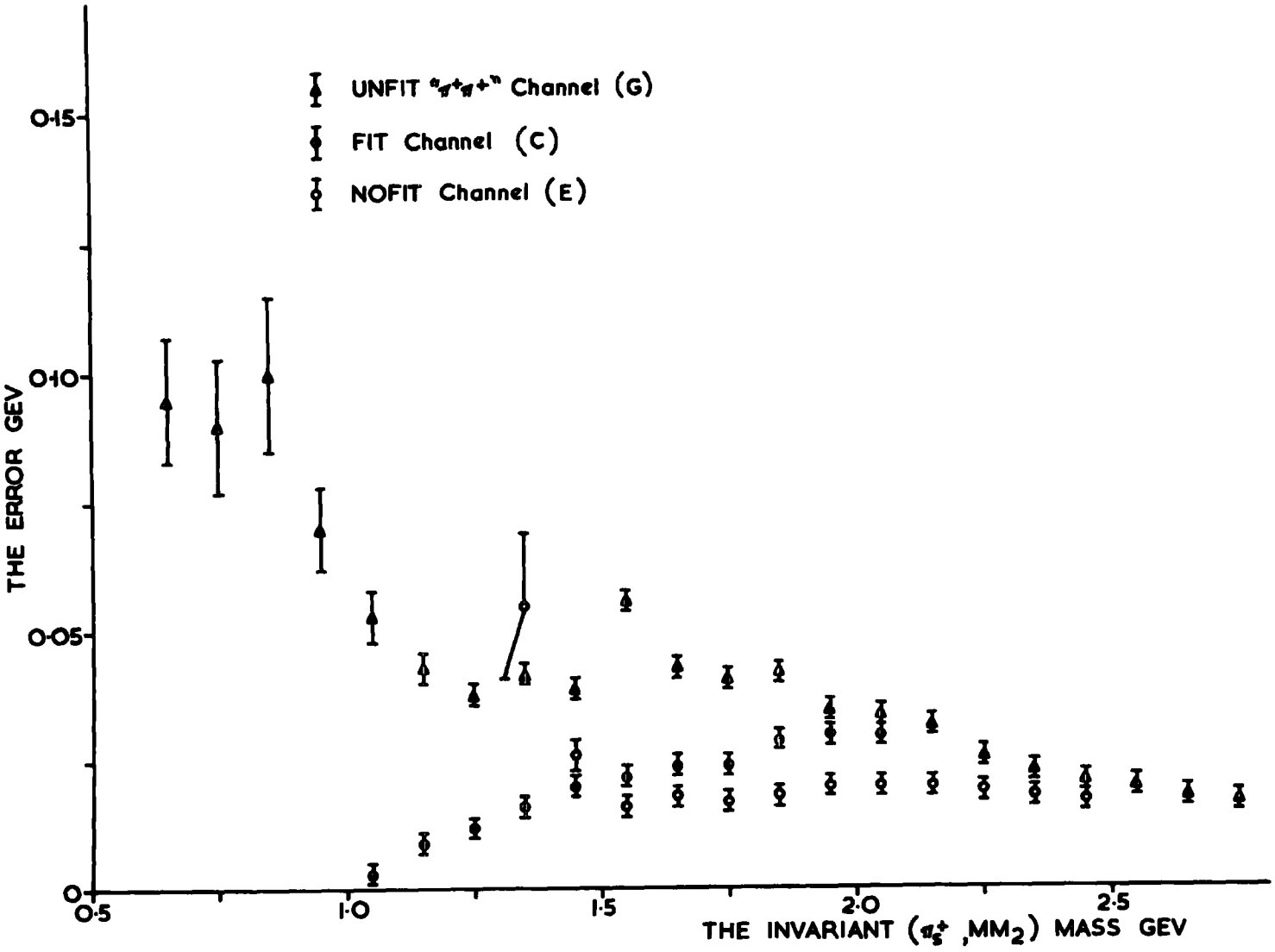

FIG. (4–12) THE ERROR ON THE (π_s^+, MM_2) MASS SYSTEM AS A FUNCTION OF THE (π_s^+, MM_2) MASS FOR THE INELASTIC TWO PRONGED (π_s^+ π_f^+) EVENTS.

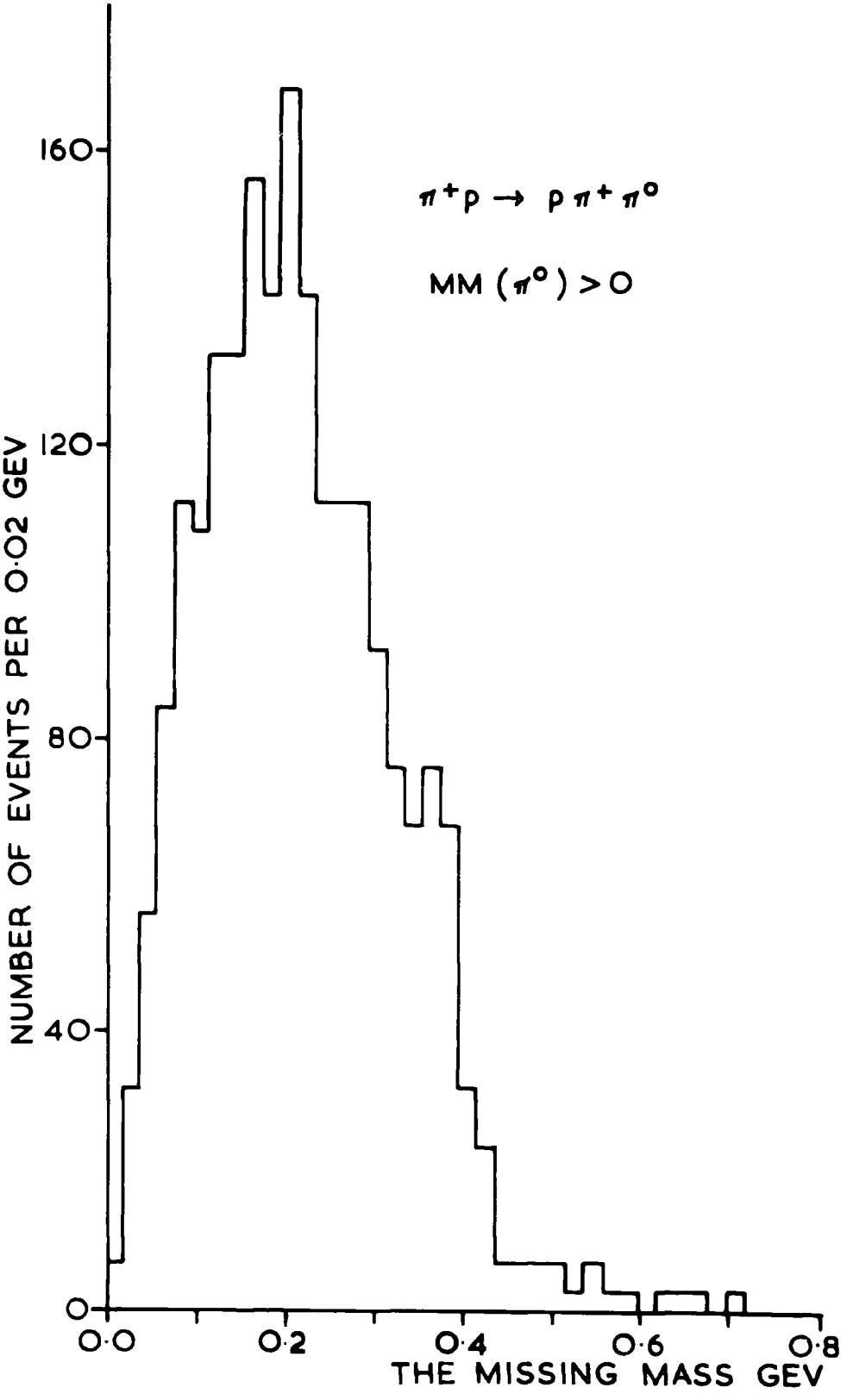

FIG. (4 – 13) THE MISSING MASS SPECTRUM FOR THE 1-c (π^0) FIT EVENTS AT 5 GEV/C.

0.018 ± 0.001 Gev^2. The displacement arises from the distortion in going from missing mass squared (MM^2) to missing mass (MM_1). In the missing mass distribution it can be shown that the maximum occurs at MM_1 when

$$MM_1^2 = MM_o^2/2 + (MM_o^4 + 2\sigma^2)^{1/2}/2 \qquad 4.14$$

where σ is the standard deviation of the missing mass squared distribution and MM_o^2 is the mean value which should be equal to the π^o - mass squared. In the present case the standard deviation squared is much greater than MM_o^4 and then

$$MM_1^2 = MM_o^2/2 + \sigma/(2)^{1/2} \qquad 4.15$$

Substituting $MM_o = (0.018)^{1/2}$ Gev and $\sigma = 0.060 \pm 0.001$ Gev^2 in the equation 4.15 then the peak occurs at $MM_1 = 210$ Mev. Only when (MM_o^2/σ) is large the missing mass and missing mass squared peaks coincide as shown in figure (4-15).

This effect is most pronounced for small missing masses, so that no distortion is expected, for example, at missing masses in the η^o region in the channel (F) or at the neutron region in the $\pi^+ \pi^+$ channel (C).

Similarly, in the case of the channel (C), the error on the missing mass, see figure (4-9), at the neutron mass region (mass = 940 Mev) is about E = 120 Mev and leads to a full width at half height of Γ_f = 280 Mev. Again, this corresponds in figure (4-15) to the observed width of the neutron peak in the missing mass spectrum to $\pi^+ \pi^+$ events which subsequently give the 1-C(n) FIT.

This agreement gives confidence in the errors which have been displayed in the earlier figures. Consequently, it also gives confidence in the consideration of the mass resolutions

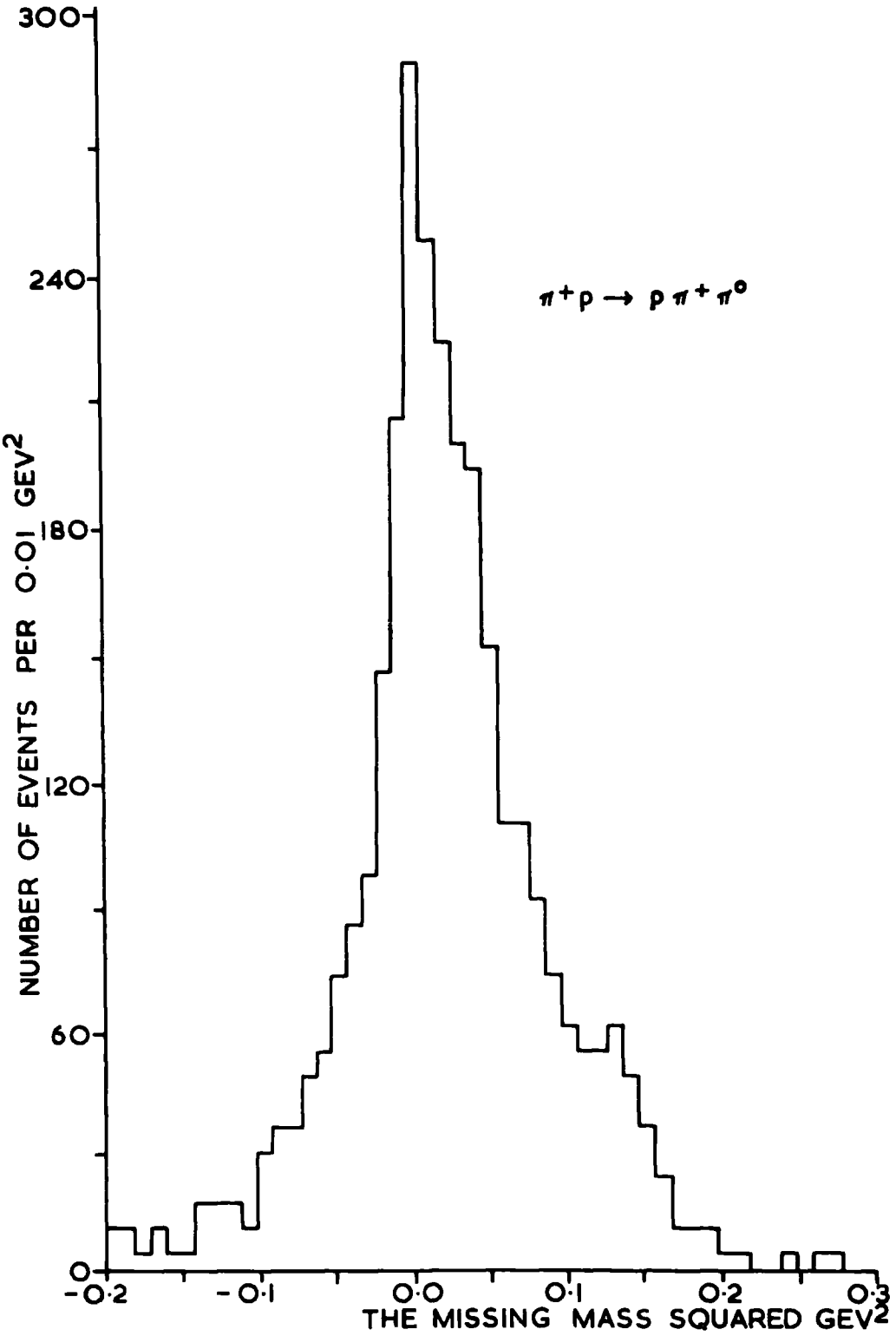

FIG. (4-14) THE MISSING MASS SQUARED SPECTRUM FOR THE 1-C(π^0) FIT EVENTS AT 5 GEV/C

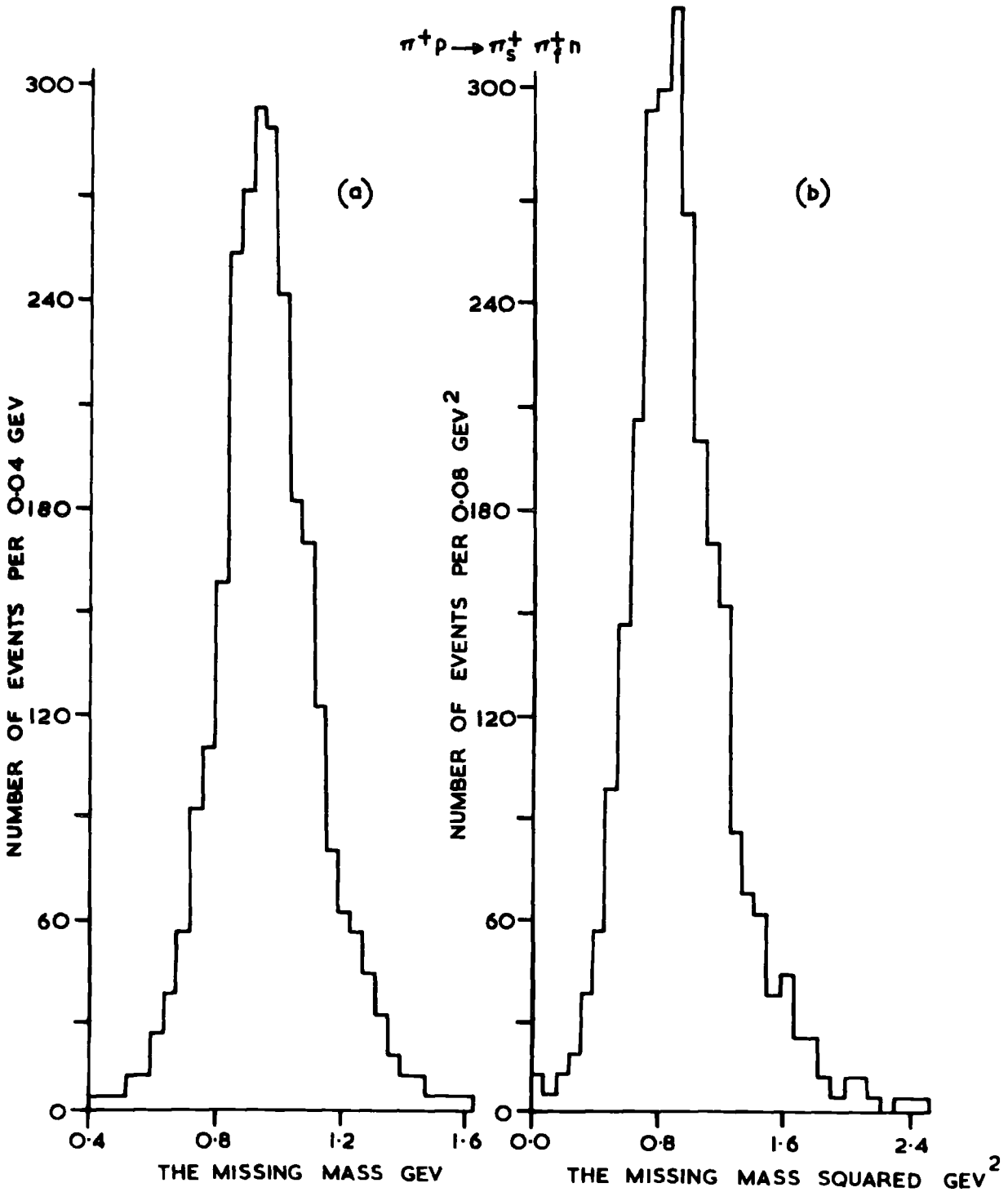

FIG. (4-15) (a) THE MISSING MASS AND (b) THE MISSING MASS SQUARED FOR THE 1-C (n) FIT EVENTS AT 5 GEV/C.

to be expected in the NOFIT channels and in the expected widths of resonance mass signals.

CHAPTER 5

ESTIMATION OF RESONANCE PRODUCTION IN THE TWO PRONGED NOFIT CHANNELS

The selection of events and the resolution of the two pronged NOFIT channels

$$\pi^+ P \longrightarrow P \pi^+ MM_1 \qquad (D)$$

$$\pi^+ P \longrightarrow \pi^+_s \pi^+_f MM_2 \qquad (E)$$

have already been discussed in chapter 4. The missing masses MM1 and MM2 are composed of two neutral secondary particles at least. For example, in channel (D) the missing mass should be two neutral pions at least, in the case of the channel (E) it will be a neutron and at least one neutral pion.

In the case where the missing mass is made from two neutral secondaries, for example two neutral pions in reaction (D), it is possible to make estimates of cross-sections for various physical processes from the reaction's equivalent 4-C FIT channel where the neutral secondaries are replaced by charged secondary particles (i.e. the four pronged channel). Similarly, when the missing mass is composed of three neutral particles then cross-sections in the above two channels can be determined from the equivalent four pronged 1-C (π^o) FIT and 1-C (n) FIT channels.

In the π^+P collisions at 5 Gev/c, the cross-section for four pronged final states (see ref.1) have already been determined, see table (5-1), and of which the 4-C FIT and the 1-C(π^o) FIT have been analysed in detail, (see ref. 1, 2, 3, 4, 5, 6 and 7).

TABLE (5-1)

FINAL STATE	No. OF EVENTS	CROSS-SECTION (mb)
4-C FIT: $P\pi^+\pi^+\pi^-$	6994	2.76 ± 0.04
1-C(π^0)FIT: $P\pi^+\pi^+\pi^-\pi^0$	7300	2.88 ± 0.04
1-C(n)FIT: $n\pi^+\pi^+\pi^+\pi^-$	2164	0.85 ± 0.02
TOTAL	16458	6.49 ± 0.06
Microbarn Equivalent is 0.40 ± 0.01 μb/event.		

In many cases the prediction can be made accurately. For example, the production of A_2^+ (see ref. 5), in the four pronged 4-C events in the channel

$$\pi^+ P \rightarrow P A_2^+ \hookrightarrow \pi^+ \rho^0 \hookrightarrow \pi^+\pi^-$$

where A^+_2 decays to $\pi^+ \rho^0$, should be accompanied by exactly the same amount of production of A^+_2 decaying into $\pi^0 \rho^+$ in the two pronged NOFIT reaction (D), where ρ^+ decays to $\pi^+ \pi^0$, as follows:-

$$\pi^+ P \rightarrow P A_2^+ \hookrightarrow \pi^0 \rho^+ \hookrightarrow \pi^+\pi^0$$

Other processes are more complicated. For example, some Δ^{++} (see ref.7) production is seen to occur in the four pronged 1-C(π^0) FIT events in the channel

$$\pi^+ P \rightarrow \Delta^{++}\pi^+\pi^-\pi^0$$

where Δ^{++} decays to P π^+. In the majority of cases the three pions (or their di-pion combination) do not resonate. The problem then is to calculate how many events of this kind will lead to two pronged NOFIT channel (D) where the three pions in the above channel are all produced in the neutral mode. For this purpose it is necessary to consider the general three body state and using Clebsch-Gordon coefficients to calculate the relative proportion of the possible charged body states.

To do this the three body state is broken down into a substate of two associated particles whose ispin is T^{12} with third component T_3^{12}. These two particles are then coupled to the third to give an overall ispin of T and its third component T_3. A particular ispin state is made up from the multiplicity of charged body states as (see ref. 8) :-

$$\left.\begin{aligned} |T^{12};\, T,\, T_3\rangle = \sum_{T_3^i} \langle T^1,\, T_3^{\,1};\, T^2,\, T_3^{\,2} \mid T^{12},\, T_3^{\,12}\rangle \times \\ \times \langle T^{12},\, T_3^{\,12};\, T^3,\, T_3^{\,3} \mid T,\, T_3\rangle |T_3^{\,1},\, T_3^{\,2},\, T_3^{\,3}\rangle \end{aligned}\right\} 5.1$$

where T^1, T^2 and T^3 are the ispins of the three particles and $T_3^{\,1}$, $T_3^{\,2}$ and $T_3^{\,3}$ are their third components respectively.

Returning to the channel

$$\pi^+ P \longrightarrow \Delta^{++}\, \pi^+ \pi^- \pi^o$$

from which we wish to determine the cross-section for

$$\pi^+ P \longrightarrow \Delta^{++}\, \pi^o \pi^o \pi^o$$

The three pions must form a state with ispin of 0, 1, 2 or 3. The fact that a Δ^{++} with $T(\Delta^{++}) = 3/2$ is produced in association can be shown to impose no limits, through ispin conservation, on the ispin of the tri-pion. The three pions are regarded as having a di-pion substate with ispin T^{12}.

As an example, T^{13} will be taken to be 2. When the di-pion is coupled to the third pion ($T^1 = T^2 = T^3 = 1$) then the total ispin (T) is 1, 2 or 3 with $T_3 = 0$. Application of equation 5.1 shows that this ispin configuration is made up of pion statesin the following way:-

$$\left.\begin{aligned} |T^{12}; T, T_3\rangle = |2;1,0\rangle = |\pi^0\pi^0,\pi^0\rangle\sqrt{2/3}\left(-\sqrt{2/5}\right)+ \\ +|\pi^+\pi^-,\pi^0\rangle\sqrt{1/6}\left(-\sqrt{2/5}\right)+|\pi^-\pi^+,\pi^0\rangle\sqrt{1/6}\left(-\sqrt{2/5}\right)+ \\ +|\pi^-\pi^0,\pi^+\rangle\sqrt{1/2}\sqrt{3/10}+|\pi^0\pi^-,\pi^+\rangle\sqrt{1/2}\sqrt{3/10}+ \\ +|\pi^0\pi^+,\pi^-\rangle\sqrt{1/2}\sqrt{3/10}+|\pi^+\pi^0,\pi^-\rangle\sqrt{1/2}\sqrt{3/10} \end{aligned}\right\} \quad 5.2$$

In equation 5.2 it can be seen how the $\pi^0\pi^0\pi^0$ state is related to other three pion states. From the squared amplitudes of the various substates, the relative proportion of $\pi^0\pi^0\pi^0$ to $\pi^+\pi^-\pi^0$ is given by:-

$$(\pi^0\pi^0\pi^0)/(\pi^+\pi^-\pi^0) = (4/15)/(2/15+9/15) = 4/11$$

Similar results are obtained for T = 2 and 3 with $T_3 = 0$ and $T^{12} = 2$

$$|2;2,0\rangle \;;\; (\pi^0\pi^0\pi^0)/(\pi^+\pi^-\pi^0) = 0$$

$$|2;3,0\rangle \;;\; (\pi^0\pi^0\pi^0)/(\pi^+\pi^-\pi^0) = 2/3$$

Since the cross-section of $\Delta^{++}\pi^+\pi^-\pi^0$ has been measured (see ref. 1, 5 and 6) to be 0.83 ± 0.02 mb (about 2076 events), then the above calculation shows that for a di-pion substate of $T^{12} = 2$ the three pions can not exist in the three neutral pion mode if the tri-pion ispin is T = 2. However, if the tri-pion ispin is 1 or 3 then the cross-section for $\pi^+P \longrightarrow \Delta^{++}\pi^0\pi^0\pi^0$(NOFIT) is either 0.30 mb for T = 1 or 0.55 mb for T = 3.

The usefulness of this kind of ispin analysis is that:-

a) it enables predictions of cross-section to be made for NOFIT channels and b) the predictions vary with the ispin of the tri-pion substates and it might be possible by comparison with the observed cross-section in NOFIT channel to be able to pinpoint the particular ispin state which is present in the reaction.

The estimates for cross-section for various physical processes in the two pronged NOFIT events determined from the corresponding four pronged reactions are given in the ensuing sections. It should be remembered in predicting the number of events and the cross-section likely to be seen in the two pronged NOFIT channels that all data (two and four pronged interactions) were obtained from the same exposure (that is the $\pi^+ P$ collisions at 5 Gev/c in the B.N.H.B.C.).

5. 1 Four Pronged Reactions

First let us assume that the missing mass in the two pronged NOFIT channels comprises two neutral particles. The reactions (D) and (E) are then described as follows:-

$$\pi^+ P \longrightarrow P \pi^+ \pi^o \pi^o \qquad \text{(i)}$$

$$\pi^+ P \longrightarrow \pi_s^+ \pi_f^+ n \pi^o \qquad \text{(ii)}$$

These two categories are equivalent to four pronged 4-C FIT interactions

$$\pi^+ P \longrightarrow P \pi^+ \pi^+ \pi^- \qquad \text{(H)}$$

An ($N \pi \pi \pi$) system then is seen to occur as channel (H) with a certain cross-section. The problem is to calculate from that cross-section what would be expected in the ($N \pi \pi \pi$) system of reactions (i) and (ii), these are the two pronged

NOFIT channels. This can be done by use of Clebsch-Gordon coefficients and following the method described earlier (that is using equation 5.1). The assumption that is made is that the N π π π system is regarded completely as one of the following configurations:-

a) the N π π π system is made up of N π and π π substates

or b) it is made from π and N π π substates

or c) it is made from N and π π π substates.

For each of these assumptions the expected contributions to channels (D) and (E) can be calculated from the observed P π^+ π^+ π^- channel. The result of the calculation for the above configurations (a, b and c) are shown in tables (5-2), (5-3) and (5-4) respectively for a pure ispin state.

TABLE (5-2)

1	2	3	4	5	6
ISPIN SUBSTATES		BRANCHING RATIOS			
(N π π π)		FIT CHANNEL	NOFIT CHANNELS		NOFIT / FIT
T(N π)	T(π π)	(H)	(i)	(ii)	
3/2	0	2/3	1/3	0	1/2
3/2	1	3/5	0	2/5	2/3
3/2	2	7/15	2/15	6/15	8/7
1/2	2	8/15	0	7/15	7/8

TABLE (5-3)

1	2	3	4	5	6
$(N\pi\pi)^+$ ISPINS		BRANCHING RATIOS			NOFIT
SUBSTATE	FINAL STATE	FIT CHANNEL (H)	NOFIT CHANNELS (i)	NOFIT CHANNELS (ii)	FIT
$\lvert T^{12} ; T, T_3\rangle$					
$\lvert 0 ; 1/2, 1/2\rangle$		2/3	1/3	0	1/2
$\lvert 1/2 ; 1/2, 1/2\rangle$		4/9	1/9	4/9	5/4
$\lvert 1 ; 1/2, 1/2\rangle$		1/3	0	2/3	2/1
$\lvert 3/2 ; 1/2, 1/2\rangle$		5/9	2/9	2/9	4/5
$\lvert 1/2 ; 3/2, 1/2\rangle$		2/9	2/9	5/9	7/2
$\lvert 1 ; 3/2, 1/2\rangle$		2/3	0	1/3	1/2
$\lvert 3/2 ; 3/2, 1/2\rangle$		26/45	2/45	17/45	19/26
$\lvert 2 ; 3/2, 1/2\rangle$		2/15	4/15	9/15	13/2

TABLE (5-4)

1	2	3	4	5	6
$(\pi\pi\pi)^+$: ISPINS		BRANCHING RATIOS			NOFIT
SUBSTATE	FINAL STATE	FIT CHANNEL (H)	NOFIT CHANNELS (i)	(ii)	FIT
$\|T^{12}$	$; T, T_3\rangle$				
$\|0$	$; 1, 1\rangle$	2/3	1/3	0	1/2
$\|1$	$; 1, 1\rangle$	1/2	1/2	0	1/1
$\|2$	$; 1, 1\rangle$	1/2	1/2	0	1/1
$\|1$	$; 2, 1\rangle$	19/30	11/30	0	11/19
$\|2$	$; 2, 1\rangle$	1/2	1/2	0	1/1
$\|2$	$; 3, 1\rangle$	1/5	4/5	0	4/1

Inspection of tables (5-2), (5-3) and (5-4) showsispin configurations corresponding to well known physical processes. For example, in table (5-2) T(N π) of 3/2 and T($\pi\pi$) of 1 will include Δ^{++} ρ^0 and T(N π) of 3/2 and T($\pi\pi$) of 0 will include Δ^{++} f^0 and so on. For these specific processes the ispin configuration is well defined. From events of this kind occurring in P π^+ π^+ π^- events their contribution to the NOFIT channels can be directly calculated from specific parts of the tables.

For the remainder of the events which do not fall into

well known processes then all possible ispin configurations have to be considered. For example for $\Delta^{++}\ \pi^+\ \pi^-$ the possible ispins are T = 3/2 for the Δ^{++} and T = 0, 1, or 2 for the dipion. All these possibilities have to be considered. As a more complicated example, N $\pi\ \pi\ \pi$, T(N π) = 1/2 or 3/2 and T($\pi\ \pi$) = 0, 1 or 2 and all four possibilities for P $\pi^+\pi^+\pi^-$ have to be taken into account.

In table (5-5) a breakdown is given of P $\pi^+\ \pi^+\ \pi^-$ events from the 4-C FIT reaction of this experiment (see ref. 1, 5 and 6) into well defined processes and remainders. The reaction final state, the total number of events and the observed numbers of events in each channel which are given in columns 1, 2 and 3 were found in the analysis of the four pronged 4-C FIT events. Column 4 gives the cross-section in each channel.

From table (5-5) it can be seen that:-

a) in the case of $\Delta^{++}\ \varrho^0$ and in the case of those P $\pi^+\ \varrho^0$ events where the π^+ is associated with the proton, there can be no contribution to the NOFIT channel (D) since the ϱ^0 can only decay by the $\pi^+\ \pi^-$ mode and not by the $\pi^0\pi^0$ mode.

b) for the PA_2^+ events and for those P $\pi^+\ \varrho^0$ events where the π^+, now, is associated with the ϱ^0 through a tri-pion state there can be a contribution to the NOFIT channel (D) through the related P $\pi^0\ \varrho^+$ events. Here, the ϱ^+ can decay to $\pi^0\ \pi^+$ to give a final state of P $\pi^+\ \pi^0\pi^0$. For the A_2^+ meson decaying to $\pi^+\ \varrho^0$ there will be an equal number of A_2^+ meson decaying to $\pi^0\ \varrho^+$ in the two pronged NOFIT channel (D).

c) where the ϱ^0 is associated with the proton as a P ϱ^0 state there can be a contribution from the related n ϱ^+ state

TABLE (5-5)

1	2	3	4
THE FOUR PRONGED 4-C FIT EVENTS			
REACTION FINAL STATE	No. OF EVENTS		CROSS-SECTION (mb)
	Total	Observed	
I - $\underline{P\pi^+\pi^+\pi^-}$: no Δ^{++}	3006	—	1·196 ± 0·017
$P\pi^+\rho^0$, $\rho^0 \to \pi^+\pi^-$; A_2^+ EXCL.		1709	0·680 ± 0·010
$P A_2^+$, $A_2^+ \to \rho^0\pi^+$		286	0·114 ± 0·002
$\pi^+ N^{*++}(1700)$, $N^{*++} \to P\pi^+\pi^-$		211	0·084 ± 0·002
$P\pi^+\pi^+\pi^-$; REMAINDER		800	0·318 ± 0·005
II - $\underline{\Delta^{++}\pi^+\pi^-}$	3935	—	1·565 ± 0·023
$\Delta^{++}\rho^0$		2186	0·870 ± 0·013
$\Delta^{++} f^0$, $f^0 \to \pi^+\pi^-$		427	0·170 ± 0·003
$\Delta^{++}\pi^+\pi^-$; REMAINDER		1322	0·525 ± 0·008
TOTAL : $P\pi^+\pi^+\pi^-$	6941		2·762 ± 0·041
Cross-sections are not corrected for unseen decay modes.			

TABLE (5-6)

Column	1	2	3	4	5	6	7	8	9	10	11	12
ROW	STATE $\|T^{I2}; T, T_3\rangle$	DECAY MODE	BRANCHING RATIOS			NO FIT / FIT	EXPECTED NUMBER OF EVENTS AND CROSS-SECTIONS (mb)					
			Fit	No fit channels			No fit channels : (D)+(E)		No fit channel (D)		No fit channel (E)	
			(H)	(D)	(E)		No. of events	Cross-sections	No. of events	Cross-sections	No. of events	Cross-sections
	$N^{*++}(1700)$											
1	$\|0; 1/2, 1/2\rangle$	$\pi\ \pi\ N$					106	0·042	106	0·042	0	0
2	$\|1/2; 1/2, 1/2\rangle$	$N\ \pi\ \pi$					264	0·105	53	0·021	211	0·084
3	$\|1; 1/2, 1/2\rangle$	$\pi\ \pi\ N$	See table (5-3) Columns 3 to 6				422	0·168	0	0	422	0·168
4	$\|3/2; 1/2, 1/2\rangle$	$N\ \pi\ \pi$					169	0·068	84	0·034	84	0·034
	$\Delta^{+}(1700)$											
5	$\|1/2; 3/2, 1/2\rangle$	$N\ \pi\ \pi$					738	0·294	211	0·084	527	0·210
6	$\|1; 3/2, 1/2\rangle$	$\pi\ \pi\ N$					106	0·042	0	0	106	0·042
7	$\|3/2; 3/2, 1/2\rangle$	$N\ \pi\ \pi$	See table (5-3) Columns 3 to 6				154	0·061	16	0·006	138	0·055
8	$\|2; 3/2, 1/2\rangle$	$\pi\ N\ \pi$					1372	0·546	422	0·168	950	0·378

The numbers and cross sections of NO FIT events (columns 7 to 12) are calculated from the number of $N^{*++}(1700)$ events seen in the four pronged 4C FIT channel, see table (5-5), which is about 211 events.

to the NOFIT channel (E) in the reaction

$$\pi^+ P \rightarrow \pi^+ n \; e^+ \hookrightarrow \pi^+ \pi^0$$

d) in the case of $\pi^+ N^{*+}(1700)$ events where the $N^{*+}(1700)$ decays to $P\pi^+\pi^-$ there can be contributions in both two pronged NOFIT channels (D) and (E) from the related $P\pi^0\pi^0$ state and $n\pi^+\pi^0$ state. The amount of the contributions are given in table (5-6), see columns 7 to 12.

e) for the $\Delta^{++} f^0$ and for those $\Delta^{++}\pi^+\pi^-$ where the π^+ is associated with the π^- through a di-pion state, there can be a contribution in the two pronged NOFIT channel (D) from the related $\pi^0\pi^0$ state since the f^0 can decay by the $\pi^0\pi^0$ mode.

f) where the π^- is associated with the Δ^{++} as a $\Delta^{++}\pi^-$ state there can be contributions in both NOFIT channels (D) and (E) from the related $\Delta^+\pi^0$ state and $\Delta^0\pi^+$ state. The branching ratios are given by:-

$$\Delta^{++}\pi^- : \Delta^+\pi^0 : \Delta^0\pi^+$$
$$1/5 : 2/5 : 2/5$$

where Δ^+ decays to $P\pi^0$ to give a final state

$$\pi^+ P \rightarrow P\pi^+\pi^0\pi^0$$

and Δ^0 decays to $n\pi^0$ to give a final state

$$\pi^+ P \rightarrow \pi^+\pi^+ n\pi^0$$

From inspection of table (5-5), using the above calculation, the expected number of events and cross-sections in the two pronged NOFIT channels for this kind of process are given in table (5-7).

TABLE (5-7)

REMAINDER: $\Delta^{++}\pi^+\pi^-$		EXPECTED NUMBER OF EVENTS AND CROSS-SECTIONS			
FIT CHANNEL (H)		NOFIT CHANNEL (D)		NOFIT CHANNEL (E)	
No. of Event	Cross-Section (mb)	No. of Event	Cross-Section (mb)	No. of Event	Cross-Section (mb)
1322	0.525 ± 0.008	2644	1.050	2644	1.050

g) in the case of P π^+ π^+ π^- (remainder) there are three possibilities, as stated earlier, where the tri-pion (or their di-pion combinations) or any pion associated with the proton do not resonate. These possibilities are:-

I - the P π^+ π^+ π^- system is made up of N π and π π substates.

II - the dipion substate is associated with the proton

III - the three pions are associated through a tri-pion state.

Inspection of tables (5-2), (5-3) and (5-4) show there can be contributions in the two pronged NOFIT channels. The expected number of events and the cross-sections for each possibility are given in tables (5-8), (5-9) and (5-10) respectively.

From tables (5-6), (5-8), (5-9) and (5-10) it can be seen how the expected cross-sections in the two pronged NOFIT channels vary with the ispin configurations through the substates.

5. 2 Five Pronged Reactions

Let us assume that the missing mass in the two pronged

TABLE (5-8)

Column	1	2	3	4	5	6	7	8	9	10	11	12
ROW	ISPIN SUBSTATES $(N\pi\pi\pi)^{++}$		BRANCHING RATIOS				EXPECTED NUMBER OF EVENTS AND CROSS-SECTIONS (mb)					
			FIT	NOFIT CHANNELS		NOFIT	NOFIT CHANNELS (D)+(E)		NOFIT CHANNEL (D)		NOFIT CHANNEL (E)	
			CHANNEL	(D)	(E)	FIT	No. of	Cross-sections	No. of	Cross-sections	No. of	Cross sections
	T $(N\pi)$	T $(\pi\pi)$	(H)				events		events		events	
1	3/2	0	See table (5-2) columns 3 to 6				400	0·159	400	0·159	0	0
2	3/2	1					533	0·212	0	0	533	0·212
3	3/2	2					914	0·363	228	0·091	686	0·272
4	1/2	2					700	0·278	0	0	700	0·278

The numbers and cross-sections of NOFIT events (columns 7 to 12) are calculated from the number of $P\pi^+\pi^+\pi^-$ (remainder) events in the four pronged 4-C FIT channel, see table (5-5), which is about 800 events.

TABLE (5-9)

Column	1	2	3	4	5	6	7	8	9	10	11	12
ROW	STATE		BRANCHING RATIOS			NOFIT / FIT	EXPECTED NUMBER OF EVENTS AND CROSS-SECTIONS (mb)					
			FIT CHANNEL (H)	NOFIT CHANNELS (D)	(E)		NOFIT CHANNELS (D)+(E)		NOFIT CHANNEL (D)		NOFIT CHANNEL (E)	
	$\lvert T^{12}; T, T_3 \rangle$						No. of events	Cross-sections	No. of events	Cross-sections	No. of events	Cross-sections
	$(N\pi\pi)^+$											
1	$\lvert 0; 1/2, 1/2 \rangle$						400	0·159	400	0·159	0	0
2	$\lvert 1/2; 1/2, 1/2 \rangle$						1000	0·398	200	0·080	800	0·318
3	$\lvert 1; 1/2, 1/2 \rangle$		See table (5-3) columns 2 to 6				1600	0·636	0	0	1600	0·638
4	$\lvert 3/2; 1/2, 1/2 \rangle$						640	0·254	320	0·127	320	0·127
5	$\lvert 1/2; 3/2, 1/2 \rangle$						2800	1·113	800	0·318	2000	0·795
6	$\lvert 1; 3/2, 1/2 \rangle$						400	0·159	0	0	400	0·159
7	$\lvert 3/2; 3/2, 1/2 \rangle$		See table (5-3) columns 2 to 6				585	0·232	62	0·024	523	0·208
8	$\lvert 2; 3/2, 1/2 \rangle$						5200	2·067	1600	0·636	3600	1·431

The numbers and cross-sections of NOFIT events (columns 7 to 12) are calculated from the number of $P\pi^+\pi^+\pi^-$ (remainder) events in the four pronged 4-C FIT channel, see table (5-5), which is about 800 events.

TABLE (5-10)

Column	1	2	3	4	5	6	7	8	9	10	11	12
ROW	STATE $\lvert T^{12}; T, T_3 \rangle$		BRANCHING RATIOS			NO FIT / FIT	EXPECTED NUMBER OF EVENTS AND CROSS-SECTIONS (mb)					
			Fit channel (H)	No fit channels			No fit channels (D)+(E)		No fit channel (D)		No fit channel (E)	
				(D)	(E)		No. of events	Cross-sections	No. of events	Cross-sections	No. of events	Cross-sections
	$(\pi\pi\pi)^+$											
1	$\lvert 0; 1, 1 \rangle$						400	0·159	400	0·159	0	0
2	$\lvert 1; 1, 1 \rangle$						800	0·318	800	0·318	0	0
3	$\lvert 2; 1, 1 \rangle$		See table (5-4), Columns 3 to 6				800	0·318	800	0·318	0	0
4	$\lvert 1; 2, 1 \rangle$						463	0·184	463	0·184	0	0
5	$\lvert 2; 2, 1 \rangle$						800	0·318	800	0·318	0	0
6	$\lvert 2; 3, 1 \rangle$						3200	1·272	3200	1·272	0	0

The numbers and cross sections of NO FIT events (columns 7 to 12) are calculated from the number of P $\pi^+\pi^+\pi^-$ (remainder) events in the four pronged 4-C FIT channel, see table (5-5), which is about 800 events

NOFIT channels is composed of three neutral secondary particles. Reactions (D) and (E) would then be written as follows:-

$$\pi^+ P \rightarrow P \pi^+ \pi^\circ \pi^\circ \pi^\circ \qquad \text{(iii)}$$

$$\pi^+ P \rightarrow \pi_s^+ \pi_f^+ n \pi^\circ \pi^\circ \qquad \text{(iv)}$$

These two channels are also equivalent to four pronged 1-C(π°) FIT and 1 -C(n) FIT events

$$\pi^+ P \rightarrow P \pi^+ \pi^+ \pi^- \pi^\circ \qquad \text{(I)}$$

$$\pi^+ P \rightarrow \pi^+ \pi^+ \pi^+ \pi^- n \qquad \text{(J)}$$

In the present case a $N \pi^- \pi^+ \pi^+ \pi^-$ can be seen to occur as channels (I) or (J) with a certain cross-section. In principle the contributions to the NOFIT channels (D) and (E) can be calculated. However, the large multiplicity of combinations of the substates makes the calculations more complex. Instead discussion will be limited to quasi two body and three body reactions involving resonances. These are given in table (5-11) where a summary is presented of the 1-C (π°) FIT reaction (I) as found in an earlier part of this collaboration (see ref. 1, 5 and 6). Column 1 shows the reaction final state of well defined processes and remainders. The total number of events, the observed numbers and their cross-section in each channel are given in columns 2, 3 and 4 respectively. From similar arguments to those presented in section 5. 1 and using table (5-11) the expected contributions to NOFIT channels are determined as follows:-

a) in the cases of P π^+ ω°, PB^+ (where B^+ decays to π^+ ω°), Δ^{++} π^- e^+ , Δ^{++} A_2° (the A_2° - meson decays to π^- e^+) and Δ^{++} ω° there can be no contribution to the two pronged NOFIT

TABLE (5-11)

1	2	3	4
THE FOUR PRONGED 1-C (π^0) FIT EVENTS			
REACTION FINAL STATE	Nº. OF EVENTS		CROSS-SECTIONS (mb)
	Total	Observed	
I- $\underline{P\pi^+\pi^+\pi^-\pi^0}$: no. Δ^{++}	2340		0·932 ± 0·014
$P\pi^+\eta^0$, $\eta^0 \to \pi^+\pi^-\pi^0$; A_2^+ EXCL.		65	0·026 ± 0·002
PA^+ , $A_2^+ \to \eta^0\pi^+$		35	0·014 ± 0·001
$P\pi^+\omega^0$, $\omega^0 \to \pi^+\pi^-\pi^0$; B^+ EXCL.		891	0 355 ± 0·010
PB^+ , $B^+ \to \omega^0\pi^+$		230	0·092 ± 0·016
$\pi^+\pi^0 N^{*+}(1700)$, $N^{*+} \to P\pi^+\pi^-$		55	0·022 ± 0·008
$P\pi^+\pi^+\pi^-\pi^0$; REMAINDER		1064	0·423 ± 0·010
II- $\underline{\Delta^{++}\pi^+\pi^-\pi^0}$	4880		1·941 ± 0·025
$\Delta^{++}\bar{e}^{\pm}\pi^{\mp}$, $\bar{e} \to \bar{\pi}\pi^0$; A_2^0 EXCL.		1831	0·728 ± 0·011
$\Delta^{++}A_2^0$, $A_2^0 \to \bar{e}^{\mp}\pi^{\pm}$		367	0·146 ± 0·022
$\Delta^{++}\eta^0$		60	0·024 ± 0·004
$\Delta^{++}\omega^0$		704	0·280 ± 0·014
$\Delta^{++}\pi^+\pi^+\pi^0$; REMAINDER		1918	0·763 ± 0·012
TOTAL : $P\pi^+\pi^+\pi^-\pi^0$	7220		2·873 ± 0·043
Cross-sections are not corrected for unseen decay modes			

channels (D) or (E) since, for example, the ω^o does not decay to $\pi^o\pi^o\pi^o$

b) for the Δ^{++} η^o, PA_2^+ (A_2^+ decays to π^+ η^o) and for those P π^+ η^o where the π^+ is associated with the η^o (or with the proton) through a π^+ η^o (or π^+P) state there can be a contribution in the NOFIT channel (D) since the η^o - meson can decay by the neutral mode (as π^o π^o π^o) as well as by the charged mode (as π^+ π^- π^o). The branching ratio is given by:-

(neutral mode) / (charged mode) = 71/29 = 2.45

Then the number of events and the cross-section expected in the NOFIT channel (D) for these well defined processes are given in table (5-12).

TABLE (5-12)

1	2	3	4	5	6	7
FOUR PRONGED 1-C (π^o) FIT CHANNEL (I)			EXPECTED NUMBER OF EVENTS AND CROSS-SECTIONS			
Reaction	No. of Events	Cross-Section (mb)	NOFIT CHANNEL (D)		NOFIT CHANNEL (E)	
			No. of Events	Cross-Section (mb)	No. of Events	Cross-Section (mb)
$P\pi^+\eta^o$	65	0.026 ± 0.002	160	0.064	-	-
PA_2^+	35	0.014 ± 0.001	86	0.034	-	-
$\Delta^{++}\eta^o$	60	0.024 ± 0.004	147	0.059	-	-
Cross-sections are not corrected for Unseen Decay Modes.						

c) for the π^+ π^o $N^*(1700)$ events where $N^{*+}(1700)$ decays to P π^+ π^- there can be contributions in both two pronged NOFIT

channels. Then the expected contributions are shown in table (5-13), see columns 7 to 12.

d) in the case of $\Delta^{++}\ \pi^+\ \pi^-\ \pi^0$ (remainder), where the three pions are associated through a tri-pion state, there can be a contribution in the NOFIT channel (D) and the amount of the different ispin configurations is given in table (5-14).

Again, from tables (5-13) and (5-14) it can be seen how the expected cross-sections in the two pronged NOFIT channels vary with the ispin configurations through the substates.

5. 3 Conclusions

I. In the case of the missing mass in the two pronged NOFIT channels comprising two neutral secondary particles it can be seen that in the majority of cases there can be contributions to these channels from resonances seen in the equivalent four pronged 4-C FIT events. The predicted signals are expected to be strong enough to be detected and it might be possible with quasi two body and three body reactions involving resonances to pinpoint the particular ispin state or ispin substate which is present in the interaction. As an example, for the $N^{*+}(1700)$ in the channels

$$\pi^+ P \longrightarrow \pi^+ P\ \pi^0\pi^0$$
$$\pi^+ P \longrightarrow \pi_f^+\ \pi_s^+\ n\ \pi^0$$

there are many possibilities for the ispin configurations through this substate, and by comparison with the observed cross-section it might be possible to determine the ispin substate.

II. If the missing mass in the two pronged NOFIT channels is composed of three neutral secondary particles it can be seen that in the majority of cases for well defined processes in the

TABLE (5-13)

Column	1	2	3	4	5	6	7	8	9	10	11	12
ROW	STATE $\|T^{12};T,T_3\rangle$	DECAY MODE	BRANCHING RATIOS I-C(π^0) FIT Channel (I)	No fit channels (D)	No fit channels (E)	NOFIT / FIT	EXPECTED NUMBER OF EVENTS AND CROSS-SECTIONS (mb) Nofit channels: (D)+(E) No. of events	Nofit channels: (D)+(E) Cross-sections	Nofit channel (D) No. of events	Nofit channel (D) Cross-sections	Nofit channel (E) No. of events	Nofit channel (E) Cross-sections
	$N^{*+}(1700)$											
1	$\|0;1/2,1/2\rangle$	$\pi\pi N$					28	0·011	28	0·011	0	0
2	$\|1/2;1/2,1/2\rangle$	$N\pi\pi$					69	0·028	14	0·006	55	0·022
3	$\|1;1/2,1/2\rangle$	$\pi\pi N$	See table (5-3) columns 3 to 6				110	0·044	0	0	110	0·044
4	$\|3/2;1/2,1/2\rangle$	$N\pi\pi$					44	0·018	22	0·009	22	0·009
	$\Delta^{+}(1700)$											
5	$\|1/2;3/2,1/2\rangle$	$N\pi\pi$					193	0·077	55	0·022	138	0·055
6	$\|1;3/2,1/2\rangle$	$\pi\pi N$					28	0·011	0	0	28	0·011
7	$\|3/2;3/2,1/2\rangle$	$N\pi\pi$	See table (5-3) columns 3 to 6				40	0·016	4	0·002	36	0·014
8	$\|2;3/2,1/2\rangle$	$\pi N\pi$					358	0·143	110	0·044	248	0·099

The numbers and cross-sections of NOFIT events (columns 7 to 12) are calculated from the number of $N^{*+}(1700)$ events seen in the four pronged I-C(π^0) FIT channel, see table (5-11), which is about 55 events.

TABLE (5-14)

COLUMN	1	2	3	4	5	6	7	8
ROW	$(\pi\pi\pi)^o$: ISPINS		BRANCHING RATIOS			NOFIT / FIT	EXPECTED NUMBER AND CROSS-SECTION IN THE TWO PRONGED NOFIT CHANNEL (D)	
	SUBSTATE	FINAL STATE	1-C(π^o)FIT CHANNEL (I)	NOFIT CHANNELS (D)	(E)			
	$\lvert T^{12} ; T, T_3 \rangle$						No. of Events	Cross-Section (mb)
1	$\lvert 1 ; 0, 0 \rangle$		1	0	0	0	0	0
2	$\lvert 2 ; 1, 0 \rangle$		11/15	4/15	0	4/11	698	0.277
3	$\lvert 2 ; 2, 0 \rangle$		1	0	0	0	0	0
4	$\lvert 2 ; 3, 0 \rangle$		3/5	2/5	0	2/5	767	1.305

The number and cross-sections of NOFIT events (columns 7 and 8) are calculated from the number of $\Delta^{++}\pi^+\pi^-\pi^o$ (remainder) events seen in the four pronged 1-C(π^o)FIT channel, see table (5-11), which is about 1918 events.

equivalent four pronged 1-C (π^0) FIT there can be no contributions in these channels. However, in the case of quasi two body and three body interactions involving resonances, the prediction of signal expected in the two pronged NOFIT channel (D) is much stronger than the observed signal in the equivalent four pronged 1-C (π^0) FIT events. For example, in the quasi two body reaction (PA_2^+) the expected signal in the two pronged NOFIT channel (D) is more than twice the observed signal in the four pronged 1-C(π^0) FIT events.

CHAPTER 6

AN ANALYSIS OF THE TWO PRONGED NOFIT $\pi^+ \pi^+$ CHANNEL

The selection of events and the resolution for the two pronged NOFIT channel (E),

$$\pi^+ P \rightarrow n \pi_s^+ \pi_f^+ (m_1 \pi^o) \qquad \text{(E)}$$

with m_1 greater than zero, have already been discussed in chapter 4 (see sections 4. 1 and 4. 4). This channel contains about 7000 events which include about 350 misclassified P π^+ MM_1 events that is the two pronged NOFIT channel (D). The total cross-section is 2.77 $\pm$ 0.03 mb after correcting for these misinterpreted events. Indeed, in examining the missing mass and the invariant mass combinations it should be remembered that they contain some misclassified events. So any unusual structure must first be considered as due to a misinterpretation of these events as π_s^+ π_f^+ MM_2 , $MM_2 = n (m_1 \pi^o)$.

An analysis of the spectra of the missing mass (MM_2) and the invariant mass combinations (π_s^+, π_f^+), (π_f^+, MM_2) and (π_s^+, MM_2) are given in the following sections.

6. 1 The Missing Mass Distribution

The missing mass comprises a neutron and at least one neutral pion. In general the programme FAKE (which is a Monte Carlo programme to simulate the production of events) suggests that the missing masses are composed of a mixture of two neutral particle states and three neutral particle states (n π^o and n π^o π^o). The mixture is approximately 50% each. Figure

(6-1) shows the missing mass (MM_2) spectrum. By using the programme FAKE about 6000 events of reaction

$$\pi^+ P \rightarrow \pi^+ \pi^+ n \pi^o \qquad \text{(ii)}$$

and the same number of events of reaction

$$\pi^+ P \rightarrow \pi^+ \pi^+ n \pi^o \pi^o \qquad \text{(iv)}$$

have been generated. For these two reactions the missing masses ($n \pi^o$) and ($n \pi^o \pi^o$) are plotted on figure (6-1) where the dash-dot curve displays the phase space background of the ($n \pi^o$) and the dashed curve shows the phase space background of the ($n \pi^o \pi^o$). It can be seen that neither of these will fit the experimental data. However, the experimental data has been fitted by mixing the above two reactions as follows:-

$$a\, x_i + b\, y_i = z_i \qquad 6.1$$

where a and b are constants to be determined in the fit and x_i, y_i and z_i are the expected numbers for $n \pi^o$, $n \pi^o \pi^o$ and the mixture events of i th bins of the missing mass. For this purpose assume that the observed number of events in the i th bin of the experimental data is N_i and constants a and b are adjusted until

$$\sum (z_i - N_i)^2 = \text{minimum} \qquad 6.2$$

This gives $a = 0.46 \pm 0.04$ and $b = 0.54 \pm 0.05$. The result of equation 6.1 is shown in figure (6-1) as a solid curve. Now, it can be seen that the phase space background of the admixture of reaction (ii) and reaction (iv) fits the experimental distribution of the missing mass quite well. Any structure in the missing mass spectrum can be seen to have no significance. Consequently, there is no evidence for the decay of neutral baryons to all neutral secondaries. This does not mean that there is no resonance

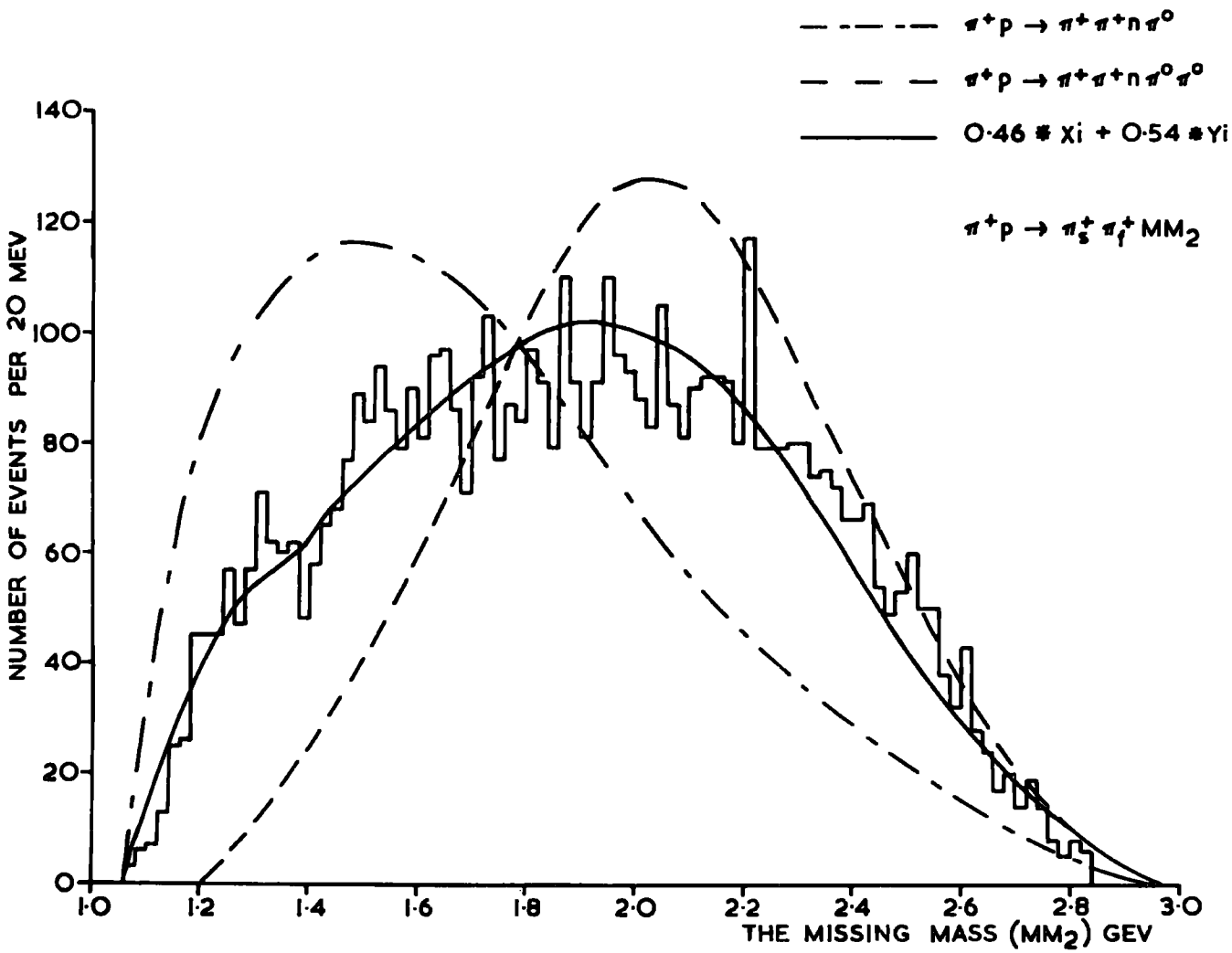

FIG. (6–1) THE MISSING MASS SPECTRUM FOR THE REACTION $\pi^+p \rightarrow \pi_s^+\pi_f^+MM_2$ AT 5 GEV/C INCIDENT MOMENTUM.

production at all. It could be that

$$\pi^+ P \longrightarrow B^+ M^+$$

where B and M refer to baryon and meson respectively. As an example, assume that the above reaction gives

$$\pi^+ P \longrightarrow \Delta^+ \rho^+ \quad \rho^+ \longrightarrow \pi^+ \pi^\circ \quad \Delta^+ \longrightarrow (N\pi)^+ \qquad \text{(vi)}$$

This could lead to either

$$\pi^+ P \longrightarrow P \pi^\circ \pi^+ \pi^\circ \qquad \text{(vii)}$$

which would be classified in channel (D), or

$$\pi^+ P \longrightarrow n \pi^+ \pi^+ \pi^\circ \qquad \text{(viii)}$$

which corresponds to channel (E).

Events of the kind channel (vi) have been generated by the programme FAKE and it is found that the missing mass to the two positive pions of reaction (viii) is very similar to the missing distribution of events of this same reaction generated as phase space by the programme FAKE, see figure (6-1) the dash-dot curve.

6. 2 The Invariant Mass Combinations

From a similar argument to that discussed (missing mass phase space) in section 6. 1, the phase space background of the invariant mass system is calculated using the programme FAKE and equation 6.1 for the admixture of reactions (ii) and (iv). Here again, the invariant mass combinations (π_s^+, π_f^+) (π_f^+, MM_2) and (π_s^+, MM_2) are given in figures (6-2), (6-3) and (6-4) respectively. The solid curve in these figures shows the phase space background and it also fits the experimental

distributions quite well.

6.2.1 The Di-Pion System

The effective mass distribution of the di-pion system is shown in figure (6-2); there is no structure to be seen.

6.2.2 The (π^+, MM_2) System

The invariant mass combinations of (π^+, MM_2) are given in two figures (6-3) and (6-4). In the first the fast pion is combined with missing mass, and in the other the slow pion is associated with the missing mass. From the subsequent analysis of these two figures it can be seen that:-

a) in the case of the (π_f^+, MM_2) mass combination there is no structure to be observed.

b) in the (π_s^+, MM_2) mass spectrum the structures seen appear to be consistant with statistical fluctuations. However, in chapter 5 (section 5. 1) it was seen that a signal was expected in the mass region at about 1700 Mev corresponding to the alternative decay mode of the $N^{*+}(1700)$ resonance (see ref. 1, 2, 3, 4 and 5). There is an enhancement at this mass in figure (6-4) and for the present purpose it will be assumed that this is significant. A check has been made to determine whether these enhancements are due to the small contamination from the wrongly interpreted P π^+ MM_1 events. For this purpose all events in the channel (E) with the invariant (π_s^+, MM_2) mass between (1600 - 1800) Mev have been reconsidered as P π^+ MM_1 and the P π^+ invariant mass plotted. Now, it was seen earlier that a characteristic of the P π^+ combination is peaking in the Δ^{++} region (see figure (4-3) in chapter 4). This is not seen in the present case which shows

FIG.(6-2) EFFECTIVE MASS DISTRIBUTION OF (π_s^+, π_f^+) SYSTEM FOR THE REACTION $\pi^+ p \rightarrow \pi_s^+ \pi_f^+ MM_2$ AT 5 GEV/C. THE SOLID CURVE SHOWS THE PHASE SPACE BACKGROUND OF THE ADMIXTURE.

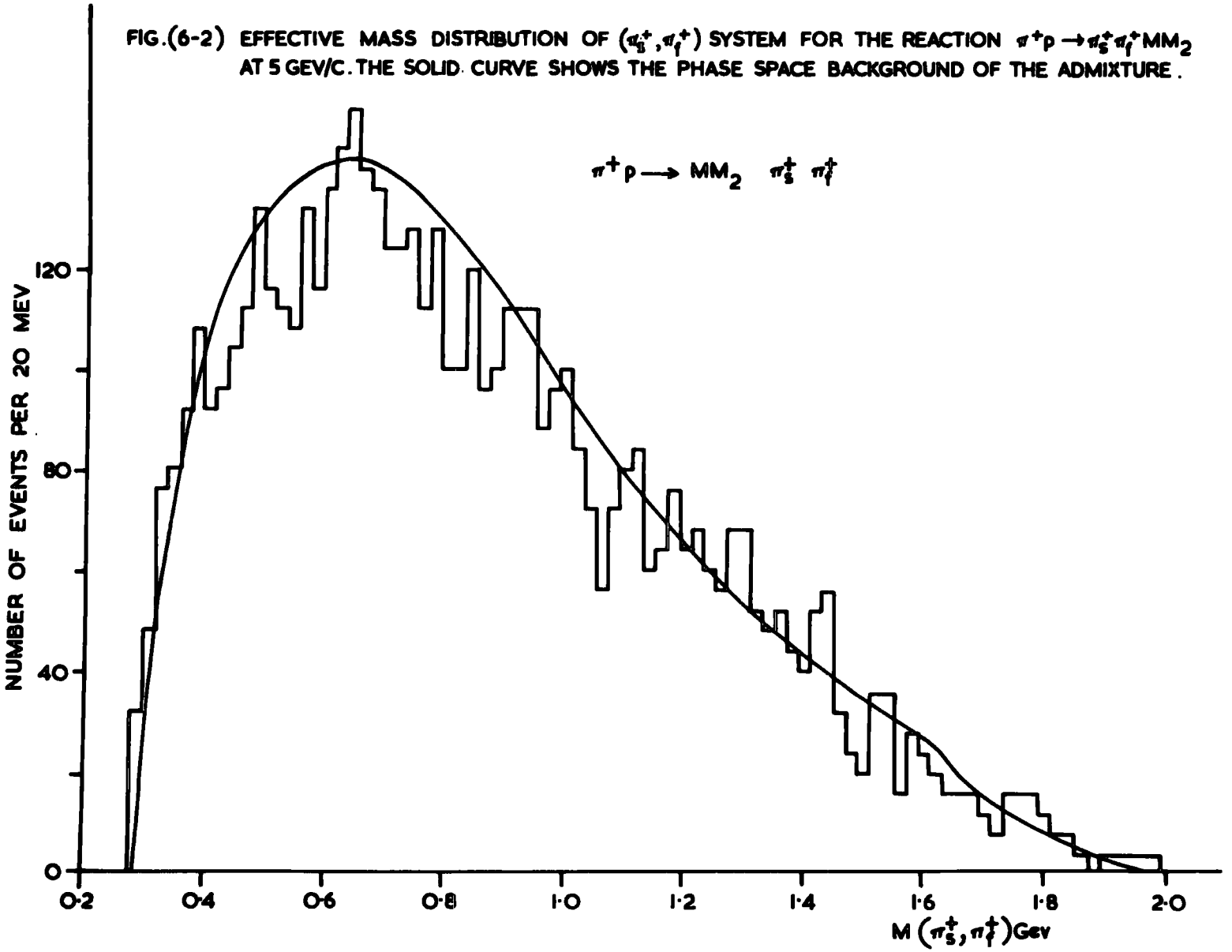

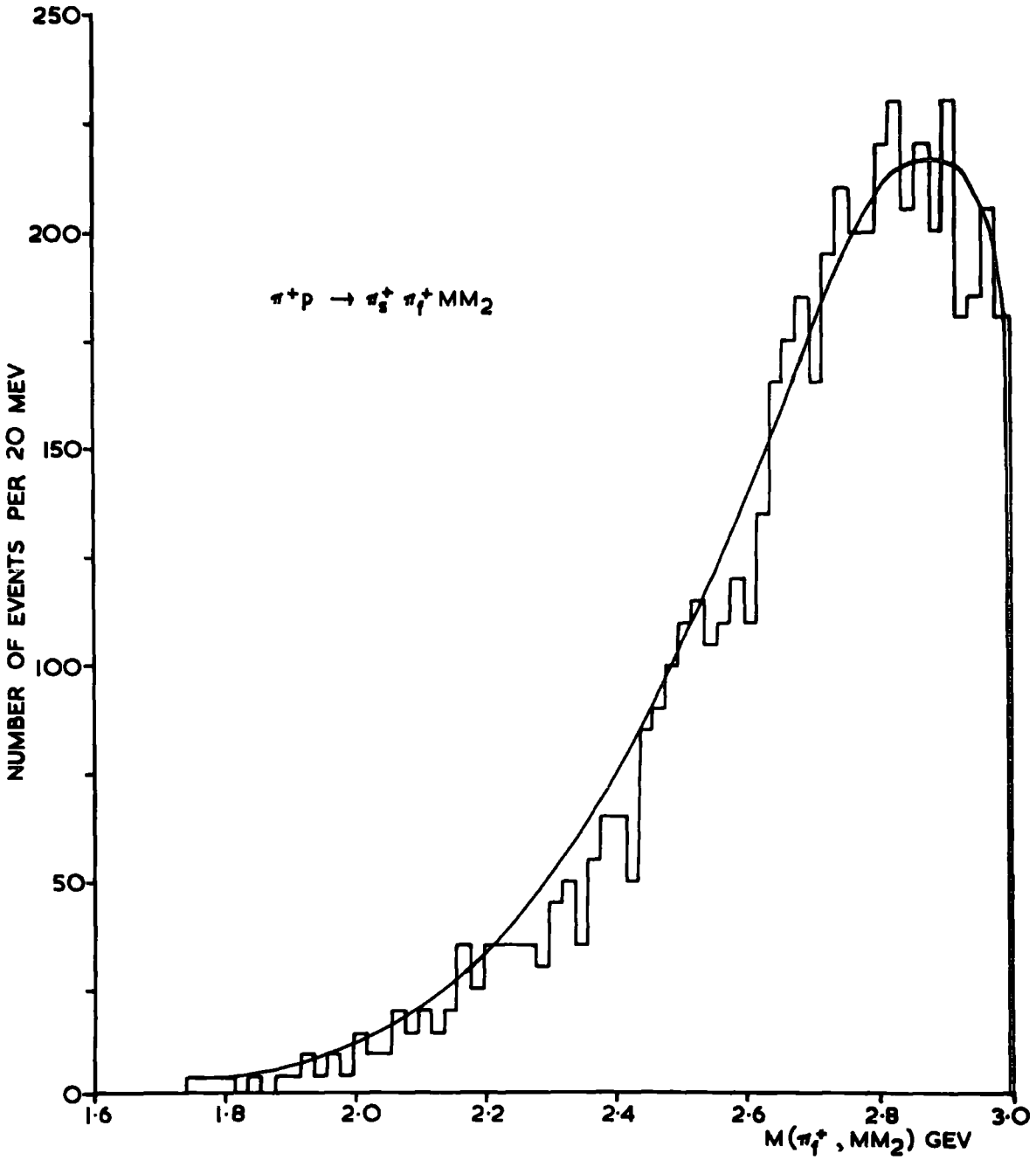

FIG. (6–3) EFFECTIVE MASS DISTRIBUTION OF (π_f^+, MM_2) SYSTEM FOR THE REACTION $\pi^+ p \rightarrow \pi_s^+ \pi_f^+ MM_2$ AT 5 GEV/C. THE SOLID CURVE DISPLAYS THE PHASE SPACE BACKGROUND OF THE ADMIXTURE.

FIG. (6-4) EFFECTIVE MASS DISTRIBUTION OF (π_s^+, MM_2) SYSTEM FOR THE REACTION $\pi^+p \rightarrow \pi_s^+ \pi_f^+ MM_2$ AT 5 GEV/C. THE SOLID CURVE SHOWS THE PHASE SPACE BACKGROUND OF THE ADMIXTURE.

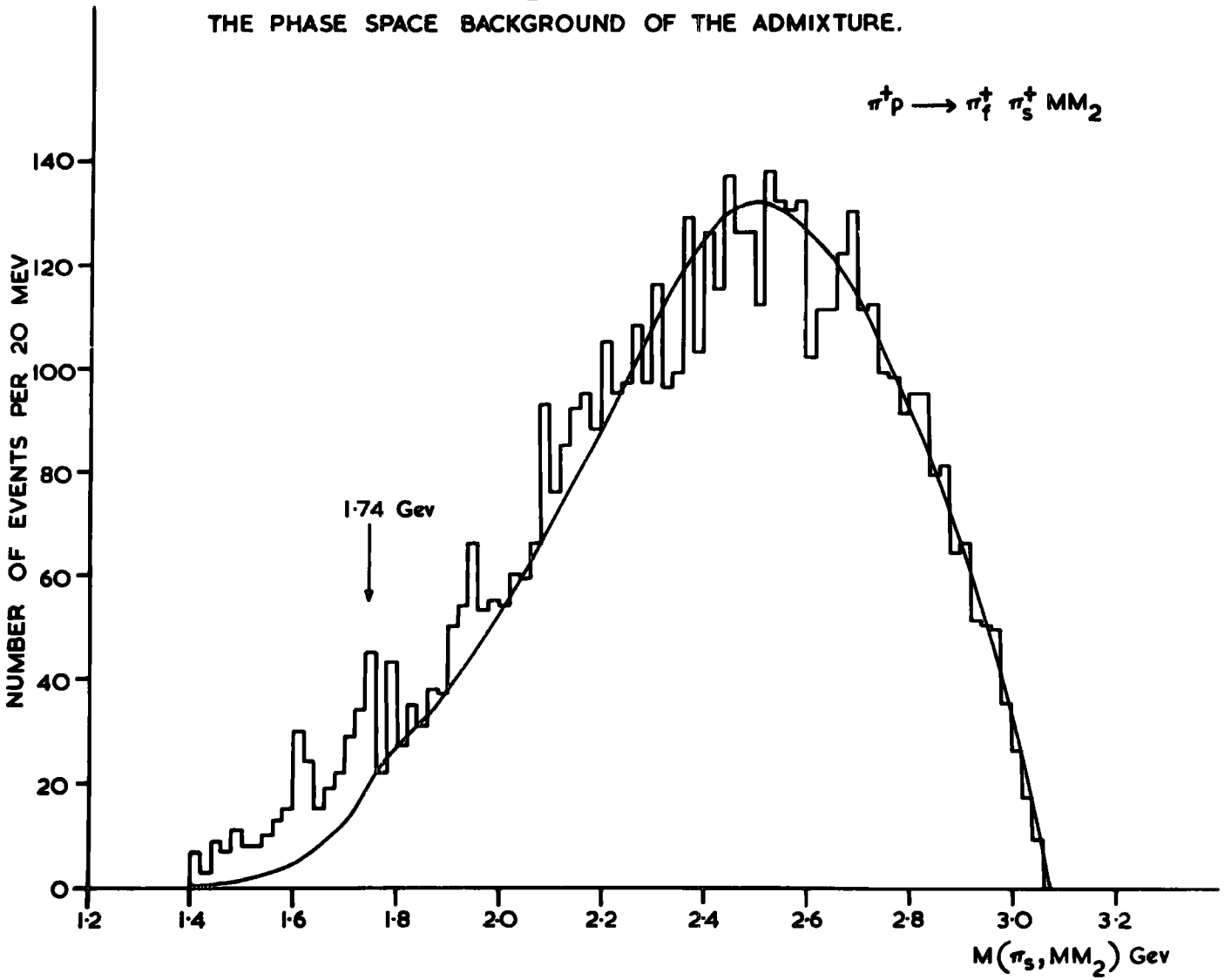

that the apparent structure at 1700 Mev is not due to the misinterpretation of the P π^+ MM_1 events.

6. 3 $N^{*+}(1700)$ in the NOFIT Channel (E)

The most likely origin of the structure at 1700 Mev in figure (6-4) is by the production of the $N^{*+}(1700)$ in the reaction

$$\pi^+ P \rightarrow \pi_f^+ N^{*+}(1700)$$
$$\hookrightarrow \pi_s^+ n \pi^o$$

where $N^{*+}(1700)$ decays to π^+_s n π^o directly. Experimentally, there is no evidence that N^{*+} decays indirectly via Δ^o π_s^+ where Δ^o decays to n π^o, since otherwise there would be a corresponding peak in the missing mass spectrum figure (6-1).

As stated earlier, the phase space background has been calculated by FAKE for reactions (ii) and (iv). The n π^o π^+ π^+ and n π^o π^o π^+ π^+ interactions have been mixed according to the same prescription as in figure (6-1) and is shown as a solid curve in figure (6-5). Figure (6-5) is a part of figure (6-4) but with the invariant ($\pi\pi_s^+$, MM_2) mass between (1400 - 2200) Mev replotted. Below 1800 Mev the phase space background is entirely made up by reaction (ii). Possibly there is an enhancement in the mass region at about 1700 Mev, where the $N^{*+}(1700)$ is expected to appear.

The lower mass region (1660 - 1900) Mev of figure (6-5) has been fitted with a background and a Breit Wigner signal added incoherently, that is

$$\text{Signal} = \text{BG} + \text{B.W.}(M_o, \Gamma_o) \qquad 6.3$$

where BG is the phase space background and B.W. is an S - wave Breit Wigner signal centred at mass M_o with width Γ_o, that is

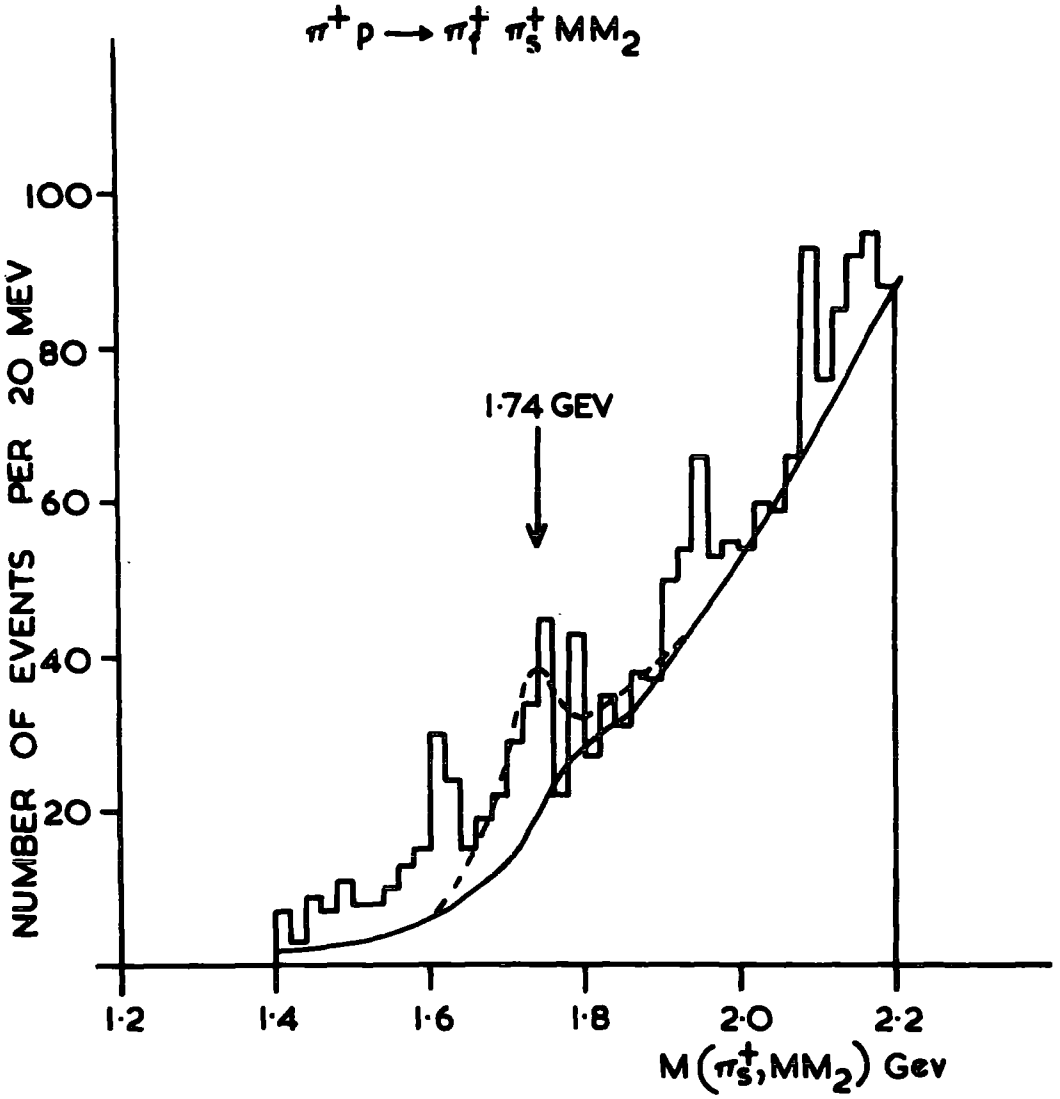

FIG.(6-5) EFFECTIVE MASS DISTRIBUTION OF (π_s^+, MM_2) SYSTEM. THE DASHED CURVE CORRESPONDS TO $M_0 = 1{\cdot}734 \pm 0{\cdot}021$ GEV AND $\Gamma_0 = 0{\cdot}084 \pm 0{\cdot}013$ GEV.

the dotted curve in figure (6-5). In the fitting M_o and Γ_o are free parameters. The result of the fitting is:-

$$M_o = 1.734 \pm 0.021 \text{ Gev}$$

$$\Gamma_o = 0.084 \pm 0.013 \text{ Gev}$$

$$N(\text{number of events above BG}) = 79 \pm 10 \text{ events}$$

$$\sigma \text{ (cross-section)} = 0.033 \pm 0.004 \text{ mb}$$

If the signal is significant then reference can be made to table (5-6) in the last chapter where predictions were made in the expected intensity of $N^{*+}(1700)$ in the NOFIT channels given that the $N^{*+}(1700)$ had been observed in the four pronged 4-C FIT channel (H). By examining columns 11 and 12 of that table the present estimated cross section of (33 ± 4) μb is consistant with the idea that the signal in $N\pi\pi$ seen at 1700 Mev is:-

a) an $N^{*+}(1700)$, see row 4 of table, or b) an $\Delta^+(1700)$, see rows 6 and 7 of the table.

It can be seen that the ambiguity in this interpretation can be resolved by searching for the signal in the other two pronged NOFIT channel (D) where for the N^{*+} interpretation there should be an equal signal to the one above, whereas in the Δ^+ interpretation there should be negligible signal.

This point will be referred to again in the chapter on channel (D).

Attempts have been made to isolate any signal in the 1700 Mev region by demanding small 4 - momentum transfer from the primary π^+ to the fast secondary π^+_f. The danger of this is that apart from removing background, the signal looked for

is also reduced. Figure (6-7) shows the effect of demanding t ($\pi^+ / \pi\pi^+_f$) to be less than 0.25 $(Gev/c)^2$. Relatively the enhancement at 1700 Mev is seen to be more significant. The Breit Wigner signal (equation 6.3) shown has been fitted to the data assuming smooth curve hand-drawn background. The fitted parameters of the Breit Wigner signal are:-

$$M_o = 1.738 \pm 0.030 \text{ Gev}$$

$$\Gamma_o = 0.100 \pm 0.016 \text{ Gev}$$

The dotted curve in figure (6-6) corresponds to this fit. The observed number of events above the background is equal to 69 ± 8, implying a cross-section of 30 ± 3 μb. These are consistant with the earlier determination.

In chapter 4 (see sub-section 4.4.3) it was seen that the expected full width at half height, for the $N^{*+}(1700)$, of about 80 Mev. This value agrees very well with the experimental values.

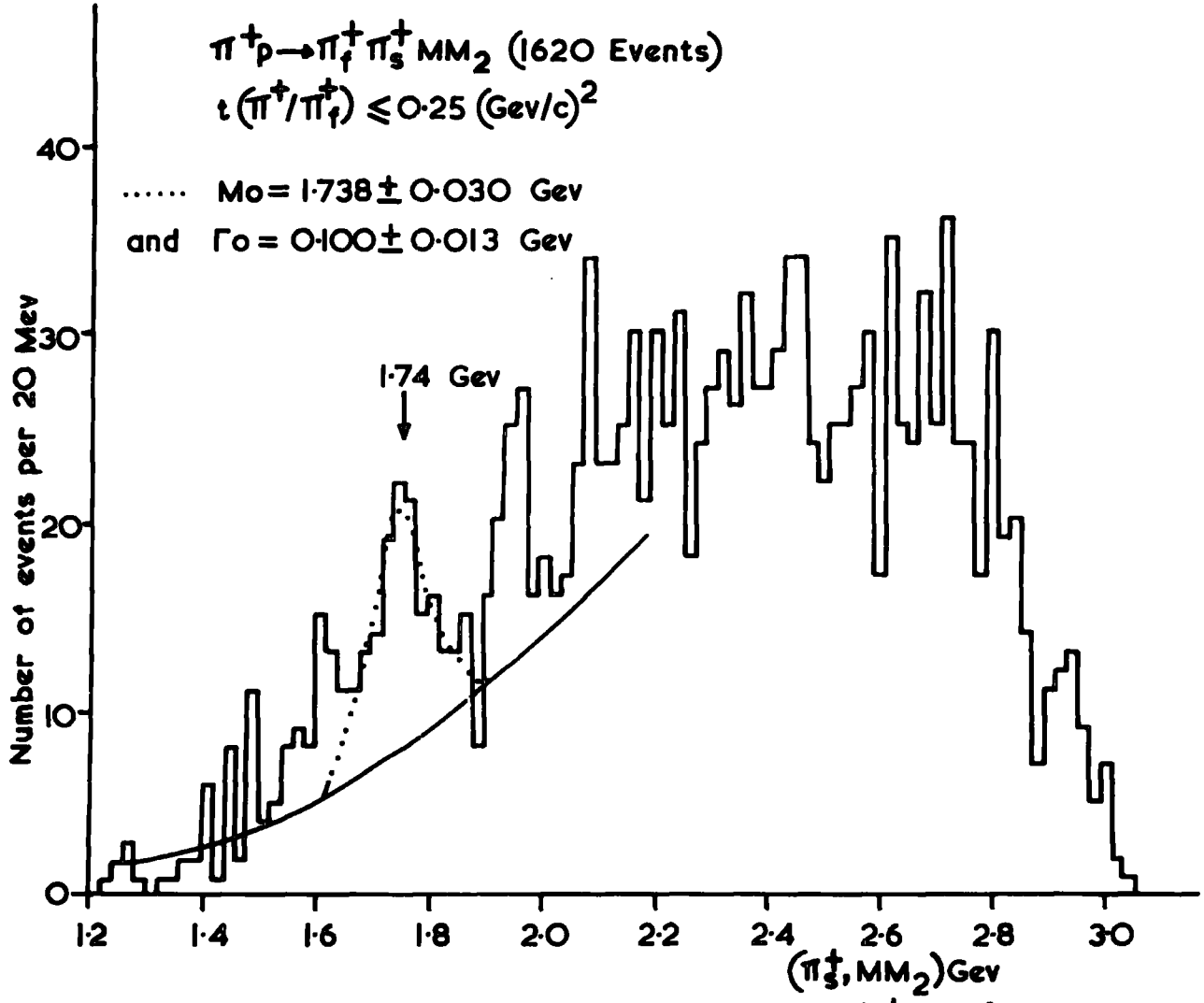

Fig. (6-6) The effective mass distribution of the (π_s^+, MM_2) system in the channel $\pi^+p \rightarrow \pi_s^+ \pi_f^+ MM_2$ at 5 Gev/c.
Distribution obtained by demanding $t(\pi^+/\pi_f^+) \leq 0.25$ (Gev/c)^2

CHAPTER 7

CHARACTERISTICS OF THE TWO PRONGED NOFIT P π^+ CHANNEL

The events belonging to this channel,

$$\pi^+ P \longrightarrow P\ \pi^+ (m_2\ \pi^o) \qquad (D)$$

with m_2 greater than 1, all have a proton slow enough to be identified (that is these are the unambiguous NOFIT events). In chapter 4 details have been given about the selection of events for this channel. It contains about 6300 events excluding 350 with a proton momentum in excess of 1500 Mev/c in the laboratory system which have been misinterpreted as π_s^+ π_f^+ MM_2 events. The total cross section is 2.78 $\pm$ 0.03 mb after correcting for these misclassified events.

An analysis of the distributions of the missing mass and the invariant mass combinations is given in the following sections. In the subsequent analysis of the missing mass it should be remembered that the signal of a resonance expected in the missing mass below 1 Gev might be distorted by the fitting process (see sub-section 4.3.1 in chapter 4). Because of this it is essential to study the missing mass distribution in both channels UNFIT and NOFIT events to determine which of these channels should be used in the subsequent analysis of the missing mass. For this purpose, the missing mass systems were each divided into 60 Mev bins. For each bin the ratio between the numbers of NOFIT records to the number of UNFIT records has been determined. In figure (7-1) these ratios are plotted as a function of the missing mass. From this figure it can be seen, for example, that in the η^o-meson region (550 Mev) 96% of the

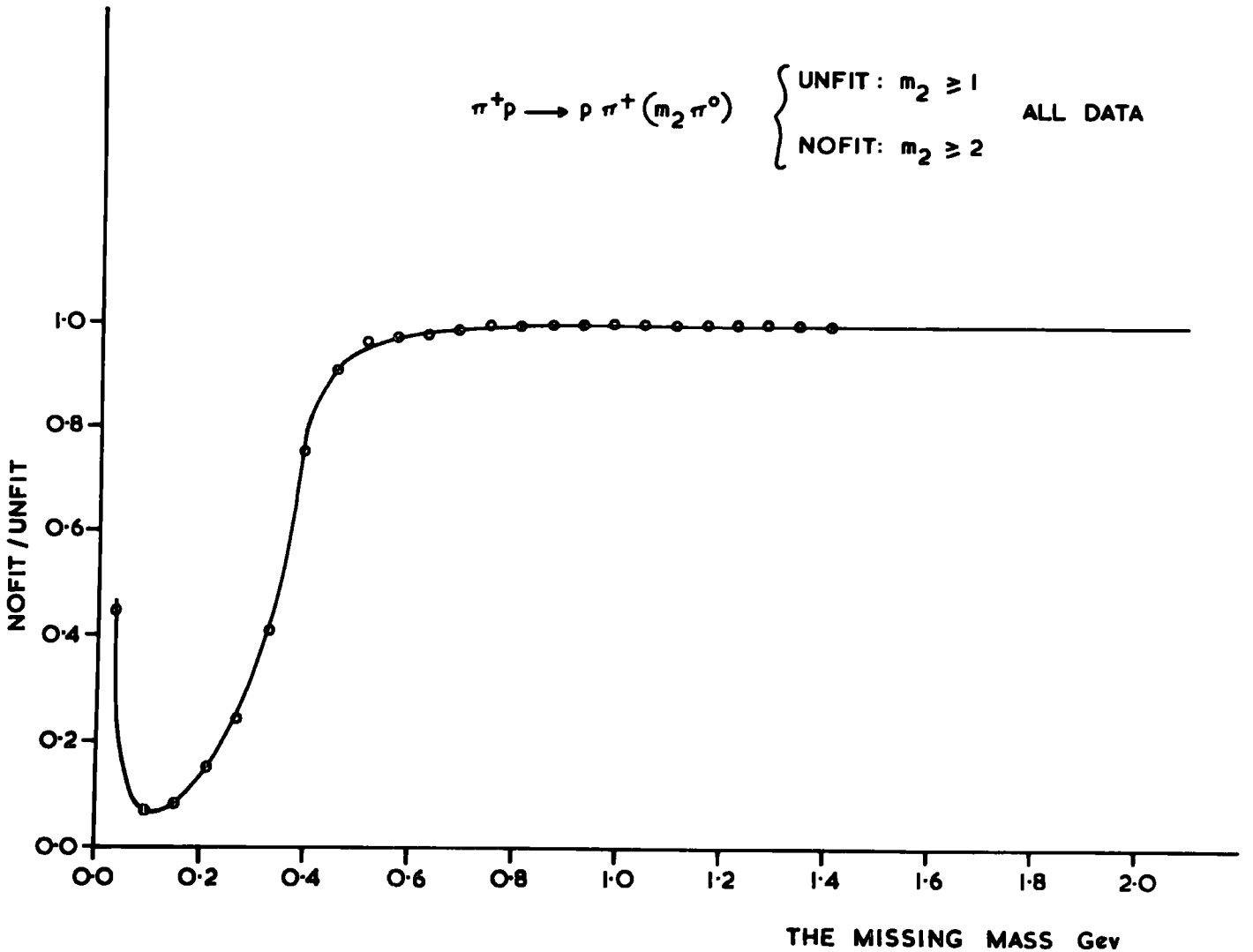

FIG.(7-1) THE RATIO OF (NO FIT/UNFIT) AS A FUNCTION OF THE MISSING MASS.

signal is contained in the NOFIT records and in the f^o-meson region (1260 Mev) all the f^o signal is in the NOFIT records rather than UNFIT records. Therefore, it is sufficient to use NOFIT rather than UNFIT records in the subsequent analysis of the missing mass.

7. 1 The Experimental Data

In this section the general features of the missing mass system and the invariant mass combinations are examined after selecting positive missing mass squared. In particular an estimate is made of the phase space background by using the programme FAKE.

7.1.1 The Missing Mass (MM_1) Distribution

The missing mass is composed of at least two neutral pions in the two pronged NOFIT channel (D). The missing mass distribution is presented in figure (7-2). Here again, programme FAKE was used to determine the phase space background for reaction

$$\pi^+ P \longrightarrow P \pi^+ \pi^o \pi^o \qquad \text{(i)}$$

with 5000 events and with the same number for reaction

$$\pi^+ P \longrightarrow P \pi^+ \pi^o \pi^o \pi^o \qquad \text{(iii)}$$

The missing masses in the above two reactions are plotted in figure (7-2) where the solid curve shows the phase space background for two neutral pions after normalising at MM_1 equal to 0.96 Gev and the dashed curves for the unnormalised three neutral pions. It can be seen that the phase space background of the three neutral pions can not be fitted successfully to the experimental data in any way whereas the phase space background of

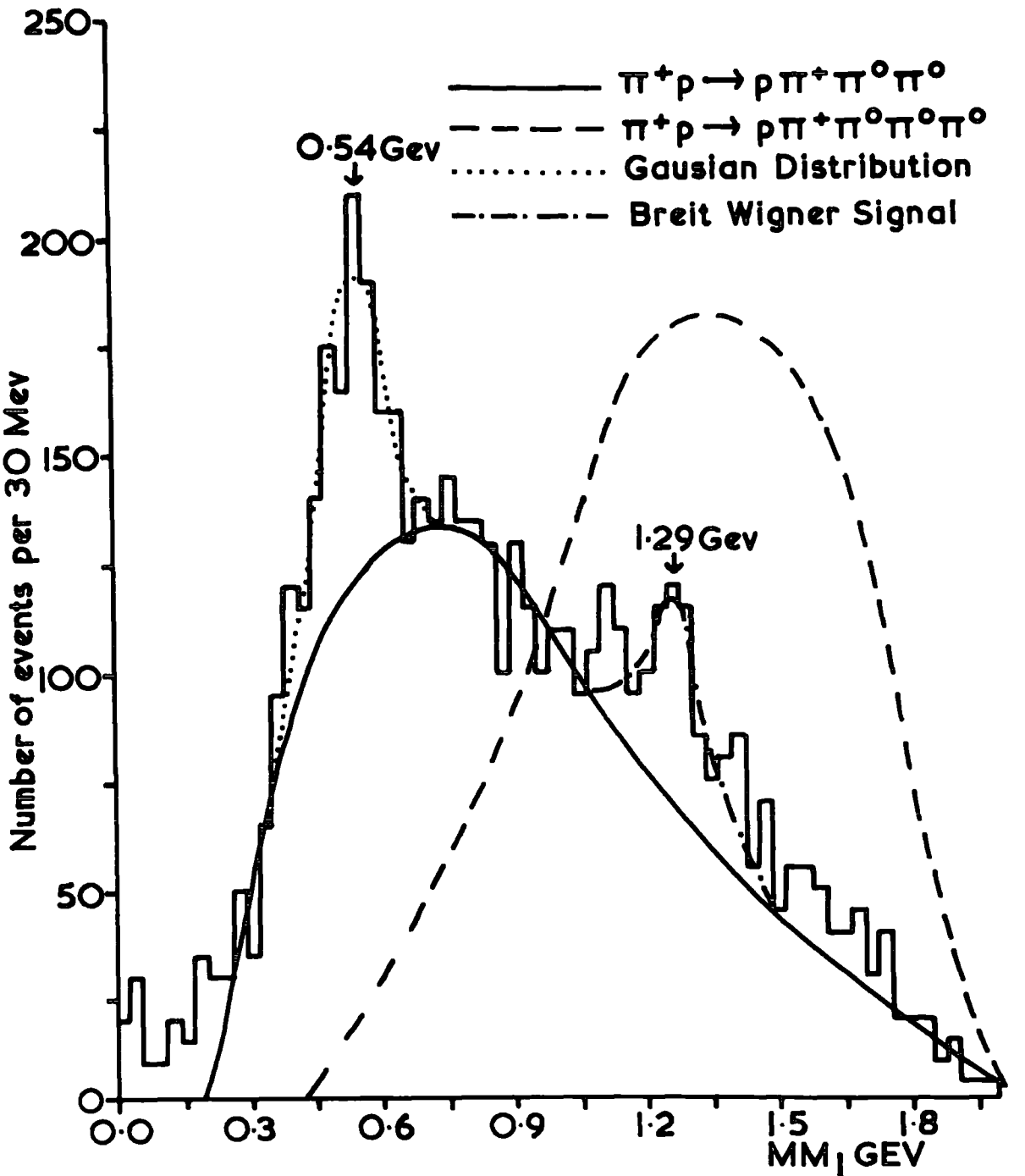

FIG(7-2) The missing mass spectrum for the reaction $\pi^+p \rightarrow p\pi^+MM_1$ (5420 events) at 5 Gev/c.

the two neutral pions fits the experimental distribution quite well. Consequently, the above two channels (i) and (iii) have been mixed by using the same method as before (see section 6.1 in chapter 6) and it is found that the majority of the missing masses corresponds to the two neutral pion phase space. The mixing required about 94% of the two neutral pion and 6% of the three neutral pion phase spaces. Therefore, in the subsequent analysis of this channel it will be assumed that the MM1 mass, in general, comprises two neutral pions only.

The significance of any structure can now be judged relative to this fitted background. It can be seen that there is evidence for the decay of neutral mesons to all neutral secondaries. For example, the structure to be seen at a mass of about 550 Mev corresponds to the η^o-meson and that at a mass of about 1280 Mev corresponds to either, or both, the f^o meson and the A_2^o meson. Here the f^o decays to two neutral pions and the A_2^o decays to $\pi^o \eta^o$ with the subsequent decay of the η^o to all neutral secondaries.

The lower mass region (300 - 750) Mev of figure (7-2) has been fitted with the two neutral pion background above and a Gaussian distribution added as follows:-

$$\text{Signal} = BG + GD(M_{1o}, D) \qquad 7.1$$

where BG is the phase space background and GD is a Gaussian distribution signal centred at mass M_{1o} with standard deviation D and is shown as the dotted curve in figure (7-2). Again, the higher mass region (1140 - 1440) Mev in the same figure has been fitted with a background and an S - wave Breit Wigner signal centred at mass $M_{h\,o}$ with width Γ_o (see section 6.3 in chapter 6) shown as dash - dot curves in the figure. In the

fitting M_{1o}, D, M_{ho} and Γ_o are free parameters. The results of the fitting are given in table (7-1) followed by the observed number of events above the BG and the cross - section for each signal.

TABLE (7-1)

The Fitted Parameters	η^o Meson Region	$f^o/A_2{}^o$ Meson Region
Central Mass (Gev)	0.540 ± 0.008	1.285 ± 0.011
Full Width at Half Height (Gev)	0.145 ± 0.006	0.185 ± 0.008
No. of Events above the Background	430 ± 20	275 ± 30
Cross - Section (mb)	0.180 ± 0.008	0.115 ± 0.013

As stated earlier in chapter 4 (see sub-section 4.3.1) that the expected full widths at half height in the η^o and the f^o regions are about 0.140 Gev and 0.180 Gev. These values agree very well with the experimental values in the table.

7.1.2 The Invariant Mass Combinations

The possible invariant mass combinations are the (P, π^+), (π^+, MM_1) and (P, MM_1). Here, in the subsequent analysis of these combinations the NOFIT channel will be used. Now, in figures (7-3), (7-4) and (7-5) are shown the effective mass distributions of the above three combinations respectively. The solid curves in these figures are the phase space background (calculated by FAKE) corresponding to two neutral pion phase

space. Here again, the significance of any structure can now be judged relative to this fitted background.

Brief descriptions of the invariant mass combinations are given as follows:-

a) The (P, π^+) System

The (P, π^+) mass spectrum is shown in figure (7-3). The only structure to be seen there is a very strong peak in the Δ^{++}(1236 Mev) region. The lower mass region, from the threshold to 1400 Mev, in this figure has been fitted with an S - wave Breit Wigner signal centred at mass M_o with width Γ_o added incoherently to the background (see equation 6.3 in chapter 6) and is shown as the dotted curve in figure (7-3). As before, M_o and Γ_o are free parameters in the fitting and the result is:-

$$M_o = 1.220 \pm 0.003 \quad \text{Gev}$$
$$\Gamma_o = 0.116 \pm 0.002 \quad \text{Gev}$$

The observed number of events above the background is equal to 1400 ± 40, implying a cross-section of 0.585 ± 0.017 mb.

From the above result it can be seen that the production of the Δ^{++} (1236), T = 3/2, in the NOFIT channel (D) is about 26%.

b) The (π^+, MM_1) System

Figure (7-4) displays the invariant (π^+, MM_1) mass distribution. None of the structure in this figure can be seen to be very significant. However, in chapter 5 (see section 5. 1) it was seen that a signal is expected in the mass region of A_2^+ (1300 Mev) corresponding to the alternative decay

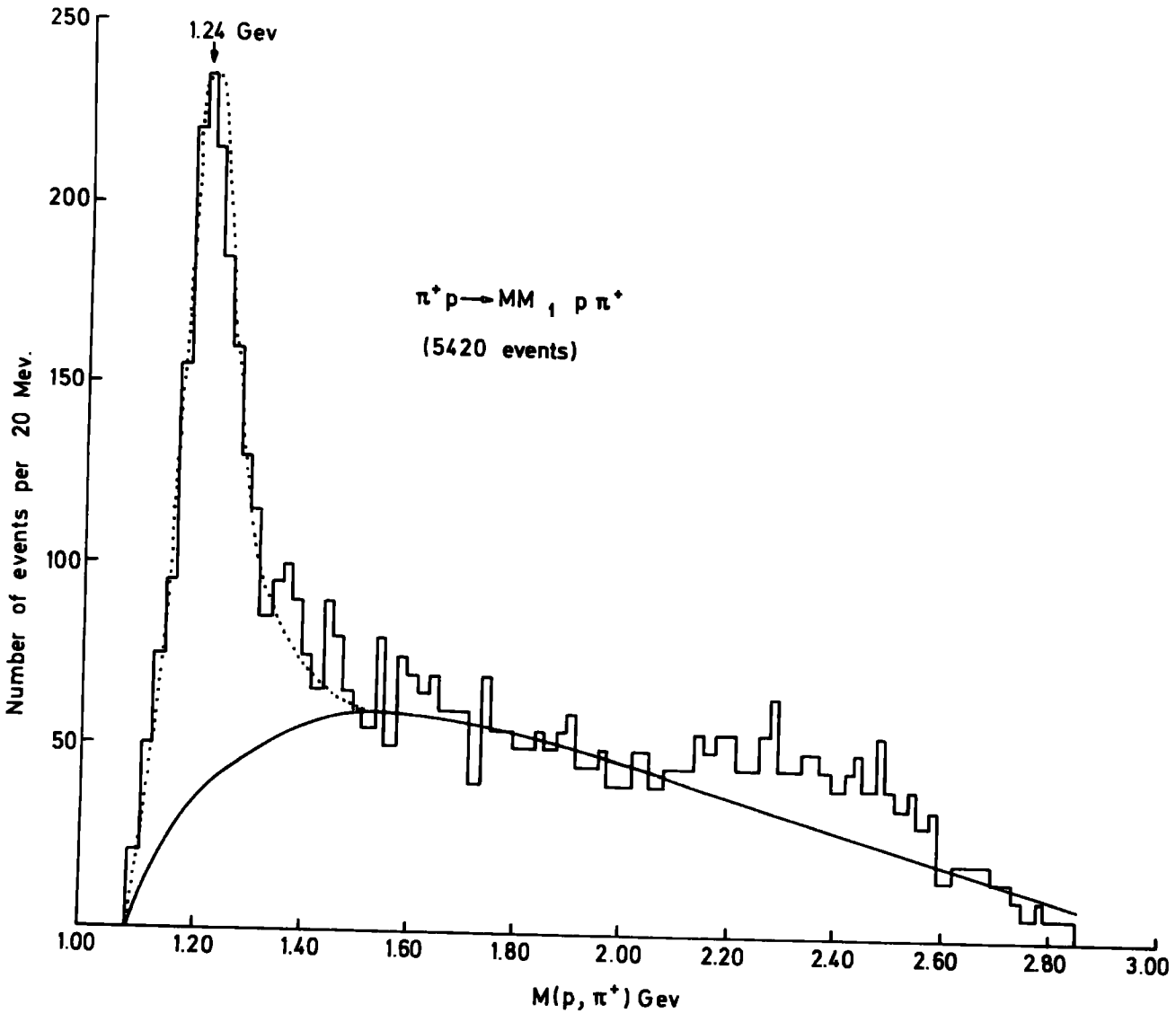

FIG. (7.3) The Effective Mass Distribution of the (p, π^+) system for the reaction $\pi^+ p \rightarrow p\ \pi^+ MM_1$ at 5 Gev/c.

mode ($\pi^0 \rho^+$) of the A_2^+ resonance. Now, relative to the phase space background of the two neutral pions there is an enhancement at this mass in the figure and for the present purpose it will be assumed that this is significant. Here again, by using an S - wave Breit Wigner signal and the background, the mass region (1170 - 1410) Mev of the figure has been fitted, the fitted mass M_o centred at mass of about 1.272 Gev with a full width at half height of about 0.182 Gev. It can be seen that the fitted Breit Wigner curve does not include all of the excess above background. In particular there is a considerable excess in the region around 1050 Mev. This could correspond to an A_1^+ (1070) signal where the A_1^+ decays to $\pi^o \rho^+$. An S - wave Breit Wigner signal and background have been used in the mass region (840 - 1170) Mev. The result of the free parameters in the fitting is:-

$$M_o\ (A_1^+) = 1.054 \pm 0.010 \text{ Gev}$$

$$\Gamma_o\ (A_1^+) = 0.154 \pm 0.007 \text{ Gev}$$

Moreover, the mass region (840 - 1410) Mev of the figure, which includes the A_1^+ and the A_2^+ signals, has been fitted by adding two Breit Wigner signals incoherently with the background. The central masses with the widths are free parameters and the number of events above the background in the A_1^+ region, $N(A_1^+)$, is a free parameter whereas the number of events above the BG in the A_2^+ region, $N(A_2^+)$, is given by:-

$$N(A_2^+) = \text{Total number above BG} - N(A_1^+) \qquad 7.2$$

The fitted curve of the double Breit Wigner signals is shown in the figure as a dotted curve. The results of the fitting (for a single Breit Wigner signal and double Breit Wigner signals

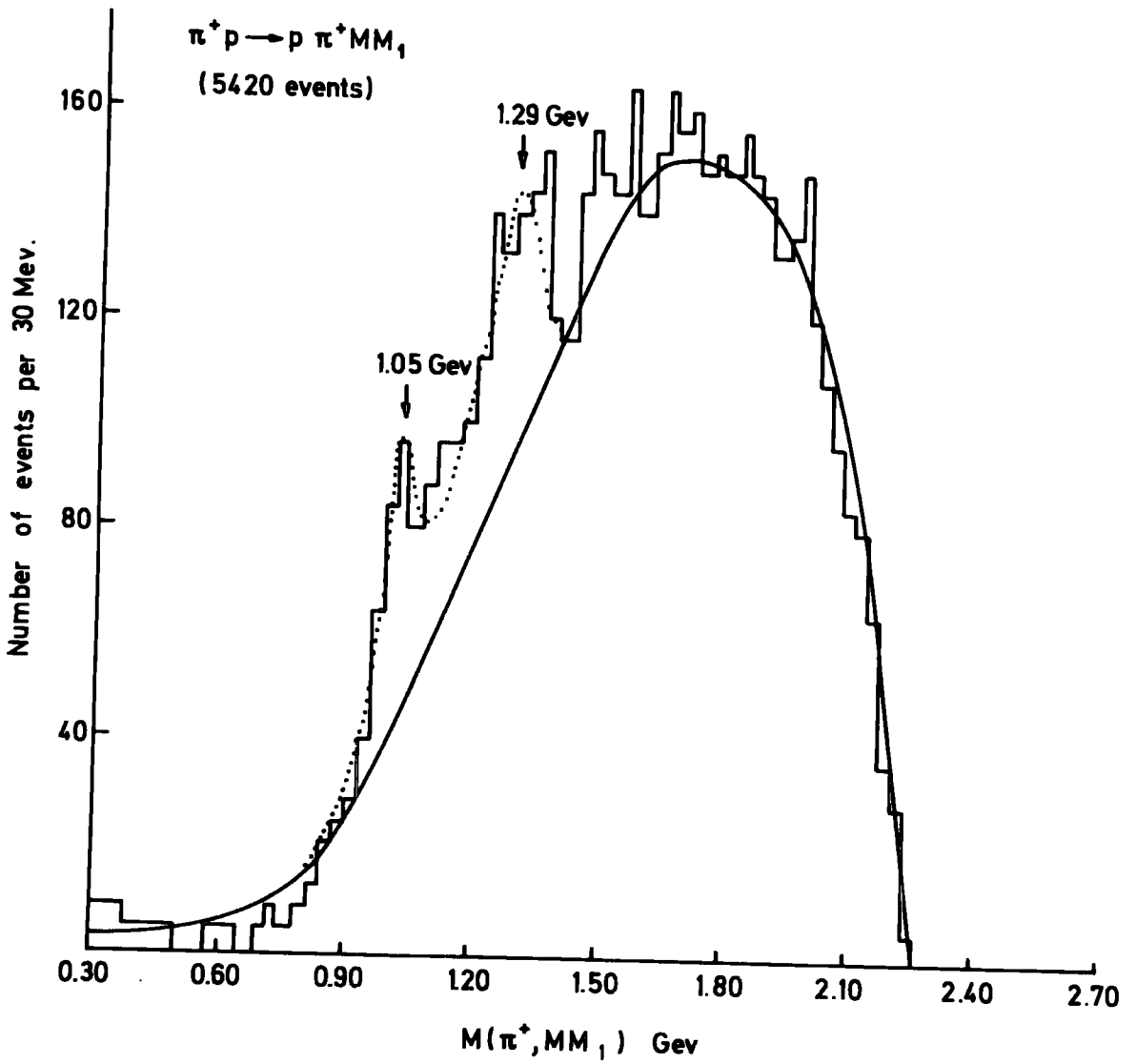

FIG. (7-4) The Effective Mass Distribution of the (π^+, MM_1) system for the reaction $\pi^+ p \rightarrow p\,\pi^+ MM_1$ at 5 Gev/c.

are given in table (7-2) followed by the observed number of events above the BG and the cross-section.

TABLE (7-2)

The Fitted Parameters	Single B.W. Signal		Double B.W. Signals	
	A_1^+ Region	A_2^+ Region	A_1^+ Region	A_2^+ Region
M_o (Gev)	1.054±0.010	1.272±0.011	1.050±0.005	1.290±0.006
Γ_o (Gev)	0.154±0.007	0.182±0.007	0.072±0.004	0.120±0.003
No. of Events above the BG	260±22	300±30	205±20	350±35
Cross-Section (mb)	0.109±0.009	0.125±0.013	0.086±0.008	0.146±0.015

Attempts have been made to isolate the signal in the 1050 Mev and 1300 Mev regions by removing the Δ^{++}; a more detailed analysis will be given later.

c) The (P, MM_1) System

In the case of the effective mass distribution of the (P, MM_1) system see figure (7-5), the structures seen appear to be consistent with statistical fluctuations. In the last chapter (see section 6. 3) it was seen that there was possible evidence for an enhancement in the $(N\pi\pi)^+$ system. There it was pointed out that the ambiguity of whether it is an N^{*+} $(T = 1/2)$ or $\Delta^+ (T = 3/2)$ could be resolved by reference to the (P, MM_1) system in the present channel. It can be seen that there is an enhancement at a mass of about 1700 Mev in figure (7-5). This could possibly correspond to the altern-

ative decay mode (P π^0 π^0) of the $N^{*+}(1700)$ resonance; details have been given in chapter 5 (see section 5. 1 and table (5-3)). If this signal is significant then reference can be made to table (5-6) in chapter 5 (see row 4 of the table). The mass region (1640 - 1860) Mev of figure (7-5) has been fitted with the background of the two neutral pions and an S - wave Breit Wigner signal (by using equation 6.3) centred at mass M_o with full width at half height Γ_o which are free parameters in the fitting. The fitted parameters of the Breit Wigner signal are:-

$$M_o = 1.740 \pm 0.018 \text{ Gev}$$

$$\Gamma_o = 0.150 \pm 0.010 \text{ Gev}$$

The dotted curve in figure (7-5) corresponds to this fit. The width Γ_o in the present channel is expected to be larger than the observed width in the NOFIT channel (E), see subsection 4.4.4 in chapter 4. However, the observed number of events above the background is equal to 80 ± 10 implying a cross-section of 0.033 ± 0.004 mb. By examining columns 9 and 10 of table (5-6) the present estimated cross section above is consistant with the idea that the signal in $(N \pi \pi)^+$ seen at a mass of about 1700 Mev is an $N^{*+}(1700)$, see row 4 of the table, and not an Δ^+ (1700), see rows 6 and 7 of the table, because for the $N^{*+}(1700)$ interpretation there should be an equal signal to the one above. In the present channel the number of events above BG is identical to the observed number of events in the channel (E).

If a resonance does occur in the P MM_1 system then the proton cannot be associated with the remaining π^+ through a $\Delta^{++}(1236)$ resonance. Hence, by demanding the absence of Δ^{++} the P MM_1

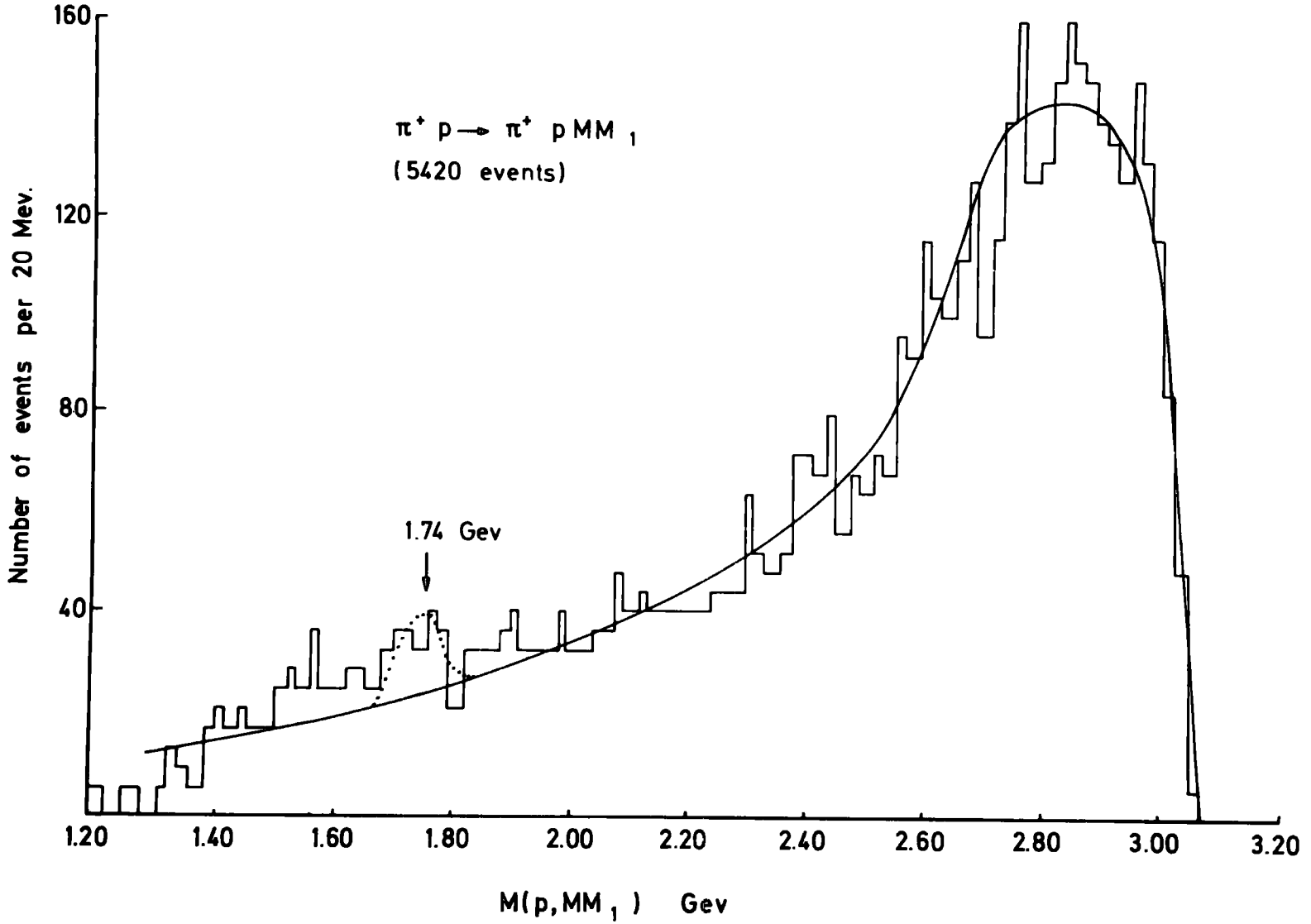

FIG. (7-5) The Effective Mass Distributers of the (p,MM$_1$) system for the reaction $\pi^+ p \rightarrow p \pi^+ MM_1$ at 5 Gev/c.

signal at 1700 Mev can be enhanced as shall be seen later in the detailed analysis.

7. 2 The Use of the Van-Hove Plot

The Van-Hove plot has been successfully used as a technique of analysis for the description of a three-body final state (see ref. 1, 2 and 3). The basic idea is that because the transverse momenta of particles are approximately constant at about 350 Mev/c, then this information is redundant. The longitudinal momentum components $q_i (i = 1, 2, 3)$ of particles or resonances in the c.m.s. of the final state are such that

$$q_1 + q_2 + q_3 = 0 \qquad 7.3$$

These three variables can be represented by a single point in a two - dimensional space. The space is defined by three axes at 120° to each other, see figure (7-6) which shows a diagrammatic representation of the hexagonal Van-Hove plot. Then q_1 is measured at right angles from axis (S1), q_2 from axis (S2) and finally q_3 from axis (S3). These define a point. In terms of the conventional (x,y) plane the coordinates of the points are given by:-

a) the longitudinal momentum q_1 of the first particle in the final state which can be plotted on the x - axis.

b) in the case of the y - axis the component to be plotted is given by:-

$$q_1 \tan 30 + q_2/\cos 30 = (q_1 + 2q_2) / (3)^{1/2} \qquad 7.4$$

The Van-Hove angle w is the angle between the y - axis, where $q_1 = 0$, and the radius vector r from the centre of the hexagon to the point. The measurement of the angle corresponds to the anticlockwise direction. The Van-Hove angle can be used

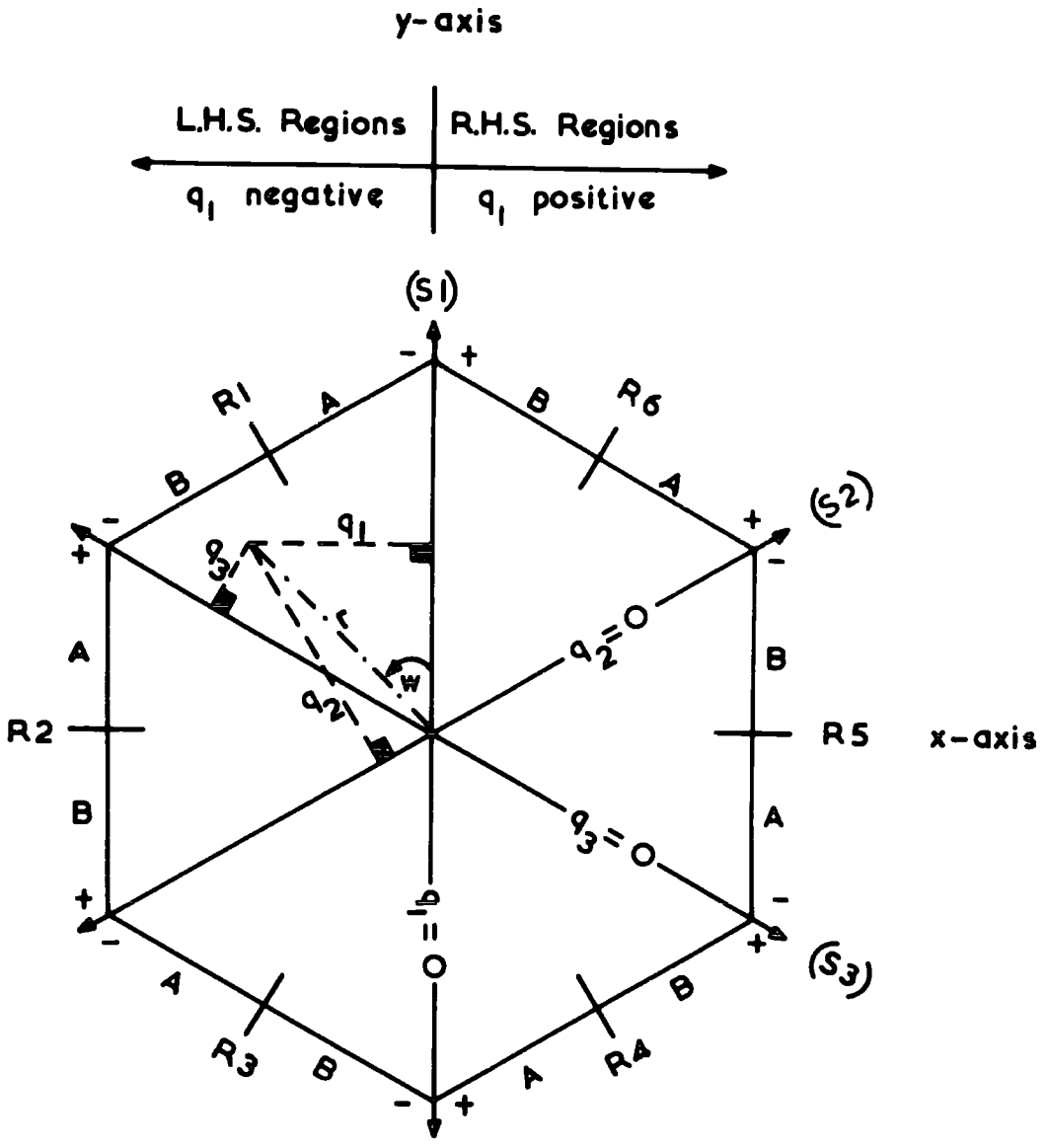

FIG. (7-6) Diagrammatic Representation of the VAN-HOVE Hexagon Plot.

to define the hexagonal plot into six regions R1, R2, R3, R4, R5 and R6 as shown in figure (7-6). Each region can be sub-divided into two sub-regions (e.g. (R1 - A) and (R1 - B)). For angle w between 0^{o} and 180^{o}, i.e. the left hand side of the hexagon, the first three regions are defined where the first particle is backward in the c.m.s., the right hand side of the plot contains the other three regions with w between 180^{o} and 360^{o} where the first particle is always forward over all these regions. The other two particles might be backward or forward in the c.m.s. depending upon the region.

As an example of the use of the Van-Hove plot consider the reaction

$$\pi^{+} P \longrightarrow P \pi^{+} \pi^{o} \qquad (B)$$

at 5 Gev/c in the same exposure. Detailed analysis already exists for this channel (see ref. 2 and 4). However, in figures (7-7), (7-8) and (7-9) the invariant mass combinations for the (P, π^{o}), the (π^{+}, π^{o}) and finally the (P, π^{+}) systems are given for all data. The data are shown again in figure (7-10) as a Van-Hove hexagon plot where, now, q_1, q_2 and q_3 refer to the longitudinal momentum components (in the c.m.s.) of the proton, the π^{+} and the π^{o} respectively. Round the extremes of the plot are shown the appropriate Feynman exchange diagrams (see ref. 5) where it is assumed that particles with low relative velocity are produced from the same vertex. These diagrams then represent the physical reactions occurring in each region. For example:-

1. in region R1 it can be seen that the proton and the π^{o} are moving together backwards in the c.m.s. and both of them are forward in region R4. This is the condition expected for

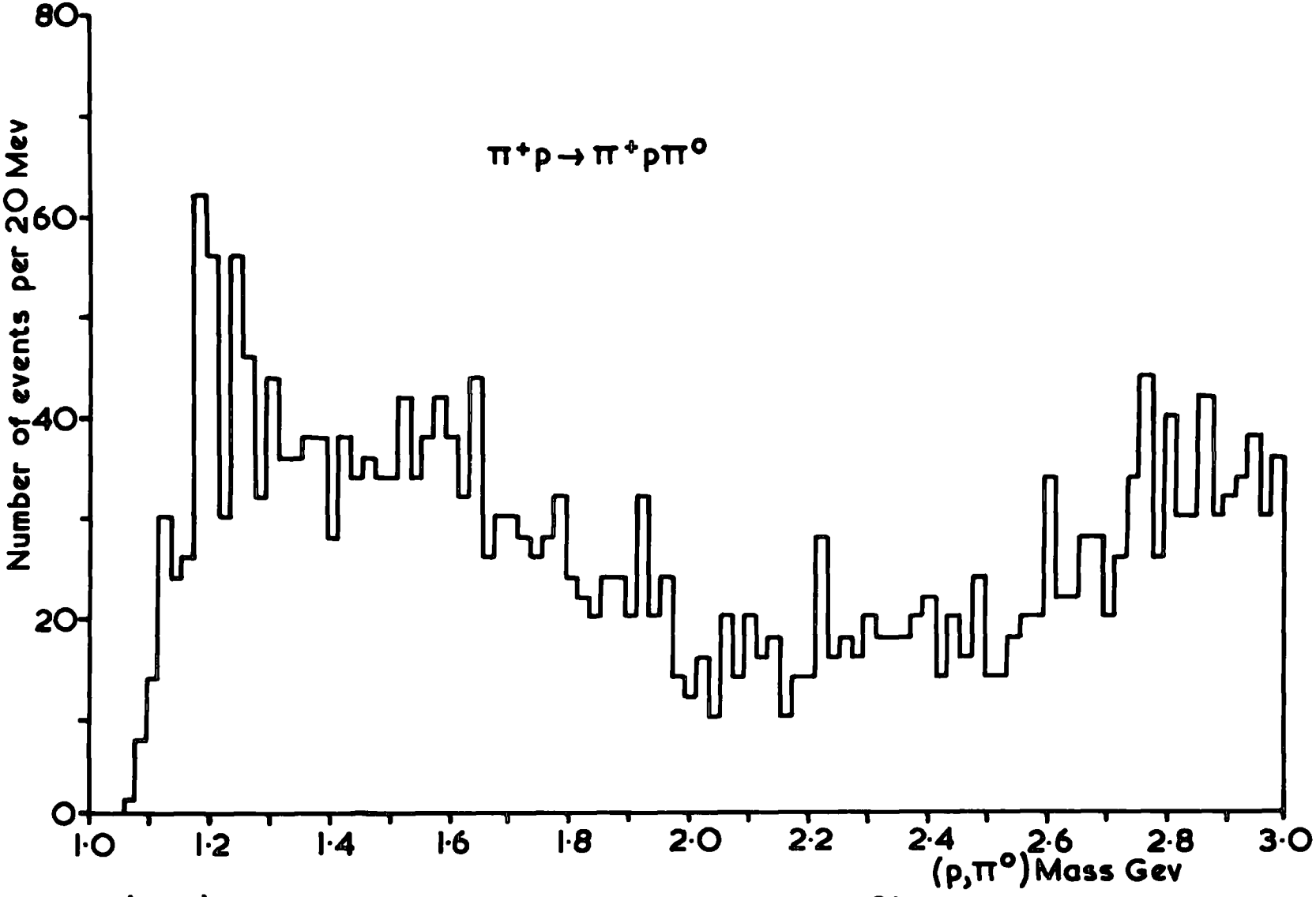

FIG.(7-7) The effective mass distribution of the $(p\pi^0)$ system for the reaction $\pi^+ p \rightarrow p\pi^+\pi^0$ at 5 Gev/c.

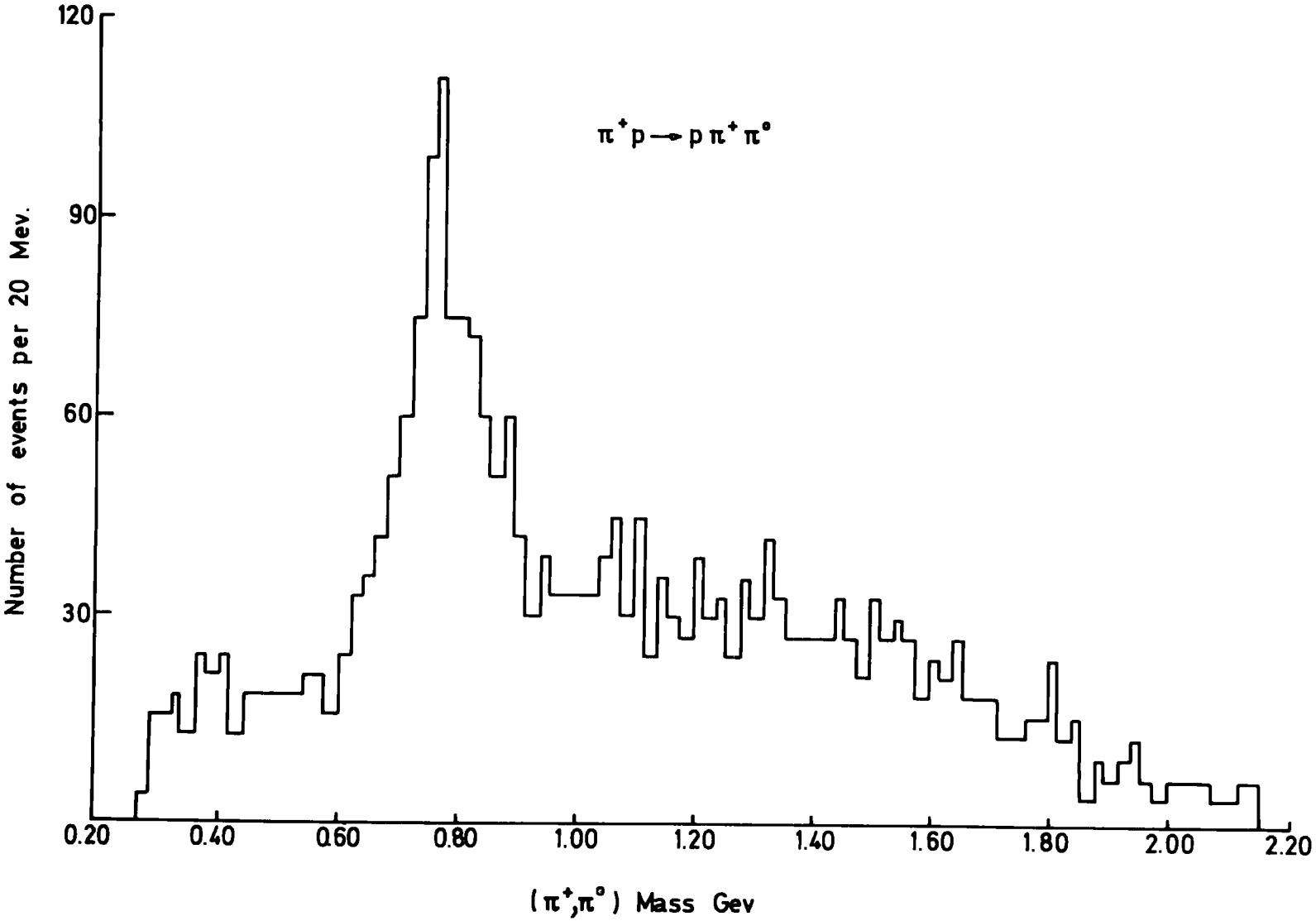

FIG.(7-8) The Effective Mass Distribution of the (π^+, π°) system for the reaction $\pi^+ p \rightarrow p\pi^+\pi^\circ$ at 5 Gev/c.

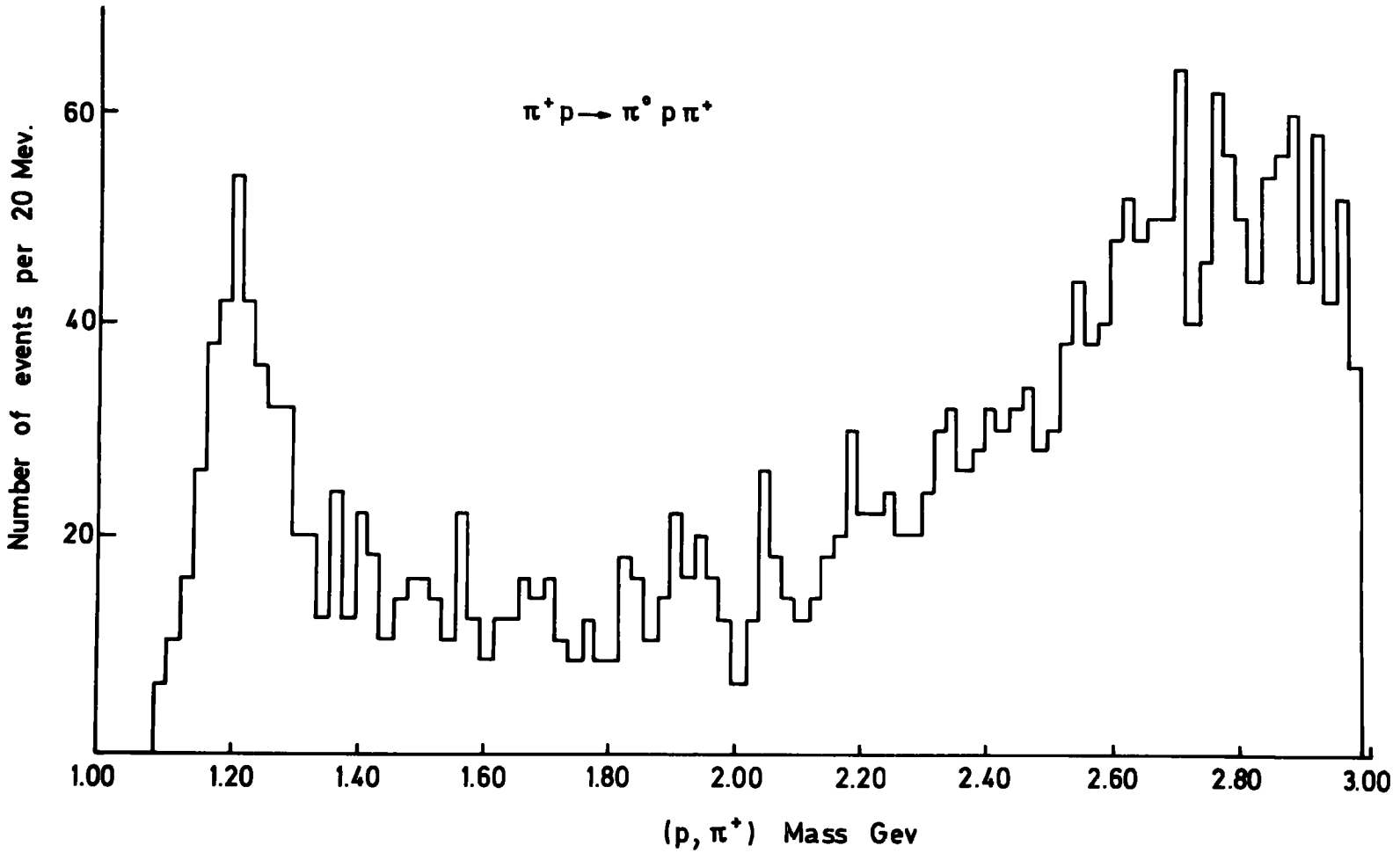

FIG.(7-9) The Effective Mass Distribution of the (p,π^+) system for the reaction $\pi^+ p \rightarrow p \pi^+ \pi^\circ$ at 5 Gev/c.

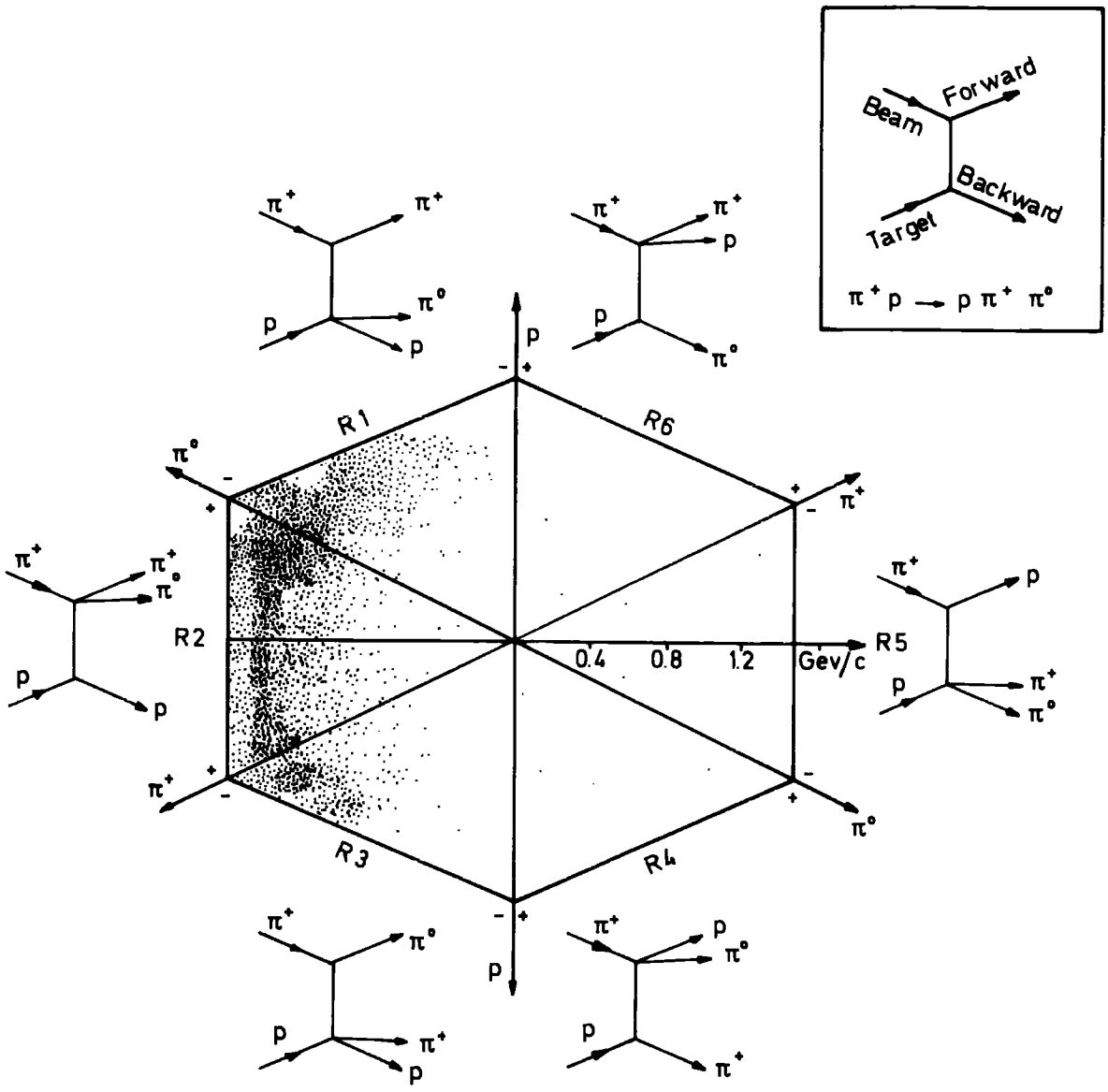

FIG. (7-10) The Hexagonal VAN-HOVE plot for the reaction $\pi^+ p \rightarrow p\pi^+\pi^\circ$ at 5 Gev/c

P π^0 production through a resonance. Hence, in region R1, Δ^+ production is expected to be manifest (backward production). Similar forward Δ^+ production might be expected in region R4.

2. in the case of region R2 the π^+ and the π^0 are both travelling together forwards in the c.m.s. and are both backward in region R5. Again, ρ^+ - meson production then is expected in regions R2 (forward production) and R5 (backward production).

3. finally, backward and forward production are expected in regions R3 and R6 respectively where the proton and the π^+ are going together and here the production of Δ^{++} is expected.

For the individual regions R1, R2 and R3 only (because about 95% of the present data, channel (B), have backward protons in the c.m.s. and are concentrated in the left hand side of the hexagonal plot) the invariant mass plots are shown in figures (7-11) for the (P, π^0), the (π^+, π^0) and the (P, π^+) in region R1 and the same invariant mass combinations are plotted in figures (7-12) and (7-13) for regions R2 and R3 respectively. It can be seen that the Δ^+, the ρ^+ and the Δ^{++} are produced only in region R1, R2 and R3 respectively and the resonant signals become much clearer than in figures (7-7), (7-8) and (7-9) which correspond to the whole Van-Hove plot. In this case, each sector seems to contain resonant production corresponding to a particular combination of particles. For example, figure (7-12) shows the invariant mass combinations in region R2 where it can be seen that:-

a) there is no structure in the (P, π^0) system,

b) a very strong peak exists at a mass of about 760 Mev,

FIG. (7-11) The Effective Mass Distribution of
(a) the (p,π°) system
(b) the (π^{+},π°) system
and (c) the (p,π^{+}) system
in sector R_1 of the VAN - HOVE plot for the reaction $\pi^{+}p \rightarrow p\pi^{+}\pi^{\circ}$ at 5 Gev/c.

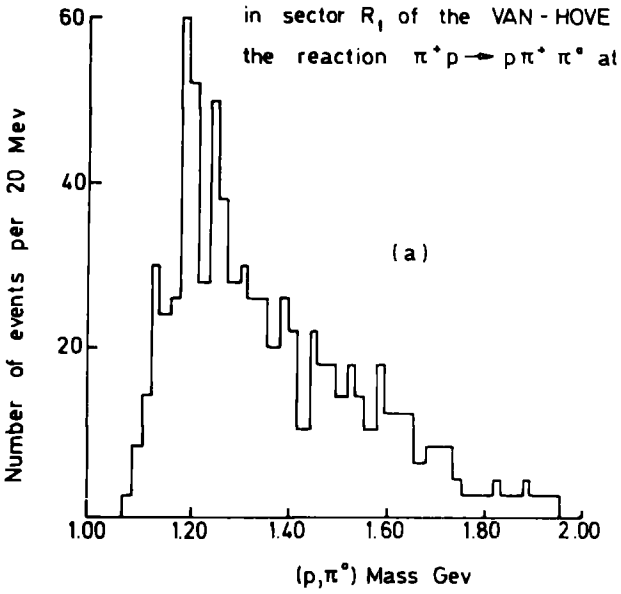

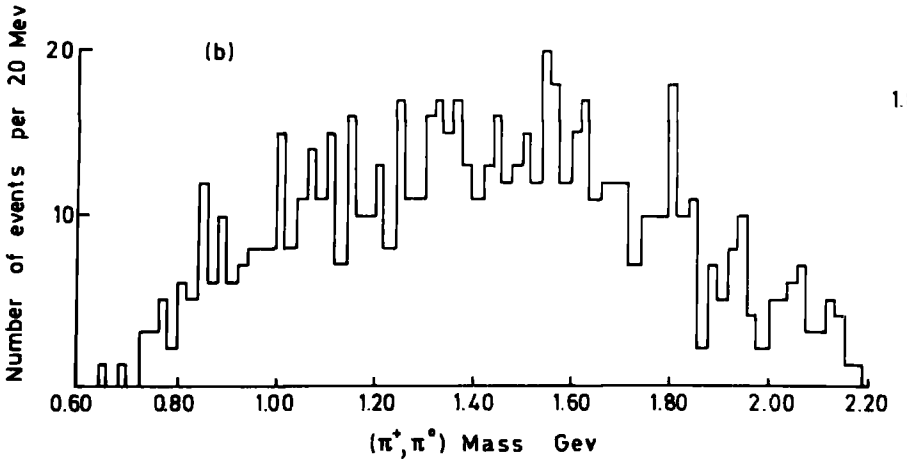

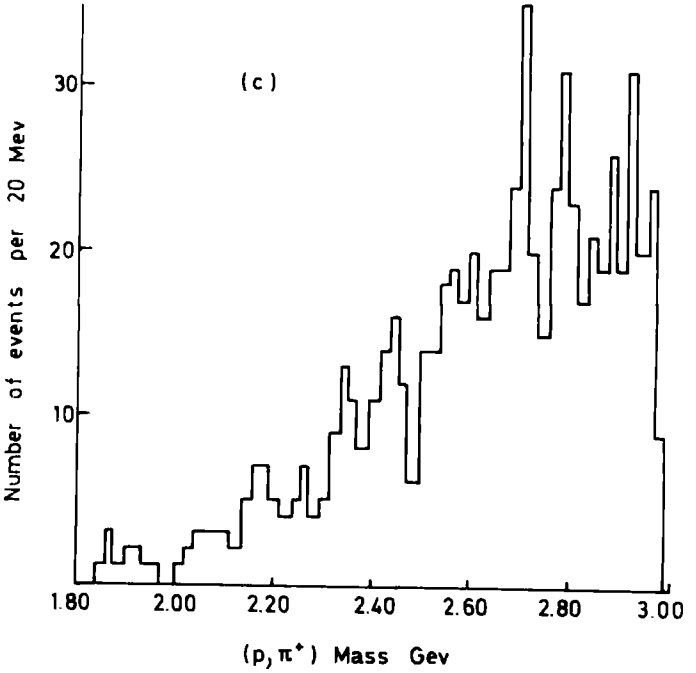

FIG. (7-12) The Effective Mass Distribution of
(a) the (p,π°) system
(b) the (π^{+},π°) system
and (c) the (p,π^{+}) system
in section R2 of the VAN-HOVE plot for the reaction $\pi^{+}p \rightarrow p\pi^{+}\pi^{\circ}$ at 5 Gev/c.

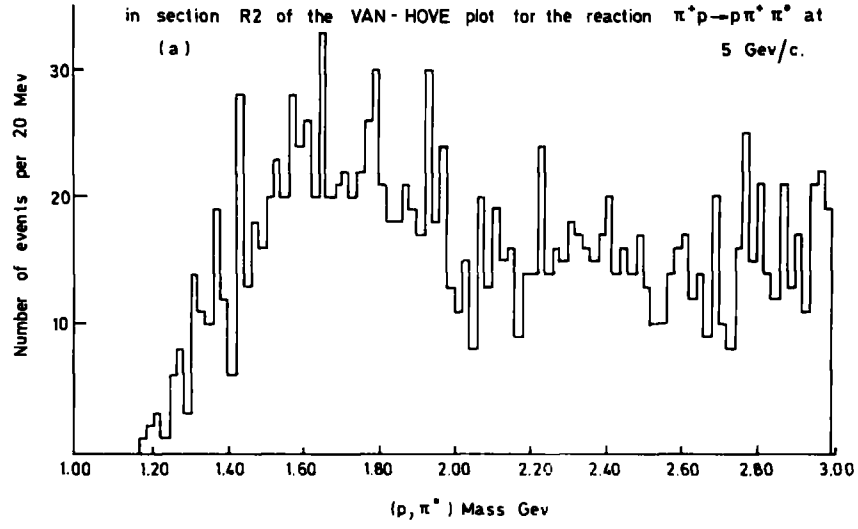

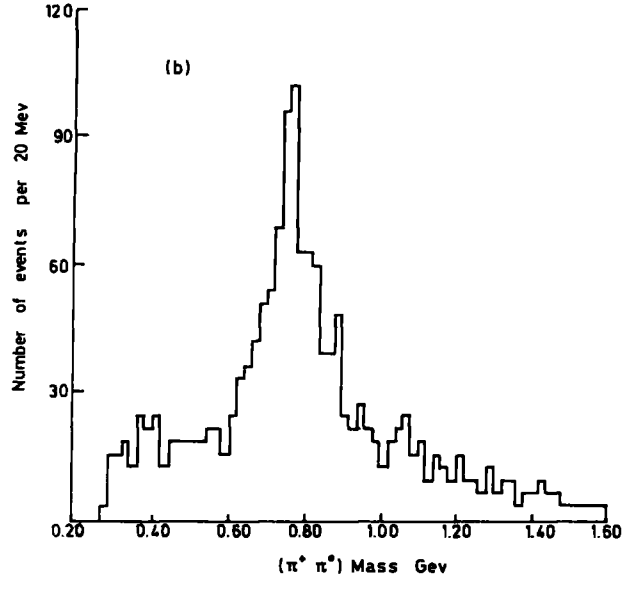

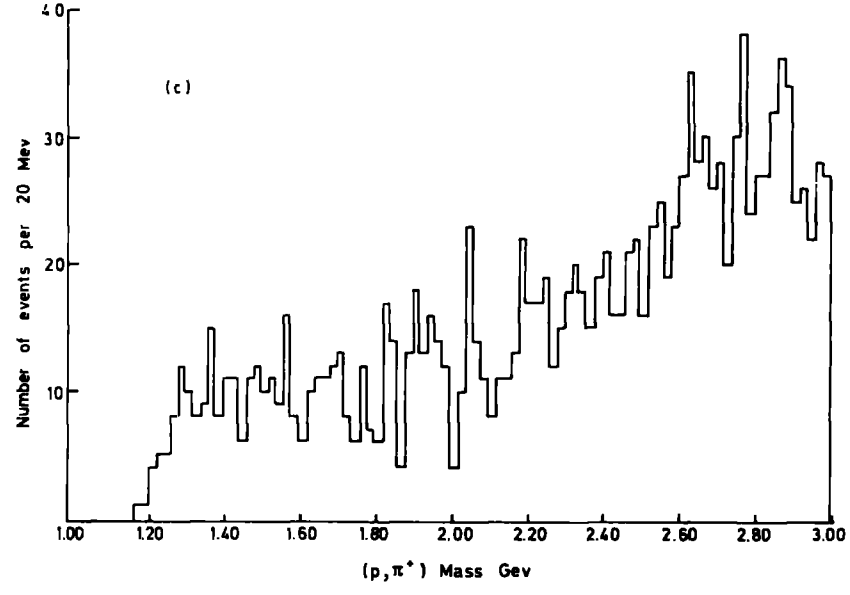

FIG.(7-13) The Effective Mass Distribution at
(a) the (p,π^0) system
(b) the (π^+,π^0) system
and (c) the (p,π^+) system
in sector R_2 of the VAN-HOVE plot for the reaction $\pi^+ p \rightarrow p\pi^+\pi^0$ at 5 Gev/c

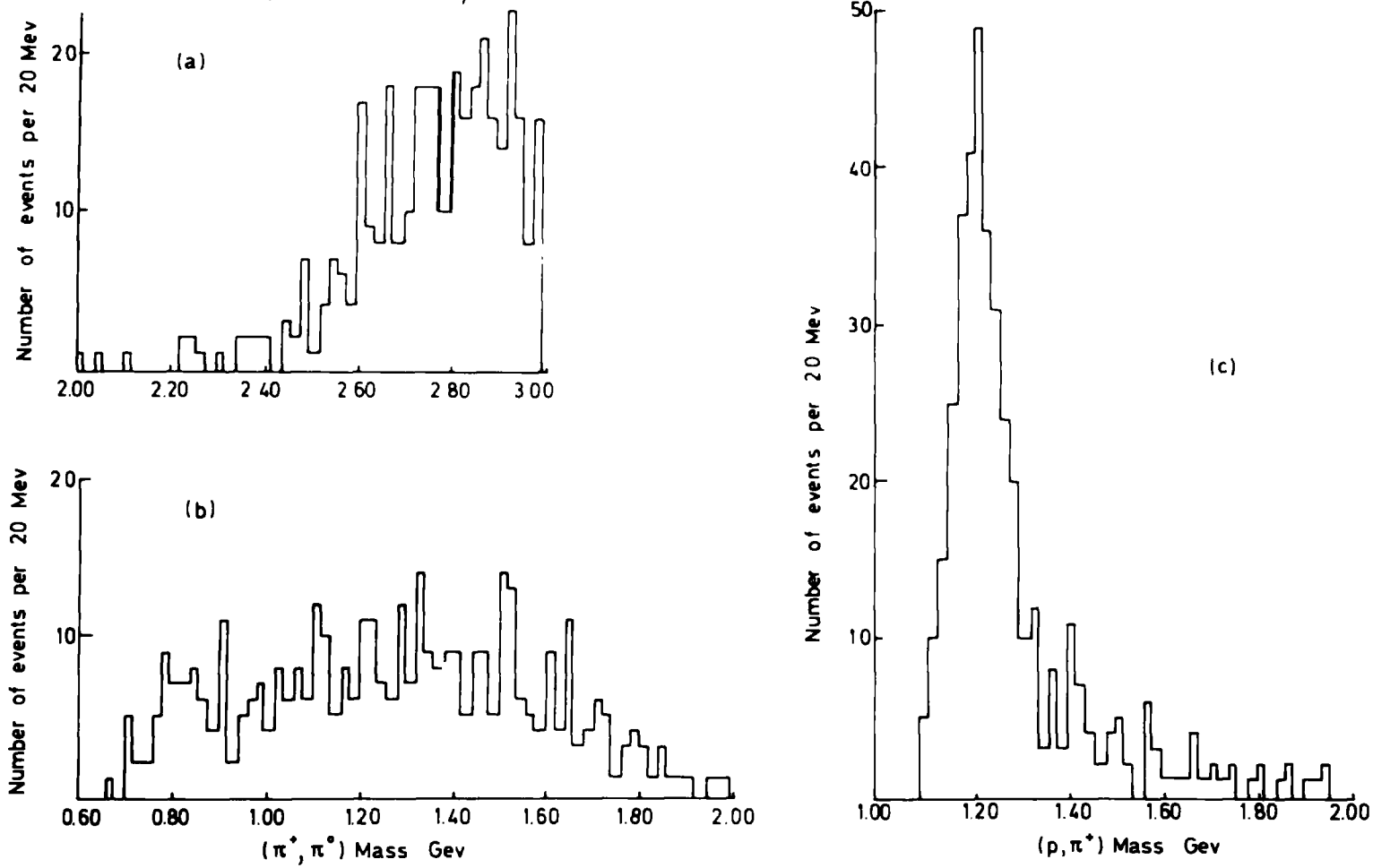

and corresponds to the ϱ^+ - meson,

c) in the (P, π^+) system there is no structure.

In using the Van Hove plot for analysis, the plot should be divided into its six regions and in each one resonant signals should be sought only in the combination of the two particles which are travelling, either both forwards or both backwards.

It is intended to apply this Van Hove analysis to the NOFIT data channel (D). Now, an essential difference is that the channel (B) comprises three particles only (for which the hexagonal Van Hove plot is appropriate) whereas the NOFIT data are composed of at least four particles in the final state. However, if the missing neutral secondary particles are regarded as a single body (the so called missing mass) then the outgoing particles in the NOFIT channel (D) are reduced to three particle states. It is important to realise that for each value of the missing mass there is a Van Hove hexagon whose radius depends upon missing mass. So the Van Hove plot in the case of the NOFIT events will correspond to the superposition of many Van Hove hexagons. However, the general discussion about the contents of regions of the plot will still hold. Consequently, q_1, q_2 and q_3 refer to the longitudinal momentum components (in the c.m.s.) of the proton, the π^+ and the missing mass. Here again, the hexagonal Van Hove plot in the case of the NOFIT reaction

$$\pi^+ P \rightarrow P\ \pi^+\ MM_1 \qquad (D)$$

is displayed in figure (7-14) with the appropriate Feynman diagrams round the extreme of the plot for each region. From a similar argument to that discussed earlier for the channel (B) it is expected then that resonant signals for the following

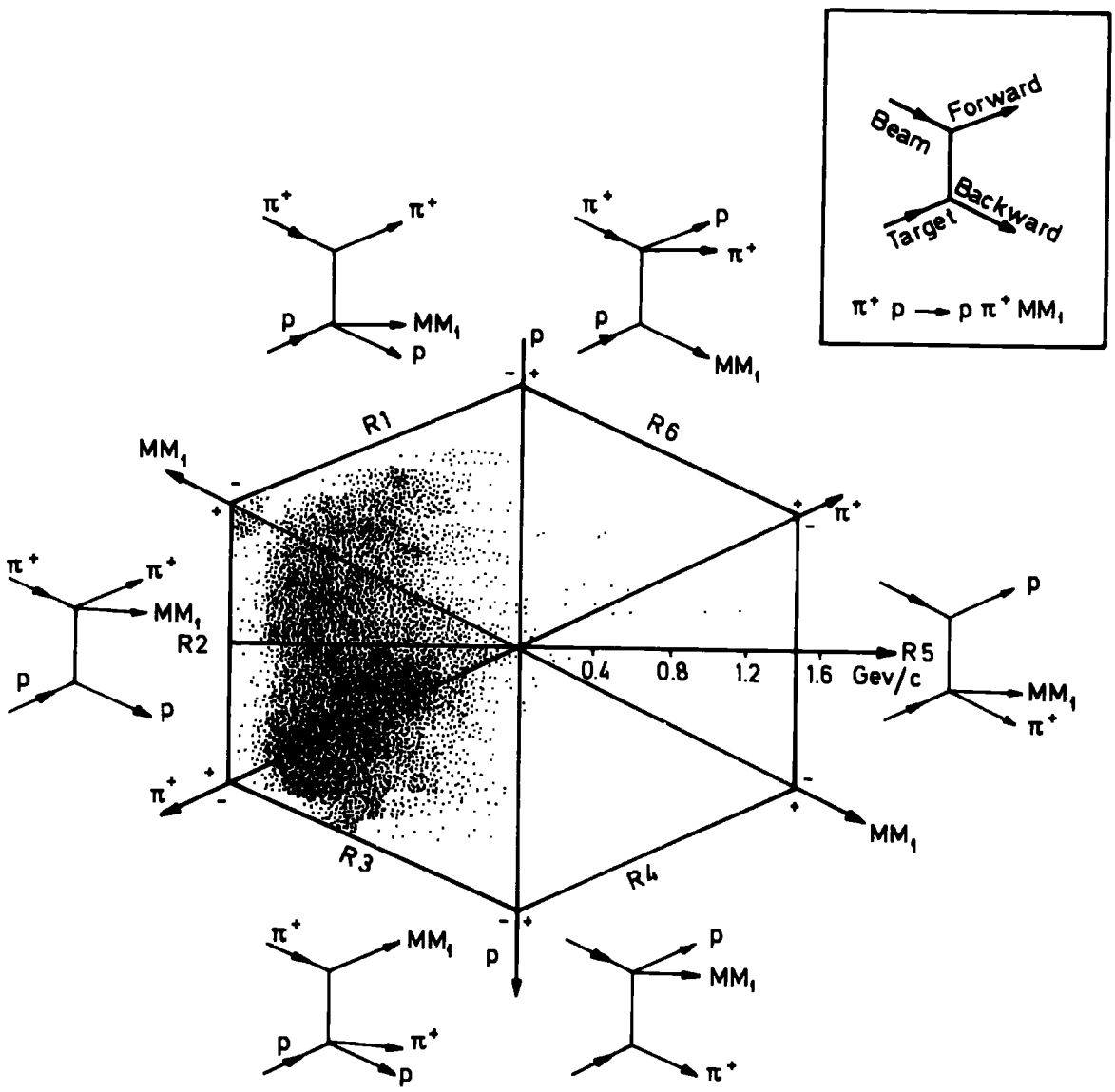

FIG. (7-14) The Hexagonal VAN-HOVE plot for the reaction $\pi^+ p \rightarrow p\pi^+ MM_1$ at 5 Gev/c.

particle combinations will correspond to the individual regions as shown in table (7-3).

TABLE (7-3)

Particle Combinations	Expected Regions	
	L.H.S.	R.H.S.
(P, MM_1)	R1	R4
(π^+, MM_1)	R2	R5
(P, π^+)	R3	R6

It is worth emphasising again that only combinations of particles travelling both forwards or both backwards should be used.

Since the (P, π^+) system, see figure (7-3), displays the strongest resonant signal then sector R3 (R6) will be considered first, followed by sector R2 (R5) and finally by sector R1 (R4). Here again, the left hand side sectors (R1, R2 and R3) where the proton is backward in the c.m.s. will be used since the remaining regions (proton forward) are very poor statistically. The ensuing sections discuss the invariant mass combinations for each sector.

7.3 Analysis of Region R3

In this region (w = 120° to 180° in the c.m.s.) the proton and the π^+ - meson are travelling together backwards and the missing mass is then forward. It contains about

1790 events after selecting the positive missing mass squared.

7.3.1 The (P, π^+) System

As stated earlier Δ^{++} production (backward) can only be expected in the sector R3. Figure (7-15) shows the invariant (P, π^+) mass combination in this region. Indeed, most of the signal is resonant relative to an approximate phase space background. This background is given as a solid curve as shown in the figure, Here again, an S - wave Breit Wigner signal and phase space background (see equation 6.3) were used to fit the mass region (1080 - 1400) Mev of the figure. The central mass M_o and the width Γ_o (full width at half height) are free parameters in the fitting. The result of the fitting is:-

$$M_o = 1.212 \pm 0.003 \quad \text{Gev}$$

$$\Gamma_o = 0.115 \pm 0.002 \quad \text{Gev}$$

The fitted Breit Wigner curve is shown in the figure as a dotted curve. The number of events above the background is equal to 1390 ± 40 which is equivalent to a cross-section of 0.581 ± 0.017 mb. These are consistent with the earlier determination by using the full data.

Since this sector R3 is dominated by Δ^{++} then the missing mass can be examined for a quasi two-body reaction in this region.

7.3.2 The Missing Mass Distribution

Figure (7-16) displays the missing mass distribution where the solid curve, again, shows the assumed phase space background corresponding to two neutral pions (see sub-section 7.1.1). Now, relative to this background it can be seen that there are

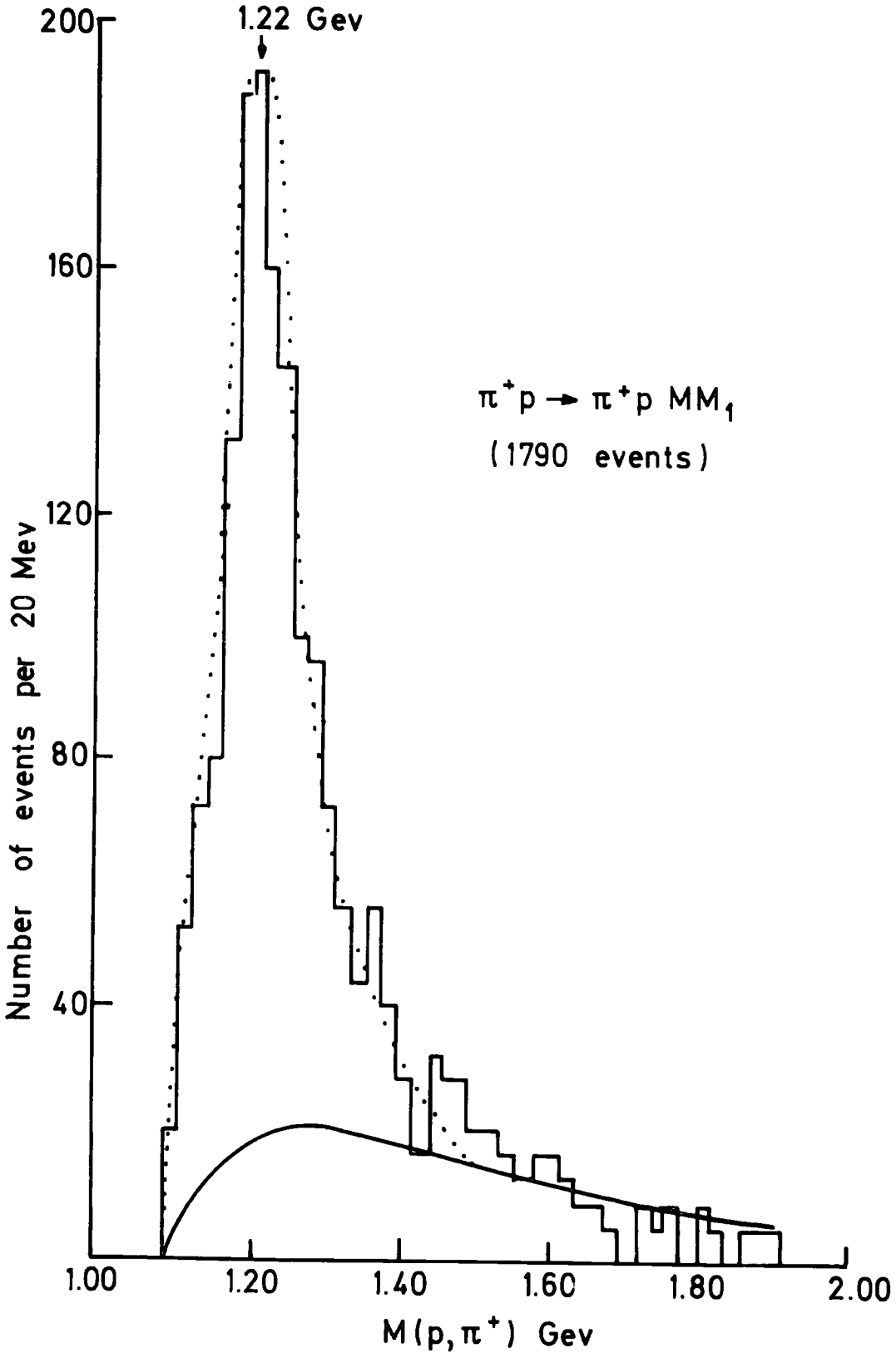

FIG.(7-15) The Effective Mass Distribution of the (p,π^+) system in sector R3

two strong peaks in the figure. The first peak appears at a mass around 570 Mev and the second at a mass of about 1260 Mev. These two significant structures correspond to the η^0-meson (for the lower mass) and to either, or both, the f^0 - meson and the A_2^0 - meson (where the A_2^0 decays to $\pi^0 \eta^0$) for the higher mass. Here again, the lower mass region (300 - 750) Mev and the higher mass region (1170 - 1440) Mev have been fitted with an approximate phase space background to which was added a Gaussian distribution (see equation 7.1) to represent the η^0 and an S - wave Breit Wigner signal for the f^0 respectively. The central masses and the full widths at half height are free parameters. The results of the fitting are shown in table (7-4) followed by the observed number of events above the BG and the equivalent cross-sections for both signals.

TABLE (7-4)

The Fitted Parameters	η^0 Region	f^0/A_2^0 Region
Central Mass (Gev)	0.560 ± 0.011	1.275 ± 0.013
Full Width at Half Height (Gev)	0.110 ± 0.008	0.180 ± 0.009
No.of Events above the BG	145 ± 20	190 ± 25
Cross-Section (mb)	0.061 ± 0.008	0.079 ± 0.010

From the above table it can be seen that the results obtained for the central masses and widths are consistent with the earlier results which were given in table (7-1). The dotted curve and the dash-dot curve show the fitted Gaussian distribution and the

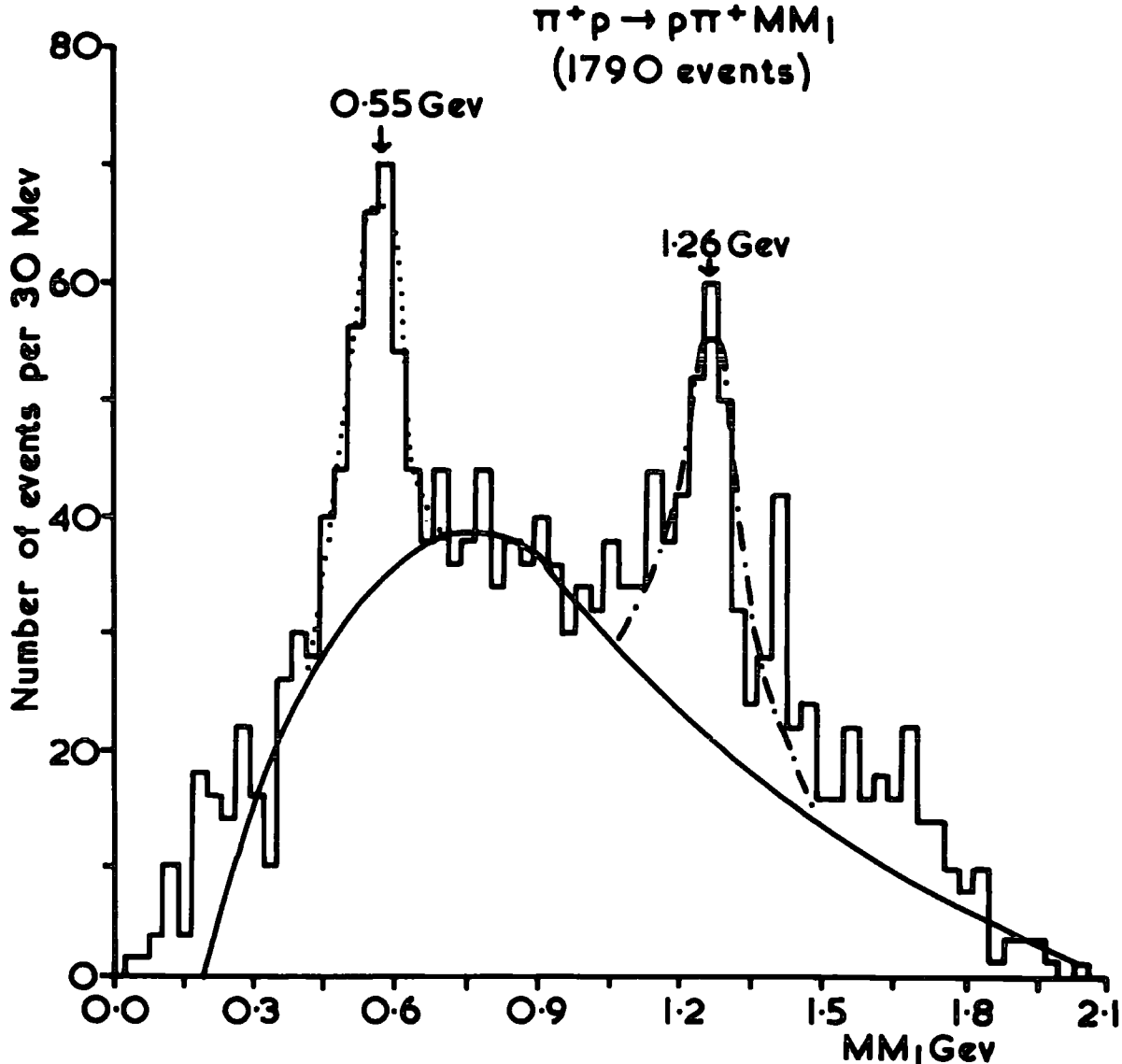

FIG.(7-16) The missing mass spectrum in section R3

Breit Wigner signal in figure (7-16).

As the sector R3 was dominated by Δ^{++} then these two signals correspond to Δ^{++} η^{o} and Δ^{++} f^{o}/A_2^{o} production (η^{o} and f^{o} decaying neutrally). For this purpose reference can be made to tables (5-5) and (5-11) in chapter 5 to predict the number of these two signals relative to the alternative decay modes of η^{o}, f^{o} and A_2^{o} in the four pronged 4-C and 1-C(π^{o}) FIT events for the same exposure. Moreover, the ambiguity in the Δ^{++} f^{o}/A_2^{o} interpretation can be resolved by looking at the prediction of the Δ^{++} f^{o} in the four pronged FIT and the two pronged NOFIT channels. This can be done by use of Clebsch-Gordan coefficients to calculate the branching ratios for each case. These branching ratios are:-

$$\eta^{o}\text{(neutral mode)}/\,\eta^{o}\text{(charged mode)} = 71/29$$

$$f^{o}\ \text{(neutral mode)}/f^{o}\ \text{(charged mode)} = 1/2$$

In table (7-5) the reaction final state is given in column 1. Columns 2 and 3 show the expected and observed number of events above the background. The cross-section corresponding to the observed number is shown in column 4.

It can be seen that the resonance in the f^{o}/A_2^{o} region is consistent with this being entirely due to the f^{o}.

7. 4 Analysis of Region R2

The sector R2 indicates that the π^{+} - meson and the MM_1 are going together forwards and the proton is backward (w = 60^{o} to 120^{o} in the c.m.s.). It contains about 2720 events, again, after removing the negative missing mass squared.

TABLE (7-5)

1	2	3	4
Reaction Final State	NUMBER OF EVENTS		Cross-Section (mb)
	Expected	Observed	
Δ^{++} MM_1 ; (η^o, f^o/A_2^o)INCL.	-	1390 ± 40	0.581 ± 0.017
	147	145 ± 20	0.061 ± 0.008
Δ^{++} f^o	213	190 ± 25	0.079 ± 0.010
Δ^{++} MM_1 ; (η^o, f^o/A_2^o)EXCL.	-	1055 ± 35	0.441 ± 0.015
Δ^{++} MM_1 ; REMAINDER	-	400 ± 34	0.167 ± 0.014
Microbarn equivalent is 0.418 ± 0.003 μb/event			

7.4.1 The (π^+, MM_1) System

An outline of the production of resonances in the (π^+,MM_1) system has been given in the sub-section 7.2.2 by using the whole data. It was seen earlier that the Δ^{++} production is dominant in region R3. Therefore, in the present region(R2)the Δ^{++} channel is excluded. The invariant (π^+, MM_1) mass combination is displayed in figure (7-17) fitted with an approximate phase space background. The significance of any structure can now be judged relative to the fitted background. By reference to figure (7-4) and table (7-3) it can be seen that the A_1^+ - meson and the A_2^+ - meson production (forward) corresponding to the alternative decay mode (π^o ρ^+) of the A_1^+ and the A_2^+ resonances and the other alternative decay mode (π^+ η^o) of the A_2^+ can only be expected in the sector R2. From the figure (7-17) relative to the assumed background it can be seen

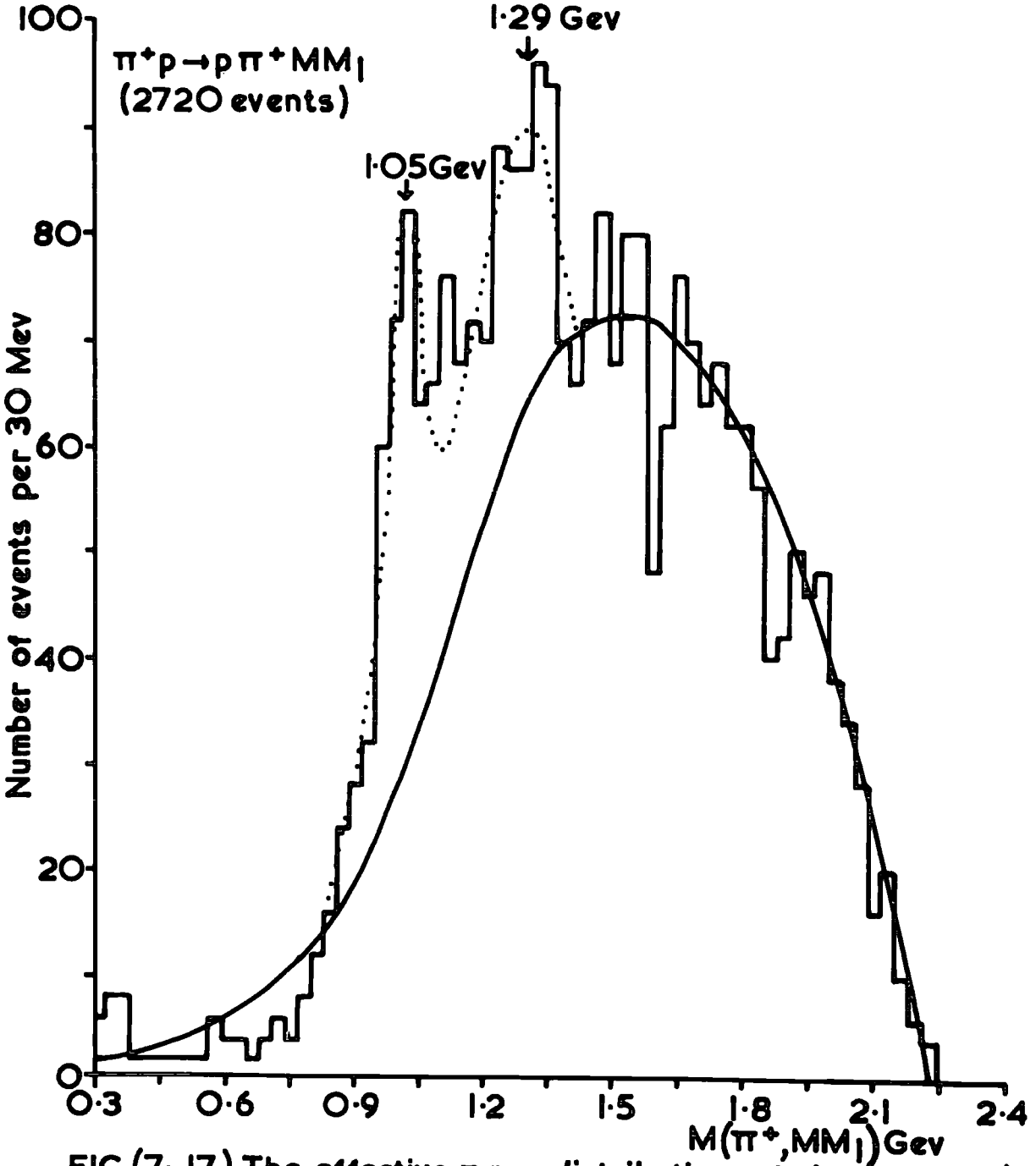

FIG.(7-17) The effective mass distribution of the (π^+, MM_1) system in section R2

that there are two peaks corresponding to the A_1^+ and the A_2^+ resonances. As before, the background and an S - wave Breit Wigner signal were used to fit the mass region (840-1170) Mev, for the A_1^+ signal, and the mass region (1170-1410) Mev, for the A_2^+ signal. Moreover, by adding two Breit Wigner signals incoherently with the background the mass region (840-1410) Mev has been fitted. The central masses and the widths are free parameters for a single Breit Wigner signal and the number of events above the BG in the A_1^+ signal $N(A_1^+)$ is a free parameter in the fitting, whereas the number of events above the BG in the A_2^+ signal is given by equation 7.2. The results are presented in table (7-6). The double Breit Wigner signals are displayed as a dotted curve in figure (7-17). Table (7-6) contains the observed number of events above the BG and the cross-section.

By reference to table (7-2) it can be seen that the results in table (7-6) are consistent with the earlier determination. This means that of the signals (A_1^+ and A_2^+ resonances) are contained in the sector R2.

TABLE (7-6)

The Fitted Parameters	Single B.W. Signal		Double B.W. Signal	
	A_1^+ Region	A_2^+ Region	A_1^+ Region	A_2^+ Region
M_o (Gev)	1.060 ± 0.010	1.280 ± 0.013	1.040 ± 0.004	1.275 ± 0.012
Γ_o (Gev)	0.190 ± 0.007	0.200 ± 0.009	0.090 ± 0.003	0.140 ± 0.006
No. of Events above the B.G.	258 ± 20	342 ± 25	200 ± 20	355 ± 35
Cross-Section (mb)	0.108 ± 0.008	0.143 ± 0.011	0.084 ± 0.008	0.148 ± 0.015

From the analysis of the four pronged 4-C and 1-C(π^0)FIT events, for the same exposure, it was found that the A_2^+ - meson can be produced via two channels (Δ^{++} excluded) as follows:-

$$\pi^+ P \longrightarrow P A_2^+ \longrightarrow \pi^+ \rho^0 \longrightarrow \pi^+ \pi^-$$

$$\pi^+ P \longrightarrow P A_2^+ \longrightarrow \pi^+ \eta^0 \longrightarrow \pi^+ \pi^- \pi^0$$

Reference can be made to tables (5-5) and (5-11) in chapter 5 to predict how many events of these kinds could be expected in the two pronged NOFIT events (again, Δ^{++} excluded). Now, when A_2^+ decays to $\pi^+ \rho^0$ it, should be accompanied by exactly the same amount of A_2^+ production decaying into $\pi^0 \rho^+$ in the two pronged NOFIT channel (D). When A_2^+ decays to $\pi^+ \eta^0$, then the branching ratio of η^0(neutral mode) to η^0(charged mode) is equal to 71/29. However, the result is given in table (7-7) of the prediction of A_2^+ - meson by using the result of the double Breit Wigner signal fitting. Column 1 showsthe reaction final state; the expected number and the observed number are given in column 2 and 3 and finally the cross section corresponding to the observed number is presented in column 4.

TABLE (7-7)

1	2	3	4
Reaction Final State	NUMBER OF EVENTS		Cross-Section (mb)
	Expected	Observed	
P A_1^+ ; $A_1^+ \rightarrow \pi^0 \rho^+, \Delta^{++}$ EXCL.	-	200 ± 20	0.084 ± 0.008
P A_2^+ ; $A_2^+ \rightarrow \pi^0 \rho^+, \Delta^{++}$ EXCL.	286	355 ± 35	0.148 ± 0.015
P A_2^+ ; $A_2^+ \rightarrow \pi^+ \eta^0, \Delta^{++}$ EXCL.	86		
P $MM_1 \pi^+$; REMAINDER	-	2165 ± 30	0.905 ± 0.013

From the above table it can be seen that the missing mass spectrum might contain an η^o - meson signal. But the prediction of the η^o - meson is expected to be about 86 events which is a very weak signal above the background in the A_2^+ region (1170-1410) Mev.

7. 5 Analysis of Region R1

The condition of this sector is that the proton and the MM_1 are moving together backwards and the π^+ - meson is then forward ($w = 0^o$ to 60^o in the c.m.s.). The number of events included in it is about 910, again, after selecting the positive missing mass squared. Moreover, all the A_1^+ and A_2^+ resonances and the Δ^{++} production are dominant in the other two sectors R2 and R3 respectively. Therefore, any structure in the (P, MM_1) system should be manifest in this region. As stated earlier the MM_1 in the two pronged NOFIT channel (D) is composed of two neutral pions. Now, if the $N^{*+}(1700)$ signal is true then it should appear in this region where the N^{*+} decays to P π^o π^o

7.5.1 The (P, MM_1) System

The distribution of the invariant (P,MM_1) mass system is given in figure (7-18). The solid curve shows an approximate phase space background. By reference to figure (7-5) it can be seen that the structure in the mass region of about 1700 Mev becomes much clearer. This structure corresponds to the $N^{*+}(1700)$ decaying by the alternative decay mode (P π^o π^o). An outline of the $(N\ \pi\ \pi)^+$ system and the expected number of the $N^{*+}(1700)$ or $\Delta^+(1700)$, estimated from the analysis of the four pronged 4-C FIT events, have been given in chapter 5 (see

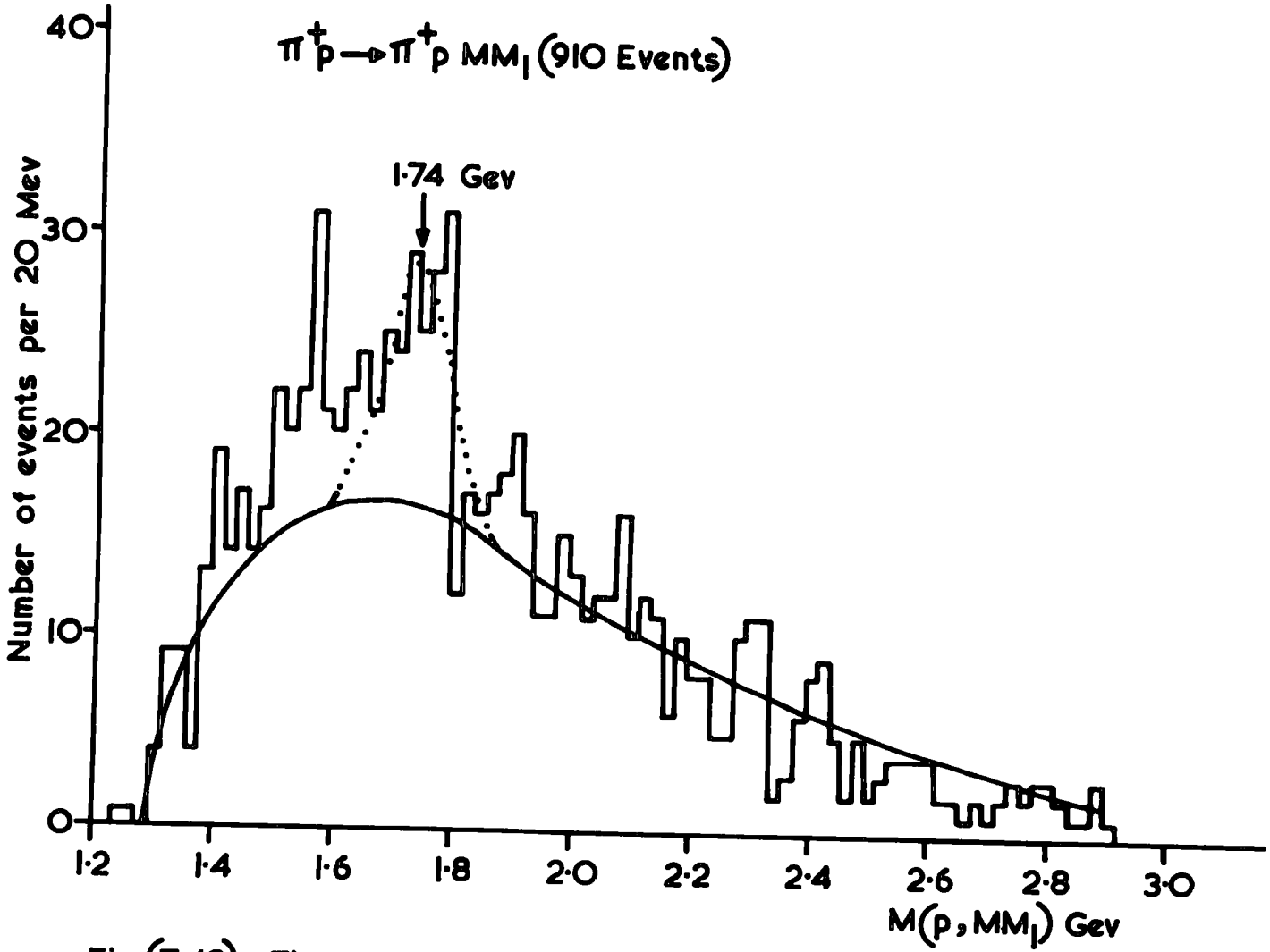

Fig. (7–18) The effective mass distribution of the (p, MM$_1$) system for region RI.

section 5.1 and tables (5-5) and (5-9). However, in sub-section 7.1.2 it was found that the structure at a mass of about 1700 Mev could possibly correspond to an $N^{*+}(1700)$ and not an $\Delta^{+}(1700)$. The assumed background and an S - wave Breit Wigner signal were used to fit the mass region (1640 - 1860) Mev of figure (7-18) where the central mass and the width are free parameters in the fitting. The fitted curve is shown as a dotted curve in the figure. The result of the fitting is:-

$$M_o = 1.745 \pm 0.013 \text{ Gev}$$

$$\Gamma_o = 0.115 \pm 0.009 \text{ Gev}$$

The observed number above the BG is equal to 75 ± 8 events which is equivalent to a cross-section of 0.031 ± 0.003 mb. These results are consistent with the earlier determination.

Since the $N^{*+}(1700)$ does occur in the $(N\pi\pi)^{+}$ system then the two distributions of the (P, MM_1) and the (π_s^{+}, MM_2) in both NOFIT channels, (D) and (E), could be added together by demanding the absence of the other resonances in the NOFIT channel (D) (e.g. A_1^{+}, A_2^{+} and Δ^{++} productions) and $t(\pi^{+}/\pi_f^{+})$ to be less than 0.25 $(\text{Gev/c})^2$ in the NOFIT channel (E). For this purpose, figure (7-19) shows the $(N\pi\pi)^{+}$ mass system. Relatively, the enhancement at 1700 Mev is seen to be more significant. An S- wave Breit Wigner signal added incoherently to the assumed smooth hand-drawn background have been fitted in the mass region (1640 - 1860) Mev. Here again, the central mass and the width are free parameters in the fitting. The results of this fitting and the results of the determination earlier (by using (P, MM_1) and (π_s^{+}, MM_2) separately) are summarised in table (7-8). From this table it can be seen

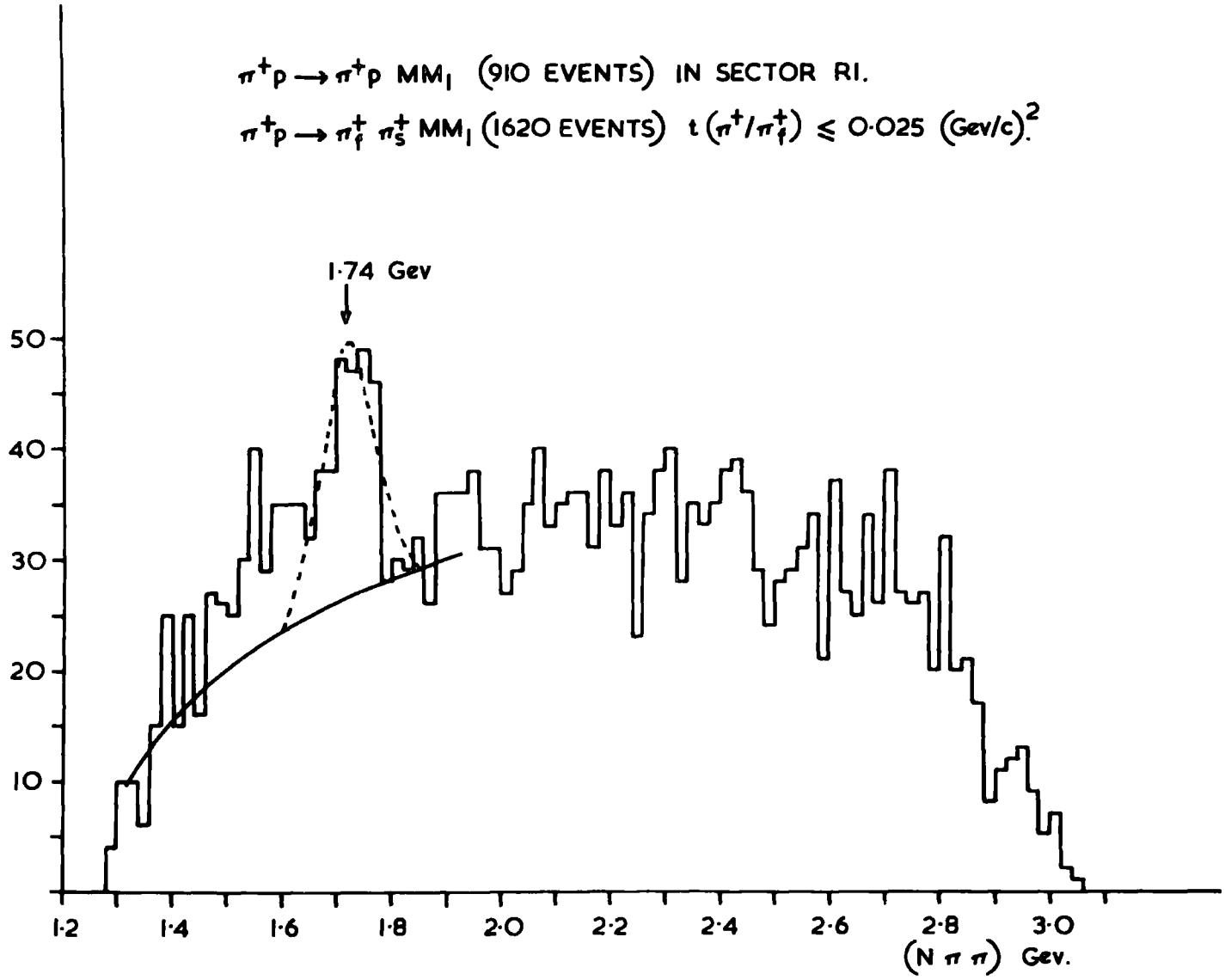

FIG. (7–19) THE EFFECTIVE MASS DISTRIBUTION OF THE $(p, MM_1) + (\pi_s, MM_2)$ SYSTEM. BOTH CURVES ARE DEFINED IN THE TEXT.

that the earlier results and the last result are in a good agreement with each other.

TABLE 7-8)

The Fitted Parameters	$(N\pi\pi)^+$ system in the Two Pronged NOFIT Events		
	$n\,\pi_s^+\pi^o$	$P\,\pi^o\pi^o$	$n\pi_s^+\pi^o + P\pi^o\pi^o$
M_o (Gev)	1.738 ± 0.030	1.745 ± 0.013	1.745 ± 0.009
Γ_o (Gev)	0.100 ± 0.016	0.115 ± 0.009	0.114 ± 0.007
No. of Events above the B.G.	69 ± 8	75 ± 8	152 ± 12
Cross-Section (mb)	0.030 ± 0.003	0.031 ± 0.003	0.064 ± 0.005

The numbers of events observed in the two NOFIT channels in table (7-8) suggest that the particle of mass 1700 Mev decays equally into P MM_1 and π_s^+ MM_2. This information is sufficient to identify the particle as an N^{*+} rather than an Δ^+ particle decaying to $N\pi\pi$ in which there is an $N\pi$ sub-state with T = 3/2 (see table (5-6), row 4). The numbers of events are in good agreement with the expected values predicted from the decay of the $N^{*+}(1700)$ seen in the four pronged 4-C FIT events and this lends strong support to the real existence of this baryon resonance.

7. 6 Summary

This channel is dominated by the production of the Δ^{++} which is produced in about 26% of the events. Using the sector R3 of the Van Hove plot it has been possible to isolate

largely the Δ^{++} from the P π^+ background. Using these Δ^{++} events the missing mass spectrum shows that there is considerable quasi two body Δ^{++} η^o and Δ^{++} f^o production.

In sector R2 there is firm evidence for A_1^+ and A_2^+ production in the π^+ MM_1 combination which corresponds to quasi two body P A_1^+ and P A_2^+ production.

Finally in sector R1 the P MM_1 distribution together with the π_s^+ MM_2 spectrum (from π_s^+ π_f^+ MM_2 NOFIT) provides strong evidence for the existence of the $N^{*+}(1700)$ which decays to N π π .

CHAPTER 8

GENERAL CONCLUSIONS

This thesis is in two parts. In the first part some consideration was given to the validity of error formula used in film analysis. It was seen that:-

1 - at the maximum length of available primary tracks the measurements are limited by measuring error only.

2 - by selecting secondary tracks of particles of low momentum the measurements are limited by measuring error and Coulomb scattering, and the transition has been clearly seen.

3 - the internal error (E_i) and the external error (E_e) are consistent with one another. However, both of them underestimate in the same way the experimental error (D_c) which is given by:-

$$D_c^2 = A^2 + S^2 E^2 \quad \mu m^{-2}$$

where A and S are constants and E is the internal or the external error. In particular for long primary tracks the error is badly underestimated by the internal or external error formulae.

Secondly, an account has been given of resonance production in the two pronged NOFIT events in the following two reactions of 5 Gev/c incident momentum π^+P interactions:-

(a) $\pi^+ P \rightarrow P\ \pi^+\ MM_1$

(b) $\pi^+ P \rightarrow \pi_s^+\ \pi_f^+\ MM_2$

It should be remembered that the programme FAKE was used to generate the phase space background and it was found that the missing mass (MM_1) in channel (a) comprises two neutral pions

(about 94%) whereas the missing mass (MM_2) in channel (b) is composed of a mixture of two and three neutral particle states (i.e. n π^o and n π^o π^o, about 50% each).

In channel (a) besides the strong production of the $\Delta^{++}(1236)$ there are significant amounts of the η^o and f^o/A_2^o mesons observed. Also, A_1^+ and A_2^+ signals are detected. An enhancement of $N^{*+}(1700)$ production is seen where N^{*+} decays into P π^o π^o.

In the case of channel (b) the only structure that has been observed is that of the $N^{*+}(1700)$ where N^{*+} decays to n π_s^+ π^o.

Table (8-1) presents a summary of the production of resonances in both channels. Column 1 shows the channel and the decay mode. The expected number of events which is predicted from the equivalent reaction in the four pronged events is given in column 2. Columns 3 and 4 show the observed number of events with corresponding cross-section. The fitted parameters such as the central mass (M_o) and the full width at half height (Γ_o) are displayed in columns 5 and 6 respectively.

The table demonstrates the potential richness of the NOFIT channels (in particular the P π^+ MM_1 channel). It shows that if the problem of P/π^+ ambiguities can be resolved and also if the precision of invariant mass combinations in these channels is fully appreciated then good samples of quasi two and three body reactions can be obtained. Indeed, in some cases (involving the η^o - meson) the sample is richer than the corresponding four pronged 1-C(π^o) FIT channel.

Obviously some quasi two body channels are completely lost to analysis in the NOFIT data, where basically it is the missing mass which is being examined. For example, the reaction $\pi^+ P \rightarrow \Delta^+ \rho^+$ can be predicted from the reaction $\pi^+ P \rightarrow \Delta^{++} \rho^o$

TABLE (8-1) Summary of the Production of Resonances in the Two Pronged NOFIT Channels.

1	2	3	4	5	6
Channel and Decay Mode	Number of Events		Cross-section	The Fitted Parameters	
	Expected	Observed	(mb)	Mass (Gev)	Width (Gev)
(a) $\Delta^{++}\eta^{\circ}$, η° goes into neutral mode	147	145 ± 20	0.061 ± 0.008	0.560 ± 0.011	0.110 ± 0.008
(a) $\Delta^{++}f^{\circ}$, $f^{\circ}\rightarrow\pi^{\circ}\pi^{\circ}$ (1)	214	190 ± 25	0.079 ± 0.010	1.275 ± 0.013	0.180 ± 0.009
(a) $\Delta^{++}MM_1$, MM_1 goes into neutral mode	—	1055 ± 35	0.441 ± 0.015	1 212 ± 0.003	0.115 ± 0.002
(a) $p\,A_1^{+}$, $A_1^{+}\rightarrow\pi^{\circ}\rho^{+}$; $\rho^{+}\rightarrow\pi^{+}\pi^{\circ}$	—	200 ± 15	0.084 ± 0.008	1.040 ± 0.004	0.090 ± 0.003
(a) $p\,A_2^{+}$, $A_2^{+}\rightarrow\pi^{\circ}\rho^{+}/\pi^{+}\eta^{\circ}$	372	355 ± 35	0.148 ± 0.013	1.275 ± 0.012	0.140 ± 0.006
(a) $\pi^{+}N^{*+}(1700)$, $N^{*+}\rightarrow p\pi^{\circ}\pi^{\circ}$ (2)	84	75 ± 8	0.031 ± 0.003	1.745 ± 0.013	0.115 ± 0.009
(b) $\pi^{+}N^{*+}(1700)$, $N^{*+}\rightarrow n\pi^{+}\pi^{\circ}$ (2)	84	69 ± 8	0.030 ± 0.003	1.738 ± 0.030	0.100 ± 0.016
(a) $p\pi^{+}\eta^{\circ}$; $A_2^{+}\rightarrow\pi^{+}\eta^{\circ}$ INCL	246	200 ± 14	0.084 ± 0.006	(1) Strictly these should be f°/A_2° but from the results in four pronged 4-C and 1-c(π°) FIT $\Delta^{++}A_2^{\circ}$ and $p\pi^{+}f^{\circ}$ are not seen.	
(a) $p\pi^{+}A_2^{\circ}$, $A_2^{\circ}\rightarrow\pi^{\circ}\eta^{\circ}$ (1)	—	85 ± 9	0.035 ± 0.004		
(a) $p\pi^{+}$ MM_1 ; Remainder	—	3115 ± 55	1.302 ± 0.023	(2) These two channels correspond to ispin sub-state $T^{12} = 3/2$, see row 4 in table (5-6).	
(b) $\pi_s^{+}\pi^{+}{}_f$ MM_2 ; Remainder	—	6912 ± 72	2.737 ± 0.030		

in the four pronged data to occur in 2186 cases (see table (5-5) in chapter 5) in this experiment. On decay of the Δ^+ to $P\pi^o$ or $n\pi^+$ and of the e^+ to $\pi^+\pi^o$ then the two charged secondary particles, $P\pi^+$ or $\pi^+\pi^+$, are not associated nor are the two unseen neutral particles. These events must fall into the categories of "remainder" in table (8-1).

A further possible application of NOFIT analysis can be made in the $\pi\pi$ interaction. It was seen in the analysis using the Van Hove plot that sector R3 was almost completely dominated by the production of Δ^{++}. This, with result from phase space calculations that the missing mass neutral particles in this channel are 94% $\pi^o\pi^o$ leads to the possibility that these selected events from the two pronged NOFIT channel allow an investigation of the interaction $\pi^+\pi^- \rightarrow \pi^o\pi^o$ to be made by use of the Chew-Low extrapolation and by other methods (see ref. 1, 2 and 3). As is well known this kind of analysis requires very large statistics. However, as a preliminary survey the events of sector R3 have been assumed to be events of the kind $\pi^+P \rightarrow \Delta^{++}\pi^o\pi^o$ and the cross-section for $\pi^+\pi^- \rightarrow \pi^o\pi^o$ estimated as a function of the di-pion centre of mass energy. A Durr-Pilkuhn form factor was used (see ref. 4 and 5). The results are shown in figure (8-1). The cross-section $\sigma(\pi^+\pi^- \rightarrow \pi^o\pi^o)$ takes place through the isospin states T = 0, 2. The part corresponding to T = 2 can be calculated from the $\pi^-\pi^- \rightarrow \pi^-\pi^-$ cross-section. Using the $\pi^-\pi^-$ results for T = 2 (see ref. 5 and 6), the T = 2, $\pi^+\pi^- \rightarrow \pi^o\pi^o$, cross-section has been calculated and is shown as the solid curve in the figure. The difference between the curve and results represents the T = 0 contribution. The figure illustrates this further important

aspect of NOFIT interactions that they can be used for detailed work on the $\pi\,\pi$ interaction.

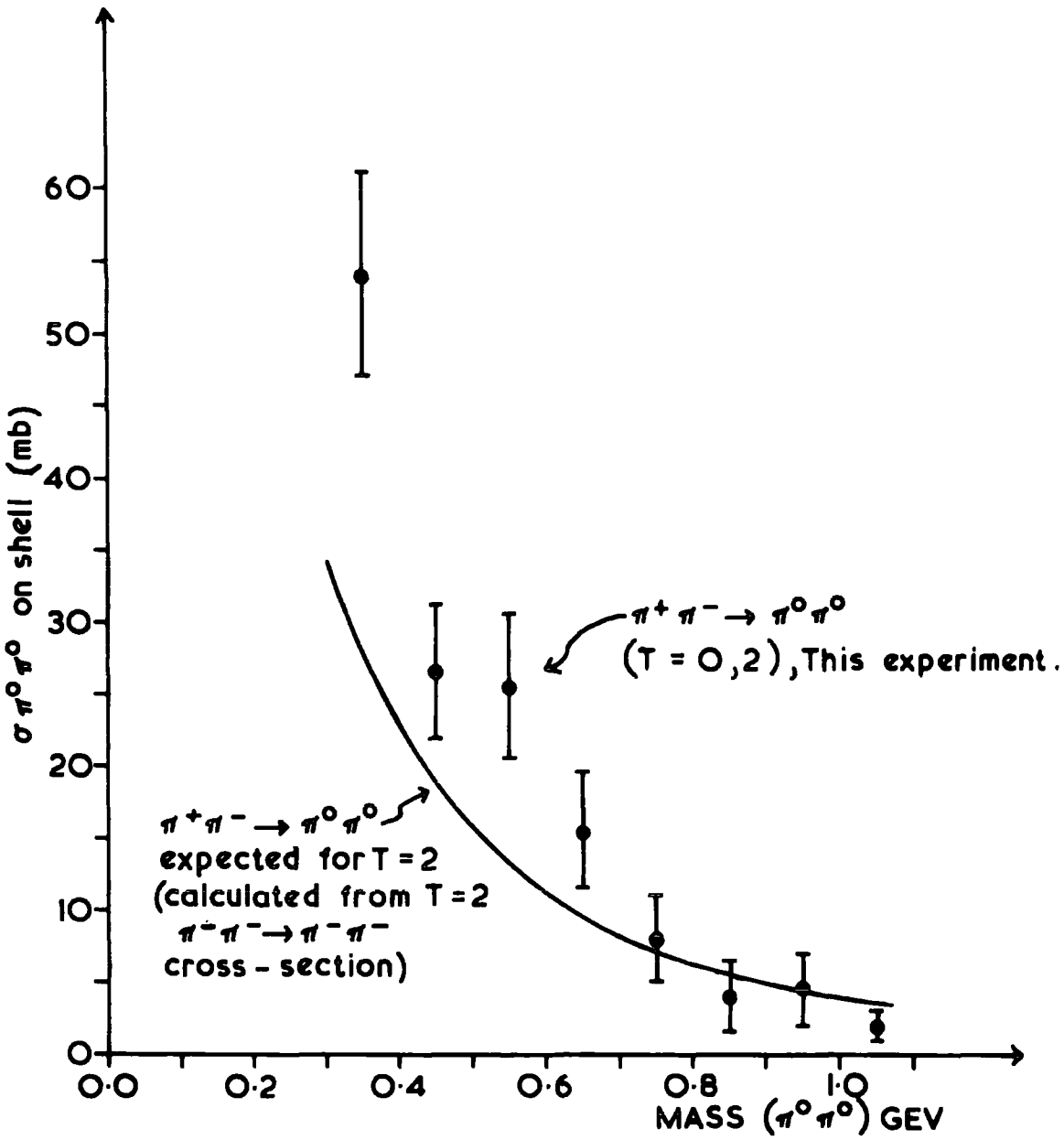

FIG.(8-1) THE DI-PION CROSS-SECTIONS ($\sigma\pi^0\pi^0$) ON SHELL DETERMINED IN THE ANALYSIS OF $\pi^+p \rightarrow \Delta^{++}\pi^0\pi^0$ EVENTS AT 5 GEV/C.

ACKNOWLEDGEMENTS

The author wishes to thank Professor G.D. Rochester and Professor A.W. Wolfendale for their encouragement and interest in the work. He wishes to acknowledge his indebtedness to his supervisor Dr. J.V. Major for his guidance, his assistance and many helpful suggestions in all phases of this work. He would like to thank his colleagues in the High Energy Nuclear Physics Group for their help with various stages of the work.

His thanks are due to the technical staff of the Physics Department, in particular to Mrs. J. Gibson, Mrs. D.C. Pickles and Mrs. T. Richardson for their help in drawing the figures. He would also like to thank the computing staffs at the different laboratories, the computing staff at Durham University in particular. He would like to thank Mrs. J. Lincoln for her careful typing of this thesis.

The author wishes to thank his wife Nabiha for her constant encouragement during his absence from her and the family.

Finally, he would like to thank the Government of the Kingdom of Saudi Arabia, the University of Riyad in particular, for a maintenance grant during the work and for travelling grants.

This work has been financed by the Science Research Council.

REFERENCES

Chapter 1

1 - D.J. Schotanus, et al.,
Nuclear Physics, B22 (1970) 45

2 - C.L. Pols, et al.,
Nuclear Physics, B25 (1970) 109

3 - H. Drevermann, et al.,
Physical Review, Vol.161 (1967) 1356

4 - A. Citron, et al.,
Physical Review, Vol.144 (1966) 1101

Glaser, D.A.,
Physical Review, Vol.87 (1952) 665

Chapter 2

1 - E. Keil and W.W. Neale,
CERN/TC/02, 63-3 (1963)

2 - Z.I. Bhuiyan,
Ph.D. Thesis, Durham University (1967) 23

3a- W.T. Welford,
Applied Optics, Vol.2 (1963) 981

3b- Parameters of 1.5 m Hydrogen Bubble Chamber,
CERN/TC/NBC, 64-1 (1964)

4 - B.N. Fabian, et al.,
The Review of Scientific Instruments,Vol.34 (1963) 484

5 - The Magnetic Field of the British 1.5 m Bubble Chamber,
CERN/TC/NBC, 63-2 (1963)

6 - G. Kellner,
CERN/TC/NBC, 65-4 (1965)

7 - D.B. Thomas,
CERN, 67-26, Vol.I (1967) 215

8 - R.L. Gluckstern,
Nuclear Instruments and Methods, 24 (1963) 381

9 - C.M. Fisher, see ref. 7, page 25

10 - C.M. Fisher,
RHEL, HEP/MISC/8 (1970) 5

Chapter 4

1 - D.J. Schotanus, et al., see ref. 1 in chapter 1

2 - E. Cibra, et al.,
Nuclear Physics, B23 (1970) 533

3 - Bonn-Durham-Nijmegen-Paris (E.P.) - Torino Collaboration
Nuclear Physics, B16 (1970) 221

Chapter 5

1 - C.L. Pols, et al., see ref. 2 in chapter 1

2 - Z.I. Bhuiyan, see ref. 2 in chapter 2, page 68

3 - Bonn-Durham-Nijmegen-Paris-Strasbourg-Turin Collaboration,
Physics Letters, Vol.28B (1968) 72

4 - Topical Conference on High-Energy Collisions of Hadrons,
CERN, 68 - 7, Vol.II (1968)150

5 - B-D-N-P-T Collaboration, see ref. 3 in chapter 4

6 - E. Cibra, et al., see ref. 2 in chapter 4

7 - G. Rinaudo, et al.,
Nuclear Physics, B25 (1971) 351

8 - Elementary Particle Physics, by Gunner Kallen, (1964) 430

Chapter 6

1 - P. Fleury, et al.,
Physics Letters, Vol.26B (1967) 686

2 - K.F. Galloway, et al.,
Physics Letters, Vol.27B (1968) 250

3 - V.E. Barnes, et al.,
Physical Review Letters, Vol.23 (1969) 1516

4 - E. Cibra, et al., see ref. 2 in chapter 4

5 - G.V. Beketove, et al.,
Soviet Journal of Nuclear Physics, Vol.13 (1971) 605

Chapter 7

1 - L. Van Hove,
Nuclear Physics, B9 (1969) 331

2 - G. Rinaudo, et al., see ref. 7 in chapter 5

3 - P.L. Bastien, et al.,
Physical Review, Vol.3D (1971) 2047

4 - D.J. Schotanus, et al., see ref.1 in chapter 1

5 - R.P. Feynman,
Physical Review, Vol.76 (1949) 469

Chapter 8

1 - G.F. Chew and F.E. Law,
Physical Review, Vol. 113 (1959) 1640

2 - E. Ferrari and F. Selleri,
Nuovo Cimento Supplements, 24 (1962) 453

3 - Z. Ming Ma, et al.,
Physical Review Letters, Vol.23 (1969) 342

4 - H.P. Durr and H. Pilkuhn,
Nuovo Cimento, 40 (1965) 899

5 - G. Wolf,
Physical Review, Vol.182 (1969) 1538

6 - E. Colton, et al.,
Physical Review, Vol.3D (1971) 2028

APPENDIX (I)

THE GENERAL EXPRESSION OF THE EXPECTED DISTRIBUTION OF THE MEASURED CURVATURES ABOUT THEIR ERROR

In chapter 3 (see section 3. 5) it was found that the estimated error in THRESH (i.e. internal error) and the calculated error in GRIND (i.e. external error) are underestimates of the true experimental error. The problem to be resolved is how are the measured error E (internal or external error) related to the experimental error D_c. Experimentall, it was found that:-

$$D_c^2 = A^2 + S^2 E^2 \qquad \text{A.1}$$

where A and S are constants. What is the general formula of the expected distribution of the measured curvatures about this error by using the above equation to determine the error ?

For this purpose, assume that there are No primary tracks leading to the measured curvatures C_j and their E_j ($j = 1,2,..,N_o$). The curvatures are individually measured. Their weighted mean C_o is given by:-

$$C_o = \sum_{j=1}^{N_o} (C_j/E_j) \Big/ \sum_{j=1}^{N_o} (1/E_j) \qquad \text{A.2}$$

Also, the mean value of the measured errors E_o has been given by:-

$$E_o = \sum_{j=1}^{N_o} (E_j/N_o) \qquad \text{A.3}$$

Then, the standard deviation D_c of the normalised distribution of the curvature (by using $(C_j - C_o)/E_j$) and the measured errors D_e have been determined.

Now, assume that the N_o values of the curvature (using

primary track) which have the weighted mean C_o and standard deviation D_c are distributed about D_c as follows:-

$$dN = \left(N_o/(2\pi)^{1/2}\right) \text{Exp}\left(-(C - C_o)^2/2D_c^2\right) dC/D_c \qquad A.4$$

and their errors will be distributed about D_e as

$$d(dN) = \left(dN/(2\pi)^{1/2}\right) \text{Exp}\left(-(E - E_o)^2/2D_e^2\right) dE/D_e \qquad A.5$$

$$d(dN) = \left(N_o/2\pi\right) \text{Exp}\left(-(C - C_o)^2/2D_c^2\right) \text{Exp}\left(-(E-E_o)^2/2D_e^2\right) *$$

$$* \quad dC\ dE/D_c\ D_e \qquad A.6$$

where substitution has been made for dN. The number of the tracks is required at $(C - C_o)/E = X$ and for a certain track length E is constant, therefore, $dX = dC/E$. Rewrite equation A.6 in terms of X and dX

$$d(dN) = (N_o/2\pi) \text{Exp}\left(-X^2E^2/2D_c^2\right) \text{Exp}\left(-(E-E_o)^2/2D_e^2\right) *$$

$$* \quad E\ dx\ dE/\ D_c\ D_e \qquad A.7$$

This expression contains two integrations, one over dX and the other over dE. To determine the number of tracks when the measured errors vary between $(-\infty)$ and $(+\infty)$ integrate equation A.7 with respect to E, which is given by:-

$$dN = (N_o\ dX/2\pi\ D_cD_e) \int_{-\infty}^{\infty} \text{Exp}\left(-X^2E^2/2D_c^2\right) \text{Exp}\left(-(E-E_o)^2/2D_e^2\right) *$$

$$* \quad E\ dE \qquad A.8$$

To integrate this expression, we are looking for some simplification. Now, it can be seen that:-

$$\text{Exp}\left(-X^2E^2/2D_c^2\right) \text{Exp}\left(-(E-E_o)^2/2D_e^2\right) =$$

$$= \text{Exp}\left(-(X^2E^2/2D_c^2 + E^2/2D_e^2 - E\ E_o/D_e^2 + E_o^2/2D_e^2)\right) =$$

$$= \text{Exp}\left(-(E^2(X^2/2D_c^2 + 1/2D_e^2) - E\ E_o/D_e^2 + E_o^2/2D_e^2)\right) \qquad A.9$$

The exponent in equation A.9 is of the form

$$(YE - Z)^2 = E^2Y^2 - E\ 2YZ - Z^2 \qquad A.10$$

From equations A.9 and A.10 it can be seen that

$$Y^2 = X^2/2D_c^2 + 1/2D_e^2 \quad \text{and} \quad 2YZ = E_o/D_e^2$$

$$Y = \left(X^2/2D_c^2 + 1/2D_e^2\right)^{1/2} \text{ and } Z = E_o/2Y\,D_e^2$$

$$Y = \left((X^2D_e^2 + D_c^2)/2D_c^2\,D_e^2\right)^{1/2}$$

therefore, $Z = (E_o/2D_e^2)\left(2\,D_c^2D_e^2/(X^2D_e^2 + D_c^2)\right)^{1/2}$

where substitution has been made for Y.

$$Z^2 = (E_o^2D_c^2/2D_e^2)\,(X^2D_e^2 + D_c^2)^{-1}$$

The exponent in equation A.9 becomes

$$\text{Exp}\left(-((YE - Z)^2 - Z^2 + E_o^2/2D_e^2)\right) =$$

$$= \text{Exp}\left(-((YE - Z)^2 + E_o^2\,X^2(X^2D_e^2 + D_c^2)^{-1}/2)\right)$$

put $YE - Z = Q$ and then $dQ = Y\,dE$

Therefore, the above exponent becomes

$$\text{Exp}\left(-(Q + E_o^2X^2(X^2D_e^2 + D_c^2)^{-1}/2)\right)$$

where substitutions have been made for Z^2 and $(YE - Z)$.

The equation A.8 becomes

$$dN = (N_o dX/2\;D_cD_e)\int_{-\infty}^{\infty} \text{Exp}\left(-(Q + E_o^2X^2(X^2D_e^2 + D_c^2)^{-1}/2)\right) \times$$

$$\times\ ((Q + Z)/Y^2)dQ \qquad \text{A.11}$$

here again, substitutions have been made for E and dE. Indeed, equation A.11 contains two integrations, these are:-

$$\int_{-\infty}^{\infty} \text{Exp}(-Q^2)Q\,dQ = 0$$

and $$\int_{-\infty}^{\infty} \text{Exp}(-Q^2)\,Z\,dQ = Z(\pi)^{1/2}$$

These are leading to

$$dN = (N_o/2\pi D_c D_e Y^2)\left(E_o D_c (\pi)^{1/2}/D_e (2(X^2 D_e^2 + D_c^2))^{1/2}\right) \times$$
$$\times \text{Exp}\left(- E_o^2 X^2/2(X^2 D_e^2 + D_c^2)\right) dX$$

and finally

$$dN = (N_o/(2\pi)^{1/2})\ (X^2 D_e^2 + D_c^2)^{-3/2} E_o D_c^2/E \times$$
$$\times \text{Exp}\left(- E_o^2\ X^2/2(X^2 D_e^2 + D_c^2)\right) dX \qquad \text{A.12}$$

where substitutionshave been made for Q and Z.

As stated earlier that $X = (C - C_o)/E$ and $dX = dC/E$ for a certain track length, therefore, $D_e = 0$(i.e. the standard deviation of the error) then equation A.12 becomes

$$dN = (N_o/(2\pi)^{1/2})\ (E_o/D_c)\ \text{Exp}(-X^2 E_o^2/2D_c^2)\ dX \qquad \text{A.13}$$

This expression presents the general formula of the expected shape of the distribution of the curvature about the measured error by using the weighted mean of the curvature and plotting $(C - C_o)/E$ which is the normalised distribution. The slope of the general formula is given by:-

$$d(\ \text{Log}_e\ dN/dX)/dX^2 = - E_o^2/2\ D_c^2 \qquad \text{A.14}$$

Experimentally it was found that

$$D_c^2 = A^2 + S^2\ E_o^2$$

where D_c is the standard deviation and E_o is the mean value of the measured errors (internal or external error) over all date (see table (3-1) columns 9 and 10). The expected slope can be determined by:-

$$t = - E_o^2/\ 2\ (A^2 + S^2\ E_o^2)$$
$$\doteqdot (1 - A^2/S^2 E_o^2)/2\ S^2 \qquad \text{A.15}$$

A brief discussion about the general expression and the expected slope which are given in equation A.13 and A.14. One sees that if $E_o = D_c$, then equation A.13 goes to a a Gaussian distribution and the slope in equation A.14 becomes equal to - 0.5. On the other hand, if D_e not equal to 0 in equation A.12, then the slope is always steeper than - 0.5.

Experimentally, we assume that the normalised distribution of the curvature about the measured error is given by:-

$$N = K \, \mathrm{Exp}(-X^2 m) \qquad \text{A.16}$$

where K and m are constants. On the other hand the number in each interval is given by:-

$$dN = K \, \mathrm{Exp}(-X^2 m)dX \qquad \text{A.17}$$

where $X = (C - C_o)/E$, and the total number N_o is

$$N_o = K \int_{-\infty}^{\infty} \mathrm{Exp}(-X^2 m)\, dX$$

$$= K(\pi/m)^{1/2}$$

Rewrite the equation A.17 when $K = N_o (m/\pi)^{1/2}$

$$dN = N_o(m/\pi)^{1/2} \, \mathrm{Exp}(-X^2 m)dX \qquad \text{A.18}$$

where m leads to the expected slope. From equations A.13 and A.18 it can be seen that:-

$$m = \left(E_o/D_c(2)^{1/2}\right)^2$$

The slope of equation A.18 is given by

$$d(\mathrm{Log_e}\, dN/dX)/dX^2 = - m$$